THE DETERMINATION OF SMALL TIME DIFFERENCES IN THE FORMATION OF PLANETARY OBJECTS

Thesis by

Dimitri Anastassios Papanastassiou

In Partial Fulfillment of the Requirements

For the Degree of

Doctor of Philosophy

California Institute of Technology

Pasadena, California

1970

(Submitted December 1, 1969)

Acknowledgment

I would like to thank Professor G. J. Wasserburg who directed this research and shared his secrets, knowledge and prejudices without hesitation, and whose explosive enthusiasm about, among other things, six digit numbers put life into occasionally dreary measurements. I would like to thank Professor T. Lauritsen for sending me off to a new world, and Professor W. A. Fowler for trusting me not to get lost there. Professor D. S. Burnett first taught me how to run a mass spectrometer and has since not stopped discussing problems and new ideas.

I thank all my co-authors for allowing me to use the intact published papers in this thesis. The work reported on the lunar samples is a cooperative effort. Professors Wasserburg and Burnett guided and actively worked in every aspect of this project; Dr. Hermogenes Sanz participated in the first measurements.

The international atmosphere of the Lunatic Lab has been most enjoyable, especially discussions with the natives (J. C. Huneke and F. A. Podosek) and non-natives (H. G. Sanz, O. Eugster and F. Tera). I thank P. Young, U. Derksen and C. Bauman for keeping the mass spectrometer in top shape and J. Brown and T. Wen for helping with the analyses.

This work was supported in part by the National Science Foundation [GP-15911] and Office of Naval Research [Nonr-220(47)]. I received a one-year scholarship from the General Atomic Division of General Dynamics.

Finally I wish to dedicate this thesis to my wife who put up with me and helped me all these years.

THE DETERMINATION OF SMALL TIME DIFFERENCES IN THE FORMATION OF PLANETARY OBJECTS

by Dimitri A. Papanastassiou

ABSTRACT

A new solid source single focusing, sector magnet mass spectrometer was developed with a programmable magnetic field analyzer of stability $|\Delta B/B| \leq 2 \times 10^{-5}$. Digital data are obtained during a completely automatic sequence and include the real time at which an intensity measurement is made. An on line computer analyses the data and returns the results to the operator throughout a run. The precision obtained in measuring isotopic ratios is increased by an order of magnitude over conventional similar instruments and is documented for the strontium isotopes. The $^{87}Sr/^{86}Sr$ ratio is measured to better than $\pm$ 0.007% over the extended time of the experiments.

Ca-rich achondritic meteorites having a total spread of 0.2% in $^{87}Sr/^{86}Sr$ were studied and appear to define an identical initial abundance of 0.698983 $\pm$ 0.000032. The samples lie on a well defined isochron with slope 0.0642 $\mp$ 0.0034, corresponding to an age of $4.47 \mp 0.24 \times 10^{9}$ years. The maximum deviation of data points from the isochron is 6×10^{-3}% and shows that these samples were formed over a time interval of 1.6×10^{6} years if they were derived from an environment of solar Rb/Sr abundance. The Angra dos Reis achondrite

has the distinctly lower inital Sr composition of 0.69884 ± 0.00004 and is, therefore, derived from more primitive material than any other meteorite measured. Angra dos Reis may have formed 5.4×10^6 years earlier than the other achondrites (from a solar Rb/Sr environment). The Angra dos Reis initial Sr isotopic composition should be considered as the best estimate of the primordial Sr isotopic abundance in the solar system.

Measurements on the chondrite Guarena yield an age $4.56 \mp 0.08 \times 10^9$ years and precise Sr initial composition of 0.69995 ± 0.00015. This is evidence for either a late formation of Guarena or a metamorphic event taking place 74×10^6 years after the time of formation of the Ca-rich achondrites. These measurements may yield a time index for the classification of meteorites.

Measurements on Apollo XI lunar samples are presented and discussed.

Table of Contents

1. Brief Outline of the Thesis

The purpose of this study is to apply newly developed experimental techniques of measuring isotopic ratios with high precision to the determination of the primordial strontium isotopic abundance and to demonstrate that it is possible to resolve fine time differences in the formation of planetary objects.

A brief outline of the thesis follows:
In section 2 we discuss the motivation for this study. In section 3 we summarize extensively the remaining sections of the thesis. In section 4 we present new analytical results obtained for several achondritic meteorites and the first results obtained for lunar samples returned by the Apollo XI crew. These measurements are discussed in relation to the data presented in sections 5, 6, and 7.

Sections 5, 6, and 7 are unmodified versions of published articles. In section 5 we describe the design and performance of a new on-line mass spectrometer used for this study.

In section 6 we demonstrate experimentally the precision obtained for measuring isotopic ratios; we obtain a precise value for the primordial strontium isotopic composition; and we discuss the time resolution afforded by the measurements and the apparent simultaneity of the formation of the basaltic achondrites.

In section 7 we determine a differential evolution interval for a chondrite and demonstrate that similar measurements may determine

a definite time evolution sequence for very ancient objects of the solar system.

Throughout sections 2,3 and 4 we refer to other parts of this thesis using the section and subsection designation (e.g., section 6.2.2: thesis section 6, subsection 2.2). We refer to equations, figures, and tables by using the section number followed by the appropriate number in quasi-decimal notation (e.g., Figure 6.1, Table 5.I).

2. Introduction

In this study we present precise measurements of strontium isotopic ratios. The isotope ^{87}Sr is being enriched over geologic time by the decay of ^{87}Rb which has a half life of 5×10^{10} years. By measuring changes in the ratio $^{87}Sr/^{86}Sr$ (where ^{86}Sr is not affected by long lived radioactivity) we obtain a measure of time under several assumptions whose validity can be ascertained from the systematics of this dating method.

The experimental procedure involves choosing samples with different enrichments of $^{87}Sr/^{86}Sr$. Each sample is dissolved completely and mixed with known amounts of calibrated solutions enriched predominantly in ^{87}Rb and ^{84}Sr. Rb and Sr are separated by ion exchange; the respective solutions are evaporated and a small drop is loaded on a filament ribbon of a solid source mass spectrometer. Mass spectrometer measurements are limited by two main effects: a) mass fractionation during evaporation and ionization from the filament, and b) by ion beam instabilities from irregular emission. The first effect can be corrected for by normalizing one measured isotopic ratio which is not affected by radioactivity (e.g. $^{86}Sr/^{88}Sr$) to a given value which is the average of many determinations. This normalization procedure corrects for instrumental as well as for naturally caused isotopic fractionation. The second effect is minimized by the design of the data acquisition system of the Lunatic I mass spectrometer (described in section 5). We are able to

reduce drastically the time wasted scanning between spectral lines by step scanning between peaks at a fast rate and digitally integrating the signal. The increased speed of obtaining data also results in a greater amount of data being collected during the run, whose length is determined mainly by the size of the sample. The prodigious output of the system is analyzed by an on-line computer. This procedure yields isotopic compositions reproducible to better than $\pm$ 0.007% which represents an improvement of an order of magnitude in precision over conventional mass spectrometers using surface ionization. This precision was sorely needed since the relative enrichments of $^{87}Sr/^{86}Sr$ are small. In particular using the Lunatic I we have determined an age for the basaltic achondrites, a group of meteorites which show only a 0.2% total enrichment in ($^{87}Sr/^{86}Sr$). These objects were previously lumped together and provided an origin for the isotopic composition of Sr in other Rb-rich meteorites.

The data presented here on basaltic achondrites define an age of 4.5×10^9 years for these objects in good agreement with the age of the earth and other meteorites. We find that these meteorites formed within 2-5 $\times 10^6$ years of each other 4.5×10^9 years ago. We also determine the best estimate of the primordial Sr composition in the solar system when solid bodies began to form.

The fine relative time scale established using the Rb-Sr scheme is comparable to the results obtained by extinct radioactivity effects in meteorites. The ^{129}I decay into ^{129}Xe with the much shorter 1.7×10^7

year half-life has an experimental resolution of about 2×10^6 years. Careful recent experiments by Podosek (1969 a) yield relative ages for meteorites and different parts of meteorites which show a total range of only 15×10^6 years. This range is similar to the results presented here although no samples have as yet been measured by both methods. The scheme dependent on ^{244}Pu fission and enrichment of the heavy Xe isotopes with an 8.2×10^7 year half-life appears to give similarly short formation intervals although the method is not well established (Sabu and Kuroda 1967 ; Reynolds 1968). It is indicated that the actual formation of solid objects in the early solar system has occurred over very short time intervals. These intervals apply to any process of matter condensation from the contracting solar nebula.

Measurements on the chondritic meteorite Guarena with $\pm$ 0.007% precision using sophisticated mineral separation techniques allow us to determine the occurence of an event in this object $\sim$ 75 million years after it was formed. Previously it has only been possible to determine formation times with a resolution of $\pm$ 100 million years.

By comparing our data on the achondrites with lower precision measurements of nonradiogenic samples of the earth we can place an upper limit of $\sim$ 200 million years on the relative time of formation of the earth and the meteorites if the earth is younger than the meteorites. High precision measurements in old terrestrial rocks will tighten this upper limit.

Recently returned samples from the lunar surface show very small enrichments in $(^{87}Sr/^{86}Sr)$ so that the precision reported and

documented here is absolutely necessary in dating these samples. We will report results which show that the moon is about 4.5×10^9 years old and that on its surface igneous rocks exist which yield ages as young as 3.5×10^9 years. This shows both that the moon is old and that it has remained active for a long period of time despite some opinions expressed to the contrary. The nature of the activity on the moon is not determinable yet, however, a very strong argument can be made against the possibility of the moon having formed $\sim 3.5 \times 10^9$ years ago by the "fission" of the earth.

The precision in measuring isotopic ratios can be applied to the study of the evolution of the earth's crust (Wasserburg 1966). In particular since the crust is characterized by high Rb/Sr ratios while the upper mantle has low Rb/Sr abundance, rocks which have been "reworked" in the crust can be resolved from rocks which have either recently been added to the crust from the mantle or have not been disturbed since their early addition.

The precision of $\pm$ 0.007% can correspond to about $\pm 2.5 \times 10^4$ years in certain common Rb-rich minerals on the earth. This resolution in time could permit a check of the ages obtained by ^{14}C dating.

The advance in instrumentation described and demonstrated here can now be used to study other fine isotopic effects for a variety of elements in different samples of the solar system with particular ease and efficiency. Precise Ba isotopic abundances have recently been obtained using the Lunatic I (Eugster, Tera, and Wasserburg 1969). By the use of a double spike for the determination

of mass fractionation, these authors have reported identical isotopic composition of Ba in terrestrial and meteoritic samples. These results allowed a definite refutal of previously reported Ba isotopic variations. Similar measurements for Gd (Eugster, Tera, Burnett, and Wasserburg 1969) have recently established an identical isotopic abundance for terrestrial and meteoritic Gd to 0.1% and also determined that the Norton County achondrite has been subjected to an integrated thermal neutron flux of 4.4×10^{15} neutrons. High precision measurements on Gd in lunar samples using this system provide a precise monitor of thermal neutron effects.

A similar digital data acquisition system and magnetic field analyzer have recently been added to a conventional rare gas mass spectrometer. Preliminary results indicate a significant increase in the precision of the data obtained. It is, therefore, obvious that a wealth of effects may now be studied related both to geological and extraterrestrial problems with a precision and ease of data analysis not previously possible.

3. Detailed Summary

3.1 Rb - Sr Systematics

Recent studies of meteorites by the rubidium-strontium dating method have consistently given ages in the range 4.4-4.7 x 10^9 years. In section 6.1 we present a short review of the data obtained previously to the present study. The resolution which can be achieved by using the standard dating procedures is $\pm$ 10^8 years, especially if we include systematic errors which exist among different laboratories due to the lack of high quality comparisons of adequate standards and the considerable difference in the quality of the available data. It is, therefore, clear that most events of object formation and differentiation cannot be resolved without a considerable improvement in analytical techniques and a shift of the emphasis in Rb-Sr determinations.

The Rb-Sr dating method is based on the decay scheme

$$^{87}_{37}Rb \longrightarrow {}^{87}_{38}Sr + e^- + \bar{\nu} \qquad (1)$$

with a half-life $\tau_{\frac{1}{2}} = 5 \times 10^{10}$ years. We denote by $(^{87}Sr)_I$ the number of ^{87}Sr atoms at an initial time τ_I in a given system containing Rb and Sr. As long as the system remains closed to Rb and Sr loss we obtain at any time τ

$$(^{87}Sr)_\tau = (^{87}Sr)_I + (^{87}Rb)_\tau \left[e^{\lambda(\tau_I - \tau)} - 1\right] \qquad (2)$$

where $(^{87}Rb)_\tau$ is the number of surviving atoms and λ the decay constant. Time is measured such that at present $\tau \equiv \tau_P = 0$. Since

isotopic ratios are measured more precisely than the absolute number of parent and daughter atoms, equation 2 is normalized by using a Sr isotope not affected by long term radioactive decay. For measurements at the present we obtain:

$$\left(\frac{^{87}Sr}{^{86}Sr}\right)_P = \left(\frac{^{87}Sr}{^{86}Sr}\right)_I + \left(\frac{^{87}Rb}{^{86}Sr}\right)_P [\exp(\lambda\tau_I) - 1] \quad (3)$$

where $(^{87}Rb/^{86}Sr)_P$ is the ratio of the concentrations of the specified isotopes (in moles/g sample) and τ_I is the "age" of the system, i.e., the time elapsed since the system had the unknown initial composition $(^{87}Sr/^{86}Sr)_I$. Both the age τ_I and $(^{87}Sr/^{86}Sr)_I$ are defined if we can measure at least two systems for which there is good reason to believe that they became isotopically homogenized but chemically differentiated (i.e., different Rb/Sr) at the same time τ_I and remained closed to Rb and Sr loss thereafter. Figure 1 shows a $(^{87}Sr/^{86}Sr)_\tau$ versus $(^{87}Rb/^{86}Sr)_\tau$ diagram usually termed a Rb-Sr evolution diagram. Closed systems move along -45° lines on this diagram. We show three systems A, B, and C which at τ_0 have the same Sr isotopic composition. In view of equation (3), any time thereafter the systems will continue to lie on a line (called an isochron) whose slope determines the time elapsed since τ_0, and whose y-axis intercept defines $(^{87}Sr/^{86}Sr)_{I_0}$. System S is the average of systems A, B, and C. If at time τ_1 the systems A_{τ_1}, B_{τ_1}, and C_{τ_1} become rehomogenized isotopically, we obtain new systems A'_{τ_1}, B'_{τ_1}, and C'_{τ_1} which thereafter evolve undisturbed. If the total system S remains closed, it will evolve without

any discontinuity at τ_1. At a later time, systems A', B', C' and S will yield an "age" τ_2 since the last "catastrophic" disturbance at τ_1. However, if $(^{87}Sr/^{86}Sr)_{I_0}$ were independently known, a line through $(^{87}Sr/^{86}Sr)_{I_0}$ and S_{τ_2} would yield the total time elapsed $(\tau_1 + \tau_2)$ since τ_0. Moreover the relatively high $(^{87}Sr/^{86}Sr)_{I_1}$ is an indication of a secondary event between τ_0 and $\tau_1 + \tau_2$. The lowest $(^{87}Sr/^{86}Sr)_I$ obtained during investigations of many bodies is thought of as "primordial". The method usually works in the reverse way: if the data on a set of objects result in points defining a straight line, an age and initial Sr isotopic composition are inferred along with the conclusion that the objects have not been disturbed during the inferred age.

A group of objects are usually chosen for which there is some reason to believe that they are cogenetic. The ability to draw any firm conclusions for a group of objects which is chosen for investigation is highly dependent on the amount of heterogeneity in Rb/Sr observed within the members of the group. From the nature of equation (3) a sample with low Rb/Sr and therefore small amount of radiogenic enrichment of $^{87}Sr/^{86}Sr$ is most important in determining $(^{87}Sr/^{86}Sr)_I$. A sample with high Rb/Sr results in the determination of the age for the sample even if only an approximate value for $(^{87}Sr/^{86}Sr)_I$ is used, if a sufficient range in Rb/Sr is not found.

In geological studies mineral phases with different Rb/Sr abundances are separated from a single rock or a suite of rocks which

are expected to be cogenetic from independent observations. If the studied minerals define a straight line an age is calculated under the simple assumptions of closed systems. If no such linear array is defined the system is highly disturbed and no single time of complete Sr isotopic homogenization can be inferred. Intermediate cases are also observed (Wasserburg and Steiger 1967). These authors found that in a certain granite the major phases defined a straight line on a Rb-Sr evolution diagram but that some of the minor phases indicated a small excess of radiogenic ^{87}Sr. This was interpreted as a sign of only slight redistribution of Sr which did not significantly affect the major phases and could not be dated directly.

The first meteorite studies (Schumacher 1956 , Gast 1962) involved measuring Rb and Sr in chondrites, which are relatively Rb-rich, and in achondrites, which are Rb-poor, by making the assumption that these two different classes of meteorites were formed at the same time and with the same initial Sr composition. From our data it now appears that this assumption was approximately correct. More recent attempts consisted of trying to obtain a wide enough range in Rb/Sr from phases of only one meteorite. The first successful effort yielded an age for the Weekeroo Station iron meteorite (Wasserburg, Burnett, and Frondel 1965). Rb-Sr data on silicate inclusions of several more iron meteorites (including a better determination of Weekeroo Station) have been reported (Burnett and Wasserburg 1967b) which yield ages of 4.6×10^9 years and an initial

($^{87}Sr/^{86}Sr$) composition compatible with the approximate value of 0.699 obtained from previous measurements on basaltic achondrites. A relatively precise Rb-Sr isochron for Norton County (Bogard et al. 1967) an enstatite ($Mg_2Si_2O_6$) achondrite yields an age of 4.70×10^9yr and an initial ($^{87}Sr/^{86}Sr$) = 0.7005 ± 0.001 . An internal isochron corresponding to an age $3.8 \pm 0.1 \times 10^9$ was obtained for the iron meteorite Kodaikanal (Burnett and Wasserburg 1967a) and is the only evidence for ages younger than the range $4.4\text{-}4.7 \times 10^9$yr obtained for all other meteorites by the Rb-Sr method. Less successful attempts at obtaining internal isochrons on stone meteorites have also been reported (Shields, Pinson and Hurley 1966 ; Shima and Honda 1967). Rb-Sr studies have demonstrated (when good linear arrays were obtained) that all meteorites, except Kodaikanal, formed within $\pm 1.5 \times 10^8$ years 4.6×10^9 years ago.

The ages in this and the previous studies are calculated using the $\tau_{\frac{1}{2}} = (5.0 \pm 0.2) \times 10^9$ years ^{87}Rb half-life which has been determined by measuring the ratio of radiogenic ^{87}Sr to ^{87}Rb in very Rb-rich terrestrial minerals. Concordant U-Pb ages ranging from 375 to 2700 million years were determined for these particular minerals and the assumption was made that the rubidium and uranium minerals were cogenetic (Aldrich et al. 1956).

Flynn and Glendenin (1959) have measured the specific activity and beta spectrum of ^{87}Rb with a liquid scintillator and obtain $\tau_{\frac{1}{2}} = (47 \pm 1) \times 10^9$ years. From the known spin and parity change (3, yes) a third forbidden transition is indicated and results in a

^{87}Rb Kurie plot with considerable curvature and an excess of low energy electrons. A mass spectrometric measurement would bypass both the problem of counting low energy electrons and of making assumptions about minerals during geological time. This experiment is now made feasible by the precision reported here. A precise half-life value would permit better comparisons between absolute ages obtained by different decay schemes. Internal comparisons of relative Rb-Sr ages are not affected by this uncertainty and we will not discuss it further.

3.2 Discrimination Correction

We would like to discuss the errors involved in measuring the remaining terms of equation (3). The second term on the RHS involves the ratio of the concentration of two elements. Each concentration is measured by isotope dilution, i.e., mixing the sample with a spiked solution of known isotopic composition and concentration. Mass spectrometric measurements are subject to mass fractionation errors. Measured, raw isotopic ratios vary between runs and during an individual run. This variation is found to behave in a regular fashion and, for two isotopes, it is a function of their fractional mass difference. Therefore we can define a discrimination $\underline{d}$ per mass unit by normalizing a measured isotopic ratio (unaffected by nuclear processes) to a value which is the average of many determinations. All other ratios are corrected appropriately. For the Sr isotopes the correction factor ranges almost always between $\pm$ 0.1% per mass unit during the data acquisition period.

Strontium has four stable isotopes and only one isotope is being enriched by the decay of ^{87}Rb. We can, therefore, use two isotopes (88 and 86) to calculate the discrimination factor and correct $^{87}Sr/^{86}Sr$. The fourth isotope (84) is used to calculate the concentration by using a spike solution enriched predominantly in ^{84}Sr. The only uncertainty in this procedure, as discussed in section 6.2.4 results from errors in the isotopic composition of the spike due to unknown fractionation. In the case of Rb there are only two long lived isotopes, 85 and 87. Therefore, it is not possible to calculate from a single run both a discrimination factor and the concentration of Rb in the sample. It is found that $^{85}Rb/^{87}Rb$ is constant in naturally occuring environments (Shields et al. 1963). However, the value measured by each mass spectrometer is different from the accepted Nier value (Nier 1950). The measured value remains constant for a particular instrument within a 0.5% discrimination correction per mass unit. The procedure used involves determining the average discrimination factor from many normal Rb samples and then applying this factor to the spiked sample runs. This procedure yields a constant percent type error in the ^{87}Rb concentration of $\sim$ 1.5% and results in a limiting error in the determination of the slope of an isochron, so that the age cannot be determined much more accurately for sufficiently Rb-rich samples independently of the systematic uncertainty in the decay constant.

3.3 $(^{87}Sr/^{86}Sr)_I$-Age Anticorrelation

On a Rb-Sr evolution diagram a linear array of data points is characterized by the range in Rb/Sr and by the precision of the individual data points. It is clear that a number of isochrons can be drawn through the data. A steeper isochron, corresponding to a higher age will correspond to a lower y-axis intercept, or a lower initial Sr isotopic composition. The opposite is true for a less steep isochron. Therefore, the quantities of time and initial Sr isotopic composition are anticorrelated. It is possible to distinguish between meteorites which have the same age but different initial Sr isotopic abundance. If we plot the data obtained on a $(^{87}Sr/^{86}Sr)_I$-age diagram, meteorites differing in either of these two quantities will occupy different areas of the plot. It is thus easier to see if the data on two meteorites are compatible with a simultaneous formation from a single reservoir. This anticorrelation was discussed first by Sanz and Wasserburg (1969). It has the effect of permitting better resolution of ages which are affected by the uncertainty of $\pm$ 1.5% from the unknown Rb fractionation. Such an anticorrelation plot is shown in Figure 7.5 for Guarena and the less precise data on other meteorites. There is a large degree of overlapping of the error envelopes for these meteorites so that vital information about the early history of these meteorites is not decipherable.

3.4 Initial $^{87}Sr/^{86}Sr$

As pointed out before and discussed in sections 6.2.1, 6.5 and

7.4, the quantity $(^{87}Sr/^{86}Sr)_I$ is a measure of the integrated effect of ^{87}Rb decay in a system prior to the last time τ_I at which the total system and its mineral phases were isotopically homogenized, chemically differentiated and became closed to Rb and Sr losses. Differences in $(^{87}Sr/^{86}Sr)_I$ denote differential evolution. Actual time differences may be obtained if an assumption is made about the number of reservoirs and the Rb/Sr in successive Rb-Sr reservoirs to which a particular system has been exposed. The time resolution is most favorable in cases where a meteorite is separated out of a Rb-rich reservoir and if the meteorite retains almost none of the Rb. For example a piece of chalk ($CaCO_3$) contains almost no Rb, however, the Sr in the chalk which follows chemically the Ca will probably have a modern terrestrial Sr composition $(^{87}Sr/^{86}Sr) \approx 0.709$ which is distinct from the value 0.699 found in primitive Sr from meteorites. Since the Rb in the chalk fails to account for the radiogenic ^{87}Sr, evolution in more than one Rb reservoirs is certain.

The time resolution afforded by $(^{87}Sr/^{86}Sr)_I$ depends directly on the measurement error of $(^{87}Sr/^{86}Sr)_P$. In a typical chondrite $(^{87}Sr/^{86}Sr)$ has changed from 0.699 to 0.745 in 4.6×10^9 years or by 0.01 per 10^9 years. A change of 0.01% in this ratio is equivalent to 7×10^6 years differential evolution in a reservoir with $Rb/Sr \approx 0.25$. For an error of 0.01% in the experimentally determined $^{87}Sr/^{86}Sr$ we can extrapolate to $(^{87}Sr/^{86}Sr)_I$ with similar precision if we do not propagate any errors due to the age or equivalently due to the constant percent uncertainty in $^{87}Rb/^{86}Sr$. The error contributed by the

extrapolation is (see also section 6.4).

$$\delta\left(^{87}Sr/^{86}Sr\right)_I = \left(^{87}Rb/^{86}Sr\right)_P \exp(\lambda\tau)\lambda\delta\tau \qquad (4)$$

where $\delta\tau$ is the uncertainty in age τ and $\left(^{87}Rb/^{86}Sr\right)_P$ is the measured value in the sample. This error decreases proportionately to $\left(^{87}Rb/^{86}Sr\right)_P$ and is equal to 0.01% for a 5% uncertainty in age when $\left(^{87}Rb/^{86}Sr\right)_P = 0.021$. Section 6.4 discusses this point at length; Figure 6.5 illustrates the problem, and Figure 6.6 is a nomogram for the calculation of the extrapolation error. For calculating $\left(^{87}Sr/^{86}Sr\right)_I$ with high precision we have to look at meteorites or mineral phases in meteorites with very low Rb/Sr ratios [Rb/Sr = 0.35 x $\left(^{87}Rb/^{86}Sr\right)$], assuming that we are able to measure $\left(^{87}Sr/^{86}Sr\right)_P$ with high precision.

In the following discussion we assume that we can measure $^{87}Sr/^{86}Sr$ to better than $\pm$ 0.007% which represents more than an order of magnitude improvement over previous measurements. By looking at several meteorites and mineral separates of meteorites which are characterized by very low Rb/Sr we are able to measure the primordial Sr isotopic abundance in the solar system and to exhibit the first clear indication (using the Rb-Sr technique) of the existence of small time differences in the formation of meteorites. Any resolution in time of the formation of meteorites will help in the understanding of the processes involved and may result in a specific parameter of definite genetic implication being added to the present classification scheme of meteorites (Van Schmus and Wood 1967). The genetic implications of the present meteorite classification scheme are unclear. In addition we will

present very recent data on lunar samples which would have been almost impossible to obtain without very precise Sr measurements due to the particularly low Rb/Sr ratios encountered. From the $(^{87}Sr/^{86}Sr)_I$ values obtained for several lunar rocks we make strong conclusions about some of the theories proposed previously for the origin of the moon.

We assume for the present that we can measure $(^{87}Sr/^{86}Sr)_P$ to $\pm$ 0.007% and we investigate how $(^{87}Sr/^{86}Sr)_I$ determinations can be used as indicators of differential evolution. The two different kinds of time intervals which are involved are a) intervals which could be obtained in principle from the differences in Rb-Sr ages of meteorites and b) intervals which may be calculated from differences in precise initial Sr isotopic measurements by assuming differential evolution in a Rb-rich reservoir. It was shown before that measurements of Rb-Sr ages are not sufficiently precise to resolve any time structure under (a) above.

Equation 6.2, reproduced here, measures the time $\Delta\tau$ in 10^6 years for a relative enrichment ϵ (parts in 10^4) in $(^{87}Sr/^{86}Sr)_I$ due to the decay of ^{87}Rb before separation from a reservoir with Rb/Sr elemental abundance,

$$\Delta\tau = 1.74 \times \frac{\epsilon}{Rb/Sr} \qquad (5)$$

Figure 6.7 is a plot of this relation for different values of ϵ. For $\epsilon = 1$ and a chondritic type abundance of Rb/Sr $\sim$ 0.25, $\Delta\tau = 7 \times 10^6$ years. For the higher Rb/Sr = 0.65 measured in the solar photosphere (Lambert et al. 1968, 1968a), $\epsilon = 1$ corresponds to

$\Delta\tau = 2.7 \times 10^6$ years. The process which these time intervals may describe is the separation of the material, which formed the meteorites and the planets, from the contracting solar nebula if the solar nebula was characterized by the present chondritic or solar photosphere type Rb/Sr.

The time resolution discussed is obtained if we can define $(^{87}Sr/^{86}Sr)_I$ with precision similar to our precision of $\epsilon = 0.7$ in the measured $(^{87}Sr/^{86}Sr)_P$ ratios. From equation 6.4 we require that the term involving the uncertainty $\Delta\tau$ in the age τ of a system have negligible effect on the calculation of $(^{87}Sr/^{86}Sr)_I$. For systems (i) which became chemically fractionated and physically separated from the reservoir (r) at different times $\Delta\tau_i$ we derive equation 6.4 . This equation may be modified to express specifically the uncertainty $\Delta\tau$ in the known age τ:

$$\left(\frac{^{87}Sr}{^{86}Sr}\right)^i_\tau = \left(\frac{^{87}Sr}{^{86}Sr}\right)^r_I + \left(\frac{^{87}Rb}{^{86}Sr}\right)^i_\tau \exp(\lambda\tau)$$

$$+\left\{\left(\frac{^{87}Rb}{^{86}Sr}\right)^r_{\Delta\tau_i} - \left(\frac{^{87}Rb}{^{86}Sr}\right)^i_\tau \exp(\lambda\tau)\right\} \lambda\Delta\tau_i \pm\left(\frac{^{87}Rb}{^{86}Sr}\right)^i_\tau \lambda\Delta\tau \exp(\lambda\tau) \quad . \quad (6)$$

To determine $\Delta\tau_i$ we require that

$$\left[\left(\frac{^{87}Rb}{^{86}Sr}\right)^i_\tau \Delta\tau \Big/ \left(\frac{^{87}Rb}{^{86}Sr}\right)^r_{\Delta\tau_i} \Delta\tau_i\right] << 1 \quad . \quad (7)$$

If for most systems the $\Delta\tau_i$ determined is $\Delta\tau_i << \Delta\tau$ then the term $\left(\frac{^{87}Rb}{^{86}Sr}\right)^i_\tau \exp(\lambda\tau)\ \lambda\Delta\tau_i$ will be also negligible in the calculation. For

two systems i, j the time difference $\Delta\tau_{ij} = \Delta\tau_i - \Delta\tau_j$ is defined by equation 6.5 . Again we require that the uncertainty $\Delta\tau$ be such that

$$\left[\left(\frac{^{87}Rb}{^{86}Sr}\right)_\tau^k \Delta\tau \Big/ \left(\frac{^{87}Sr}{^{86}Sr}\right)_{\Delta\tau}^r \Delta\tau_{ij}\right] << 1 \quad . \tag{8}$$

This clears up the slightly confusing equation 6.6 where $\Delta\tau_k$ is actually defined as the uncertainty in τ which we here call simply $\Delta\tau$ in order not to confuse it with the terms $\Delta\tau_i$ and $\Delta\tau_j$ which, when they appear in combination with $\left(\frac{^{87}Rb}{^{86}Sr}\right)_\tau^{i \text{ or } j}$, may be negligible with respect to the term arising from the $\Delta\tau$ uncertainty. However, at least in the case of Guarena, $\Delta\tau_{BACH}$ (c.f. section 6.5 for the definition) is almost as large as the uncertainty in age of that meteorite. For the basaltic achondrites $(^{87}Rb/^{86}Sr)_\tau \approx 0.006$; for $\Delta\tau \approx 100$ m.y. and $(^{87}Rb/^{86}Sr)_{\Delta\tau}^r \approx 0.7$ for a chondritic reservoir, equation (8) is well satisfied for $\Delta\tau_{ij} \approx 7 \times 10^6$ years. For smaller time differences (e.g., $\Delta\tau_{ij} \sim 10^6$ yr. for a chondritic reservoir) it is necessary to pick τ with correspondingly greater accuracy in order to determine $\Delta\tau_{ij}$.

From the data on the basaltic achondrites to be presented $\Delta\tau_{ij} \leq 7 \times 10^6$ years. In the calculation just reviewed we considered the case of a two stage Rb-Sr evolution, where the first stage is a universal reservoir and the second stage is the meteorite being investigated. Any differential evolution in a very low Rb/Sr reservoir is not resolvable. Any multiple stage process involving more than one Rb-rich reservoirs is also not resolvable from the single Rb-rich

reservoir because the differences D^{ij} (equation 6.5) formed by the data on the basaltic achondrites are very small.

However, we would like to review the graphical way of discussing the "prehistory" of a sample, that is the evolution prior to the last complete homogenization of the Sr isotopes. Figure 7.3 presents several simple possibilities. This is a $(^{87}Sr/^{86}Sr)$ - age diagram. For short times a system with a definite $(^{87}Rb/^{86}Sr) = \zeta$ abundance evolves along a line of slope $-\lambda\zeta$ as is clear by approximating equation (2):

$$(^{87}Sr/^{86}Sr)_\tau = (^{87}Sr/^{86}Sr)_I - \lambda\zeta(\tau-\tau_I) \qquad (9)$$

A system A of age τ_I^A and $(^{87}Sr/^{86}Sr)_I^A$ would plot as a point on such a diagram. If the system was composed of several fractionated phases, after τ_I, each phase would evolve along a different line according to its particular ζ abundance; therefore the evolution of the system after τ_I would be represented by a set of lines diverging from the point $[\tau_I^A , (^{87}Sr/^{86}Sr)_I^A]$ with negative slopes. If we know ζ in the total system prior to τ_I^A we may show the evolution along a single line. Anticipating the results of the basaltic achondrites which yield a well defined low $(^{87}Sr/^{86}Sr)_{BABI}$ composition (BABI ≡ Basaltic Achondrite Best Initial), we ask for the time required for system A to evolve from $(^{87}Sr/^{86}Sr)_{BABI}$ to $(^{87}Sr/^{86}Sr)_I^A$. This time is defined as $\Delta\tau_{BACH}$ (section 7.4) and is shown graphically in Figure 7.3a . For two systems A and B we may determine by construction if it is possible to obtain a time of simultaneous separation from a

homogeneous reservoir. This is possible only when the intersection of the lines extrapolated with slope $-\lambda$ from $\left(^{87}Sr/^{86}Sr\right)_I^{A \text{ or } B}$ and $\left(^{87}Sr/^{86}Sr\right)_I^B$ intersect in a restricted portion of the $\left(^{87}Sr/^{86}Sr\right)$-age plot as discussed in section 6.4 . This construction can be used for the Guarena data and for the lunar data and will be discussed later.

The $\left(^{87}Sr/^{86}Sr\right)$-age plot can also be viewed as the anticorrelation plot mentioned before if for each system A and B discussed we draw error envelopes as shown in Figure 7.5 . One diagonal of each envelope is defined for a system by the three points $[\tau_I \pm \delta\tau_I]$ and $[(^{87}Sr/^{86}Sr)_I \mp \delta(^{87}Sr/^{86}Sr)_I]$. The vertical diagonal is fixed by the amount of uncertainty in $\left(^{87}Sr/^{86}Sr\right)_I$ when the age is assumed fixed at τ_I. In terms of the isochron diagram this corresponds to a displacement of the isochron parallel to the best fit isochron yielding the age τ_I. Non intersecting envelopes indicate that different events either in time or in initial Sr composition are being observed. It is seen from Figure 7.5 that most of the error envelopes corresponding to relatively imprecise data are intersecting.

The increase in precision of Sr isotopic measurements which result in a better definition of $\left(^{87}Sr/^{86}Sr\right)_I$,in conjunction with the ability to separate very pure mineral phases with low Rb/Sr from a meteorite are evident in the small error envelope for Guarena in Figure 7.5 . We will next demonstrate that we can measure Sr

isotopic ratios to 0.007%.

3.5 Instrumentation

We are able to obtain a precision of better than $\pm$ 0.00005 in $(^{87}Sr/^{86}Sr)_P$. The error estimate is based on simple statistical analysis, on reproducibility of repeated analyses of standard samples over long periods of time and on data obtained with gravimetrically prepared standards enriched in $^{87}Sr/^{86}Sr$. The precision (std. dev. of the mean) of a single mass spectrometer run is better than $\pm$ 0.01% for $(^{87}Sr/^{86}Sr)_P \approx 0.700$. From results of more than one run we are able to realistically reduce this error by about a factor of two. Figure 2 shows a histogram of results obtained for Sr extracted from seawater. These runs have been repeated in a regular fashion throughout the length of this investigation. The Sr is obtained each time from a standard solution without any need for chemistry. An aliquot of the solution is evaporated and loaded on the ionization filament of the mass spectrometer. The bulk ($\sim$ 90%) of all analyses (spanning a two year period) are within $\pm$ 0.00005 of the mean.

The solid source mass spectrometer capable of such precision is described in section 5. We summarize here the main aspects of the system.

A magnetic field analyzer (section 5.3) enables us to preset the magnetic field to a maximum of 27 values and to step scan cyclically between the preset field values at the rate of 500 G/s, and with a 0.3 sec locking-in time. We are able to reproduce each field setting to 0.002% corresponding to an equivalent translation of the beam of

0.013 mm in the collector defining slit which is kept at 0.53 mm (see section 5.6) . The magnetic field dispersion is ~ 32 G per mass unit in the mass 86 region at an ion energy of 16 KV and a magnetic field of 5.6 KG for the 12" radius of curvature instrument. At each field value the ion beam intensity is measured by a vibrating reed electrometer and the output of the electrometer is integrated by a digital voltmeter. The mass identification, digital voltmeter reading and time of onset of integration are transmitted to an on-line computer. A data cycle consists of measuring the four Sr isotopes once, including background on both sides of each peak and requires ~ 35 seconds. The improvement over previous instruments lies a) in the better precision of digital output over recorder output, b) in increased speed of obtaining data which results in a decrease of random errors caused by long term (~ minutes) beam instabilities, and c) in increased amount of data obtained within the definite duration of a run which depends on the sample size and filament load condition and results in better statistics. The contribution of errors from several factors is discussed in section 6.2.2 . In practice we find that by running on line we are able to know exactly when the best data are obtainable. In particular there is a one to one correspondence between Category I so called data (section 6.2.2), defined as $\sigma_{10} \leq 0.05\%$ where σ_{10} is the standard deviation of a set of ten successively obtained ratios, and $\sigma(R_n^{88}) \leq 0.028\%$ as can also be seen from Table 6.1 .

Justification for measuring the beam intensity while the beam is

held stationary in the collector collimating slit is given in section 5.6 . Figure 5.6 shows an integral spectrum of a peak obtained digitally. The ion intensity is constant to 0.01% for 2.3 G whereas we can reproduce the magnetic field to 0.12 G . Minimum tailing is observed as shown also in Fig. 5.7 for a potassium spectrum where the ratio $^{39}K/^{40}K \approx 8 \times 10^{3}$. In this spectrum the ^{39}K intensity was 8.4×10^{-10} A . Results of preliminary studies of the precision obtained for Sr are shown in Figure 5.8 . The error envelopes drawn correspond to standard deviations expected from the counting statistics of the ions being collected despite the fact that an analog signal is being measured. Experimental spread agrees very well with counting statistics. At high intensities ($> 2 \times 10^{-11}$A ^{88}Sr) we are limited by the counting statistics for the smaller isotopes, the noise of the electrometer and the resolution of the digital voltmeter. Table 6.1 shows the various error contributions to the measured quantities. Figure 6.1 shows distributions of interpolated ratios. From the r_n^{88} (section 6.2.2) distribution we deduce a value for the error contributed by the beam instability and apply it to the smaller isotopes. We assumed approximate ratios 88:87:86 $\approx$ 10:1:1. Since $^{87}Sr/^{86}Sr \approx 0.7$, r_n^{86} is always slightly better defined than r_n^{87}. The statistical arguments in section 6.2.2 indicate that for a single run $\sigma_M(r_n^{87/88}) = 0.3$ (in parts in 10^4), where σ_M^2 stands for the variance of the mean. In section 5.6 we indicated that from a measurement of 10 sets each containing 10 ratios with a standard

deviation of $\pm$ 0.05% the mean should be defined to $\pm$ 0.005%. In section 6.2.2 and thereafter we use $\pm 2\sigma_M$ as the estimate of error, which is better than $\pm$ 0.007% for the typical case analyzed in that section. Standards enriched in $^{87}Sr/^{86}Sr$ and run on the mass spectrometer yielded the results shown in Table 6.2 and Figure 6.2 . The excellent correlation obtained for experimentally measured relative enrichments in ($^{87}Sr/^{86}Sr$) ratio versus the calculated enrichments from gravimetry and the negligible deviations of the means from the unity slope correlation line, indicate that our actual errors for the average of several runs are better than $\pm$ 0.01% and closer to $\pm$ 0.005%. This is particularly true since samples usually yield better runs (in terms of beam stabilities) than the normal runs reported in Table 6.2 .

Analytical results as well as the method followed for reducing the data are given in sections 6.2.2 and 6.3 for the basaltic achondrites. The Guarena data (section 7) were analyzed in the same fashion. These data will be reviewed and discussed during and after the presentation of new data on several more basaltic achondrites than reported in section 6 and the presentation of the first results on Apollo XI lunar samples.

4. New Data and Discussion

4.1 Achondritic Meteorites

4.1.1 Experimental Methods

The experimental methods are identical to those described in sections 6.2 and 7.2 . In particular all data were obtained on the Lunatic I mass spectrometer and analyzed statistically according to the consistent scheme described in section 6.2.2 . Category I ($\sigma_{10} < 0.05\%$) and Category II ($\sigma_{10} < 0.075\%$) data were obtained unless noted. Samples were spiked to yield $(^{88}Sr/^{84}Sr)_{meas.} \sim 30$ to avoid propagation of errors from uncertainty in the Sr spike isotopic composition (cf. section 6.2.4) . ^{87}Rb contribution to the ^{87}Sr peak during a run was monitored by measuring ^{85}Rb on the multiplier, at a gain of 1000, before and after a set of 30-40 ratios. The present procedure eliminates the need for long time integration of signals close to the noise level in the mass 85 region when using a simple Faraday cup. Agreement is good between the multiplier and the simple cup measurements of ^{85}Rb up to the limiting value $^{85}Rb/^{88}Sr = 4 \times 10^{-6}$ reported in section 6.2.4 for the simple cup measurements. The Sr and Rb contamination are the same as the Average Blank Estimate (ABE) reported in section 7.2.2, as monitored by regular blank runs. Blank correction is insignificant for the Sr runs. A 6% Rb blank correction was applied to the Stannern pyroxene sample and the two Serra de Mage separates; the Serra de Mage correction does not affect the extrapolation to Rb/Sr = 0 due to the extremely low Rb/Sr ratio for these samples.

4.1.2 Sampling

Three additional achondrites to the ones reported in section 6 have been measured: Bereba, Angra dos Reis and Serra de Mage. Precise results have been obtained on Moore County. Bereba is a eucrite, as are all the previously measured meteorites.

Angra dos Reis is the sole representative of the augite achondrite class. It consists of more than 90% augite (a Ca, Mg, Fe, Al silicate) and contains more CaO and TiO_2 (24.5% and 2.4%) than any other meteorite (Mason 1962). Two samples of Angra dos Reis were obtained, one from Dr. E. Anders at the University of Chicago (Angra dos Reis 1) and the other from Dr. J. Reynolds at Berkeley (Angra dos Reis 2). The samples were cleaned on the external surfaces by grinding with a dental burr. The chemical methods have been described before (Sanz and Wasserburg 1969) and consist of dissolving the samples in high purity HF and $HClO_4$ acids. All laboratory ware was teflon and all heating and evaporating of solutions were performed in small teflon or teflon-coated steel containers, through which high purity N_2 flowed.

Attempts were made at obtaining internal isochrons for Stannern and Serra de Mage. Stannern was chosen because our measurements in section 3 showed that it had the highest Rb/Sr ratio. However, Stannern is comparatively fine grained and has extensive intergrowth of plagioclase and pyroxene (Duke 1963). A mass of 2.6 g of Stannern was ground to a size less than 150μ and passed through the modified Frantz magnetic separator described in section 7.2.1 . A 98% pure plagioclase separate ($Ca_2Al_2Si_2O_8$) was obtained and analyzed for

Rb and Sr. The remaining bulk sample was ground to a size smaller than 40μ, rinsed in filtered acetone and passed through the Frantz. The best pyroxene (an Fe, Mg silicate) separate obtained (56 mg ~ 60% pyroxene, 40% plagioclase) was used for density separations in methylene iodide (ρ = 3.3 g/cm^3) as described in section 7.2.1C.

During the course of the Guarena study (section 7.3) we used different organic liquids and we varied the length of exposure of the samples to the heavy liquids. We observed only that a small absolute amount of sample was not recovered during the procedure. We did not find any evidence of preferential leaching of Rb or Sr by the use of these liquids.

A 90% pure Stannern pyroxene separate was obtained through the density separation and it was further separated on the Frantz yielding a separate richer than 95% in pyroxene, which was analyzed for Rb and Sr.

Mineral separations were attempted on a 0.3 g piece of Serra de Mage, a eucrite with exceptionally coarse crystal structure (1-2 mm). Plagioclase crystals were hand picked with a pair of stainless steel tweezers and analyzed for Rb and Sr. The meteorite was so friable that it could be broken apart by pressing against it with a sharp stainless steel needle. A mixture of finer grained pyroxene and plagioclase left over from the hand picking was analyzed. A pyroxene separate was obtained by magnetic separations. The data required a 20% Rb blank correction and yielded an unstable Sr run, which caused us to discard this analysis. The $^{87}Sr/^{86}Sr$ in the pyroxene was approximately

only 0.09% enriched over the other Serra de Mage separates. The two Serra de Mage analyses reported can be considered as representative of the "total" meteorite, in particular since it consists of 56% plagioclase (Duke 1963).

4.1.3 Analytical Results

We list in Table 4.1 the complete results obtained on the basaltic achondrites. The results reported in Table 6.4 are afflicted with a transcription error of the Rb concentration in the spike, so that the concentrations of Rb in Table 6.4 are too high by 1.6%. They have been corrected in Table 4.1 . The Sr concentrations have been reduced by 0.55% to conform to the latest spike calibrations at a time slightly after the original samples were analyzed. Such a correction is well within quoted errors and is only made here for consistency in the process of correcting the Rb concentrations reported previously. These corrections result in a composite 1.1% decrease in the $^{87}Rb/^{86}Sr$ for the meteorites reported in section 6. The same (opposite sign) percent change, therefore,applies to the slope and age in Figure 6.3 . The $^{87}Sr/^{86}Sr$ results are not affected by these corrections, neither is the value of $(^{87}Sr/^{86}Sr)_{BABI}$, which of course is the virtue of samples with very low Rb/Sr. The correct data appear in Table 4.1, in a similar format to Table 6.4 .

The analysis for Bereba reported is the average of three relatively unstable runs in which only Category III data were obtained. A conservative error $\delta(^{87}Sr/^{86}Sr)_m = 1.2$ is reported due to this fact.

Moore County is important along with Serra de Mage in defining the $(^{87}Sr/^{86}Sr)_{BABI}$ value. The long term precision of the Lunatic I mass spectrometer is obvious from the Moore County measurements and the results of at least 20 seawater Sr runs repeated regularly and reproducibly over the course of these experiments; Table 4.1 lists the results from sections 5, 6, 7 and from six additional runs. Figure 2 is a histogram of the seawater analyses.

The analysis of Angra dos Reis (1) consisted of three runs. One of the runs exhibited strange source focusing conditions because the sample filament became deformed during the run. The run was discarded although the result with a precision of 0.025% agreed to 0.007% with the results of the other two runs presented. The less stable run presented yielded only Category III data. However, both runs appear consistently low with respect to Moore County. The weighted average $(^{87}Sr/^{86}Sr) = 0.69892 \pm 7$.

The Angra dos Reis (2) sample was spiked with a different set of ^{87}Rb and ^{84}Sr spike solutions completely independently of the first sample. The Sr and Rb concentrations are lower by 25% and 50% respectively than in the Angra dos Reis (1) sample. The data given are for a single excellent quality Sr run ($\sim$ 200 Category I ratios).

The corrected data and the new data are shown in Figure 3 which is the updated version of Figure 6.3 . The errors plotted are estimates based on the best runs for each sample. The total range in $^{87}Sr/^{86}Sr$ is 0.2% . The achondrite data represented in this figure appear to follow the systematics of a set of closed Rb-Sr systems of

of the same initial strontium isotopic composition. The line shown was calculated from a least squares fit according to York (1966) which takes into account errors in both coordinates. In this case the error of 2% assigned to the $^{87}Rb/^{86}Sr$ ratios is negligible and the same fit is obtained by a least squares calculation considering only the the $^{87}Sr/^{86}Sr$ errors. Angra dos Reis (1) and (2) lie distinctly below the remaining data and were not used in calculating the best fit line. We obtain a slope of 0.0642 ± 0.0034 corresponding to an age $4.47 \pm 0.24 \times 10^{9}$ years ($\pm 2\sigma$ deviations) for $\lambda = 1.39 \times 10^{-11}$ yr^{-1}. The initial ratio from the best fit line is (following the notation of section 6) $(^{87}Sr/^{86}Sr)_{BABI} = 0.698983 \mp 0.000032$ in agreement with the value reported in section 6. The relative deviations from the best fit line are still as shown in Figure 6.4 . The Bereba and Serra de Mage (mixture) points lie within 3×10^{-5} of the best fit line; Serra de Mage (plagioclase) lies 3.5×10^{-5} off the line. The three samples lowest in $^{87}Rb/^{86}Sr$ are most important in defining $(^{87}Sr/^{86}Sr)_{BABI}$ and resolving it from $(^{87}Sr/^{86}Sr)_{ADOR}$, the initial ratio for Angra dos Reis.

Angra dos Reis lies clearly <u>below</u> the basaltic achondrite isochron. Angra dos Reis exhibits large fission Xe anomalies attributed to ^{244}Pu decay (Hohenberg 1969). Mueller and Zaehringer (1969) have obtained a U-He gas retention age of $(5.0 \pm 0.3) \times 10^{9}$ years for this meteorite. This result is confused by a K-Ar age obtained by the same authors of less than 2×10^{9} years indicating excessive gas loss or K contamination . These authors note that their sample of Angra

dos Reis appeared weathered even though Angra dos Reis is an observed fall. There is no way of contaminating the Angra dos Reis Sr to obtain our present result since any Sr contamination has a much higher $^{87}Sr/^{86}Sr$. Even if all the Rb in the meteorite represents contamination the ratio obtained is lower than the BABI value. Our samples were clean interior pieces and looked fresh. We may, therefore, assume that Angra dos Reis is $\sim 4.5 \times 10^9$ years old and extrapolate with no propagation of errors to $^{87}Rb/^{86}Sr = 0$. The ratios obtained are $(^{87}Sr/^{86}Sr)_I = 0.69883 \pm 8$ for Angra dos Reis (1) and $(^{87}Sr/^{86}Sr)_I = 0.69884 \pm 5$ for Angra dos Reis (2). We may, therefore, define the initial Sr isotopic composition for Angra dos Reis as $(^{87}Sr/^{86}Sr)_{ADOR} = 0.69884 \pm 4$. This value is listed in Table 4.1 along with $(^{87}Sr/^{86}Sr)_{BABI}$. The two isotopic compositions are distinct and differ by 0.02% .

The analytical results for the Stannern mineral separates are also given in Table 4.1 . This is the first attempt at obtaining an internal isochron for a Ca-rich achondrite. The data are plotted in Figure 4; the relative enrichment in $^{87}Sr/^{86}Sr$ between the pyroxene and the plagioclase is 0.16% . The pyroxene has been corrected for a 6% Rb blank contribution and we have assumed that the blank correction could be anywhere between zero and twice our average blank level. The line drawn is the basaltic achondrite isochron. The plagioclase error (for a single run) barely intersects this isochron. From the "total" meteorite and plagioclase points we calculate $\tau = 4.1 \pm 0.7 \times 10^9$ years (maximum errors) and an initial

$(^{87}Sr/^{86}Sr)_I = 0.69908 \mp 24$. These results are within experimental error of the basaltic achondrite isochron. We believe that Stannern is not resolvable from the basaltic achondrite age or initial ratio.

The modal mineral composition of Stannern is 39% plagioclase, 55% pyroxene and 6% silica and other minor phases (Duke and Silver 1967). Using the total meteorite and plagioclase Sr concentrations we obtain ~ 6.5 ppm (parts per million) Sr in the pyroxene. If we assume that our pyroxene separate contains plagioclase as the only important impurity, 2.5 ppm Sr is contributed by the plagioclase corresponding to 1.2% plagioclase impurity. The corresponding Rb contribution is 0.036 ppm, or only 0.035 ppm Rb exists in the pure meteorite pyroxene along with the 6.5 ppm Sr. These concentrations would yield a pure pyroxene $(^{87}Sr/^{86}Sr) = 0.7000$ for a 4.5×10^9 years age. A contribution of 1.2% plagioclase of $(^{87}Sr/^{86}Sr) = 0.7014$ would yield $(^{87}Sr/^{86}Sr) = 0.7004$ in the analyzed "pyroxene" fraction which is in agreement with the value measured $(^{87}Sr/^{86}Sr)_m = 0.70034$. Therefore, the data obtained for Stannern are consistent and indicate that the best spread in $(^{87}Sr/^{86}Sr)$ obtainable is 0.2% ; we obtained 0.16% spread. The pyroxene Rb concentration of 0.036 ppm Rb is about equal to our average blank estimate and therefore for a 2% blank correction we require ~ 50 mg of 100% pure pyroxene or ~ 25 mg 99% pure. Our sample (99%) weighed 9.5 mg . Conceivably one could repeat the separation with a larger original meteorite mass, however, this would not result in considerable improvement in the determination of the age or initial $^{87}Sr/^{86}Sr$. The Stannern internal

isochron is in good agreement with the basaltic achondrite age of 4.47×10^9 yr. From this we conclude that Stannern remained undisturbed during this time with respect to Rb and Sr. As discussed in section 6.4 Megrue (1966) obtained a K-Ar correlation by measuring K and Ar in "magnetic" and "non-magnetic" separates of Stannern. In view of our experience in separating the plagioclase and pyroxene fractions it is clear that Megrue is observing a dilution effect and that this objection raised by Burnett and Wasserburg (1967a) is justified. In particular the K-Ar age of 4.0×10^9 yr obtained is not better defined than K-Ar ages obtained on total samples and exhibiting some Ar loss.

Duke and Silver (1967) have argued that Moore County and Serra de Mage may belong to a different class than the other eucrites because they are not brecciated and because they show a preferred orientation of plagioclase crystals. These meteorites are also the coarsest observed. From our data there is no evidence for differential evolution of these objects with respect to the other basaltic achondrites.

4.1.4 Discussion

As shown previously (section 6.5, 7.4) initial strontium isotopic compositions are sensitive indicators of differential evolution, if measured precisely, and result in better resolution of time than obtainable from differences of isochron slopes. This high resolution is particularly true if an object is separated and chemically fractionated from a relatively high Rb/Sr parent environment and if it

develops at least one mineral phase with low Rb/Sr. Following the discussion in sections 3.4 and 6.5 we form the differences in initial Sr isotopic composition observed for the basaltic achondrites. The maximum difference from all the achondrite data, excluding Angra dos Reis, is $D(^{87}Sr/^{86}Sr)^{ij}_{max} = 9 \times 10^{-5}$ corresponding to $(\Delta\tau_{ij})_{max} = 9 \times 10^{6}$ years for (Rb/Sr) = 0.25 in a parent environment of Rb/Sr as observed in chondrites. By excluding Nuevo Laredo, $D^{ij}_{max} = 4 \times 10^{-5}$ and $(\Delta\tau_{ij})_{max} = 4 \times 10^{6}$ years; this interval now includes Moore County, Serra de Mage and Bereba. Nuevo Laredo is slightly off the basaltic achondrite isochron and may have formed 7×10^{6} years <u>after</u> the other basaltic achondrites.

Using the higher solar Rb/Sr = 0.65 abundance referred to before we may obtain time limits for the separation of material or objects from the contracting sun. For all the basaltic achondrites we obtain $(\Delta\tau_{ij})_{max} = 3.5 \times 10^{6}$ years (including Nuevo Laredo). The limit is $(\Delta\tau_{ij})_{max} = 1.6 \times 10^{6}$ years for these meteorites excluding Nuevo Laredo. This would represent maximum differential time of separation of these meteorites from the nebula. In principle this separation might occur over a slightly longer time interval if all these meteorites separated in identical although parallel processes. The Angra dos Reis data, to be discussed shortly, for which a measurable effect exists (as opposed to a limit) indicate that identical or parallel processes did not occur at least for this one case. If the basaltic achondrites are representative samples of

several planetary objects, limits of $\sim$ 2×10^6 years would be placed on the time of differential condensation of at least several planetary objects from the solar nebula.

The Angra dos Reis data present an exceedingly interesting discordancy with respect to the basaltic achondrites. The values determined for $(^{87}Sr/^{86}Sr)_{BABI}$ and $(^{87}Sr/^{86}Sr)_{ADOR}$ are well resolved. The difference corresponds to a negative enrichment over the BABI value $\epsilon = -2.0 \pm 0.7$. It is clear that Angra dos Reis formed from more primitive material than the basaltic achondrites. For a chondritic type reservoir Angra dos Reis formed 14×10^6 years before the basaltic achondrites. For the solar reservoir the time interval is 5.4×10^6 years.

Angra dos Reis is a unique meteorite (the only member of its class) which consists of over 90% augite, some olivine and troilite and no plagioclase. Angra dos Reis Xe has been analyzed by Hohenberg (1969). He finds in a stepwise heating experiment gas fractions composed of virtually pure fission Xe. By correcting for the unique spallation Xe in this meteorite which is enriched in the rare earth target elements, he is able to show that the fission component in Angra dos Reis is the same as the one found in Pasamonte (Rowe and Kuroda 1965) which has been attributed to the now extinct fissioning ^{244}Pu, with the short half-life of 82×10^6 years. Angra dos Reis is also exceptionally uranium rich (Mueller and Zaehringer, 1969) and Pu is supposed to follow chemically uranium

or the rare earths so that, since Angra dos Reis formed early enough, ^{244}Pu would have been incorporated in it. The Sr measurements indicating that Angra dos Reis is the most primitive object measured strengthen the hypothesis of in situ ^{244}Pu fission (Wasserburg, Huneke, Burnett 1969) as opposed to the possibility of Angra dos Reis having inherited some fissiogenic Xe during late formation. The amount of fissiogenic ^{136}Xe in Angra dos Reis of 18×10^{-12} ccSTP/g (cubic centimeters at standard temperature and pressure) corresponds to 5×10^{8} atom/g . The fission yield in mass 80 region is less by a factor of ten and the effect on the Sr isotopes is many orders of magnitude less than the effect observed.

From the systematics of rare earth element partition between the mineral phases, Schnetzler and Philpolts (1969) have concluded that Angra dos Reis originated under different conditions than the normal basaltic achondrites, or that there is no direct relationship between Angra dos Reis and the basaltic achondrites. In view of our results this is a distinct possibility. Using similar arguments for Moore County and Serra de Mage they find that these meteorites may have formed by crystal accumulation while some of the other achondrites measured here appear to have formed by direct cooling of a liquid. From our data we cannot make a distinction between Serra de Mage and Moore County and the other basaltic achondrites; however these arguments can hardly be formulated in a precise way.

Ganapathy and Anders (1969) have tried to explain the high U-He gas retention age for Angra dos Reis by considering short lived alpha emitters in the lanthanide region. In particular they calculate

that, if they assume a U-He age as high as 4.7×10^9 years (instead of the measured 5.0×10^9 Yr), the excess ^4He could be produced by ^{146}Sm ($\tau_{\frac{1}{2}} = 1.2 \times 10^8$ yr), if they used the measured abundance of Sm in Angra dos Reis and assumed a 40% initial ^{146}Sm abundance. These authors also note that this abundance for ^{146}Sm is high for a shielded nuclide. Even invoking shorter lived isotopes (e.g., ^{150}Gd and ^{154}Dy; 2 and 1×10^6 yr.) as possibly permitted by the primitive nature of Angra dos Reis cannot account for the excess He.

Angra dos Reis is most probably the product of great chemical differentiation since it has an essentially monomineralic composition. Presumably a much larger body of a more representative composition was formed originally with this very primitive Sr and extremely low average Rb/Sr and Angra dos Reis is the product of further differentiation of this body.

The Angra dos Reis $(^{87}Sr/^{86}Sr)_{ADOR}$ composition is the lowest, most precise value obtained and should therefore be used as the primordial Sr isotopic composition for the solar system instead of $(^{87}Sr/^{86}Sr)_{BABI}$. For example it should be used for calculating intervals similar to the ΔT_{BACH} intervals discussed in sections 6 and 7.

In section 7 we discuss the data obtained on a chondrite, the major meteoritic class. The experimental methods were reviewed here for the basaltic achondrites and in particular similar heavy liquids separations to the ones applied for Stannern were used. Experiments involving different time exposure to heavy liquids as well as different

sets of heavy liquids were reported in section 7.2.1 and 7.3 . No differential leaching of Rb or Sr was observed. The separations were essential in obtaining a Ca-rich mineral phase, specifically whitlockite $[Ca_3(PO_4)_2]$, in which the Rb is expected to be very poor. Since the feldspars are Rb-rich a very good separation of whitlockite from feldspar is important. From the data obtained (Table 7.1) we obtain a very precise internal isochron on a Rb-Sr evolution diagram (Figure 7.2) yielding an age of $4.56 \pm 0.08 \times 10^9$ years and initial composition $(^{87}Sr/^{86}Sr)_I^G = 0.69995 \mp 0.00015$. As pointed out in section 7 this is the first indication of <u>small</u> time differences in the formation or early history of a chondrite. Previous data have been consistent with an initial Sr composition $^{87}Sr/^{86}Sr = 0.699 \pm 0.001$. A detailed discussion of simple models involving evolution of Sr in different reservoirs which can at times become open to Rb and Sr is given in section 7.4 and is illustrated in Figure 7.3 . In particular if the whole meteorite evolved as a closed reservoir for a time $\Delta\tau$ starting with a homogeneous initial Sr isotopic composition equal to $(^{87}Sr/^{86}Sr)_{BABI}$ and if the meteorite became isotopically rehomogenized at the end of this interval, we may determine the interval uniquely. Using the notation of section 6.5

$$\Delta\tau_{BACH} \cong [(^{87}Sr/^{86}Sr)_I - (^{87}Sr/^{86}Sr)_{BABI}] \times [\lambda(^{87}Rb/^{86}Sr)_I]^{-1} \quad (12)$$

Since Guarena is a chondrite $\Delta\tau_{BACH}$ is the same as would be calculated if Guarena were formed at $\Delta\tau_{BACH}$ from a typical chondritic reservoir

which at $\tau = 0$ was characterized by $(^{87}Sr/^{86}Sr)_{BABI}$. We obtain $\Delta\tau_{BACH} = 74 \pm 12 \times 10^6$ yr. for Guarena. Figure 7.5 is an anticorrelation plot of age versus $(^{87}Sr/^{86}Sr)_I$. The precision of data reported by previous authors does not enable us to resolve the different meteorites or classes of meteorites, except possibly for the iron meteorite Weekeroo Station (Wasserburg, Burnett, Frondel 1965; Burnett and Wasserburg 1967b). In Figure 7.4 we show the data for Weekeroo Station (W) and for Guarena (G). From this data, neglecting the error envelopes for simplicity, we cannot form both Guarena and the Weekeroo Station silicate inclusions from a single parent environment simultaneously since the trajectories WW' and GG' do not intersect at some Sr isotopic composition lower than the value obtained for Guarena. We, therefore, require at least a two stage evolution for one of these objects and have drawn the simplest trajectory G'W''W for Weekeroo Station. The differential evolution suggested by these results is made much clearer by the latest measurements on achondrites reported here. We may form the following sequence of separation of material or meteorites from the solar nebula. Angra dos Reis defines the arbitrary zero point. The basaltic achondrites separated within 2×10^6 years of each other, 5×10^6 yr after Angra dos Reis. Nuevo Laredo followed the basaltic achondrites by $\sim 3 \times 10^6$ years and Guarena finally was separated from the reservoir $\sim 27 \times 10^6$ years after Nuevo Laredo (for Guarena we have taken into account the difference between chondritic and solar reservoir Rb/Sr). In view of the fact that these achondrites are extremely Rb-poor the simultaneity observed is most

sensitive to differential times of formation from a Rb-rich reservoir. Any local differentiation in a Rb-poor reservoir is not resolvable. It is, therefore, plausible to assume that the isochronism found for the basaltic achondrites or the approximate isochronism of Angra dos Reis and the basaltic achondrites might include Guarena. Therefore, Guarena may also have separated from the solar reservoir on a shorter time scale than the interval $\Delta\tau_{BACH}$. The $\Delta\tau_{BACH}$ interval thus is related best to a later metamorphic event. This means that the first rather fast separation of planetary objects was followed by at least some measurable live interval in these objects' history.

The most recent results using the ^{129}I - ^{129}Xe decay scheme ($\tau_{\frac{1}{2}} = 17 \times 10^6$ yr) by stepwise heating experiments (Podosek 1969 a) yield relative formation times within the narrow range of 15×10^6 yrs. Within this range meteorites can be resolved in time; for several meteorites time differences between parts of the same meteorite are obtained. The intervals measured by the ^{129}I method refer to relative times when Xe started being retained in these meteorites. Experiments by Hohenberg and Reynolds (1969) show that the ^{129}I intervals are defined even if partial loss of Xe has occurred. The relationship between the Xe retention record and the conditions under which Rb-Sr systems are not disturbed is not clear at the present. No direct comparison of the two methods exists yet due to non-overlapping samples. Both methods appear to define similar intervals for the formation of objects and during the same small total time period. No correlation between the classification schemes of meteorites and these

time differences is clear at the present. Detailed time information about the early history of the solar system may result in the better understanding of the processes of formation of the solar system.

From nuclear chronologies (Wasserburg, Schramm and Huneke 1969) a free decay interval of 1-2 x 10^8 years is required between cessation of nucleosynthesis and formation of planetary objects. From the ^{129}I and Rb-Sr data, planetary objects may have formed only during a small part of this interval due to some local instability or turbulence.

A more direct link to the end of nucleosynthesis than ^{129}I is provided by ^{244}Pu fission effects in meteorites. The status of ^{244}Pu formation intervals is not well defined at present due to the lack of knowledge of the ^{244}Pu fission spectrum, the possibility of fractionation between Pu and U and the uncertainty in the corrections that have to be applied to the heavier Xe isotopes in order to determine the fission component. In some meteorites there are clear excesses of both radiogenic ^{129}Xe and fissiogenic ^{136}Xe (Reynolds 1968) although no correlation can be seen at present between the two components. Juvinas and Moore County belong to this group of meteorites.

In section 6 we obtained a ΔT_{BACH} interval for St Severin from rather imprecise preliminary data, corresponding to 320 $\pm$ 160 m.y. Wasserburg, Huneke and Burnett (1969) have obtained an interval of 380 m.y. for the difference between retention of Xe and retention of fission tracks in St Severin whitlockite. The importance of the coincidence of the two intervals is obscured as yet by the fact that preliminary Rb-Sr data on St Severin have not yielded a well

defined isochron and also by the fact that we have insufficient knowledge of the conditions for Xe or track retention in minerals.

From the data on Guarena we obtain an interval of 74 million years for a metamorphic event. From the measurements of fission Xe in the St Severin whitlockite mentioned above these authors calculated a ($^{244}Pu/^{238}U$) = 1/30 at the time when the whitlockite first began to retain fission Xe. As these authors point out, if Pu was not enriched with respect to U during the formation of the whitlockite, this is a lower limit to the $^{244}Pu/^{138}U$ ratio at the time of formation of the solar system. The question of fractionation of Pu and U must remain open since in a recent study on St Severin (Podosek 1969b) a lower $^{244}Pu/^{238}U$ was obtained. In view of the Guarena data if other meteorites and in particular St Severin were affected by a similar metamorphic event at $\sim 75 \times 10^6$ years after their formation, and if such an event resulted in complete Xe loss, then the $^{244}Pu/^{238}U$ ratio at the <u>formation</u> of St Severin should be higher than observed by about a factor of two since ^{244}Pu has an 82×10^6 year half-life. Similarly the $^{129}I/^{127}I$ at the formation of St Severin, or a similar meteorite would be higher than observed by a factor of nine. The importance of the values for these ratios has been discussed by Wasserburg, Schramm, and Huneke (1969); for a ratio $^{244}Pu/^{238}U \geq 1/15$ these authors find that there exists no solution to the coupled equations for the relative abundances of $^{235}U/^{238}U$, $^{232}Th/^{238}U$, $^{129}I/^{127}I$ and $^{244}Pu/^{238}U$.

4.2 Lunar Samples

4.2.1 Sampling

We now present the first measurements on lunar samples returned by the crew of Apollo XI. It became obvious from the Lunar Sample Preliminary Examination Team report (PET Report, Science, 1969) that moon samples exhibit very low Rb/Sr and that, therefore, Sr measurements of the precision reported here would be necessary to resolve the history of these rocks. Typical Sr concentrations are 150 - 300 x 10^{-6} g Sr/g sample (ppm) and 1 - 6 ppm Rb which possibly over 4.5 x 10^{9} years would change $^{87}Sr/^{86}Sr$ from $\sim$ .699 to $\sim$ .705 or by 0.8% .

The PET report divided the returned samples in four groups: (1) type A, fine grained vesicular crystalline igneous rock; (2) type B, medium grained vuggy crystalline igneous rock; (3) type C, breccia; (4) type D, fines. The term "rock" refers to fragments larger than 1 cm, and fines refers to fragments smaller than 1 cm. We have analyzed fragments from the fines, and type A and B crystalline rocks.

On several of the rocks minimal or major mineral separations have been undertaken in an effort to establish an internal isochron for each rock. Samples from the fines were analyzed because this sample contains the greatest variety of small fragments similar to the larger rocks returned. A minimal description is given for the samples analyzed. Samples are denoted by numbers. The generic notation for the fines is 10085. Rock sample numbers run from 10002 to 10075 where only the last two digits vary. Additional decimal notation is used for

samples from the same rock. Except where confusion might arise we will denote samples only by their last two digits.

The samples were picked up at the Lunar Receiving Lab in standard polyethelene containers. All handling during the present investigations was done in a special isolated clean room with independent filtered air supply. This room was not previously used for other samples. Clean room procedures were used throughout the sampling, chemical separations and loading of filaments.

Several coarse pieces from the fines were sampled after the fine dust was blown off with a "squeeze" bottle. In particular plagioclase and pyroxene crystals were hand picked from one such coarse piece (10085, 1.11). Rocks 17, 44, 57, 69 and 71 have been sampled and "total" rock data are presented here. Furthermore, data for separated minerals of rocks 17 and 44 are presented. The following is a short description of the samples as they appear in Table 4.2. The sequential numbering of samples corresponds to that of Table 4.2 .

The fines sample as defined before was split into two fractions the coarse-fines (size greater than 1 mm, generic number 10085) and the fine-fines (size less than 1 mm, generic number 10084) .

1) Sample 10085,1 consisted of material obtained from the coarse-fines and was composed mainly of lithic fragments.

2) Sample 10084,12 was obtained from the fine-fines by sieving; the -420 μ size was used and consisted mainly of lithic fragments.

3) Sample 10085,1.9 was a small rock fragment consisting of plagioclase, pyroxene and ilmenite crystals.

4) Sample 10085,1.11 was a coarse grained rock about 50% plagioclase. The sample was crushed gently and plagioclase and pyroxene crystals were hand picked using a needle wetted with an appropriate agent(cf. Section 7.2.1). The crystals were rinsed with acetone. A rock fragment was picked out with tweezers and represents the "total" analysis reported in Table 4.2

5) Sample 10085,1.28 consisted of a small glass fragment, relatively transparent. A deep brown-red color was confirmed after crushing gently.

6) Sample 10017,32 is a type B crystalline rock.The exterior surface was defined by the existence of zap-pits. Interior pieces with no zap craters were used for "total" rock analyses. Part of the rock was crushed and a plagioclase separate was hand-picked and analyzed for Rb and Sr. The sample (0.6g) was further crushed in a roller, sized, and then separated on the Franz. The best pyroxene separate from the Franz ($\sim$ 60% pyroxene) was used for density separations in methylene iodide. The final sample was estimated at 90% purity and was analyzed. An ilmenite rich fraction from the Frantz was used for density separations in methylene iodide and the final ilmenite ($\sim$ 90% ilmenite + inclusions) was analyzed.

7) Sample 10044,30 consisted ofavery friable coarse grained crystalline rock. An interior piece was analyzed as the "total" rock. From electron microprobe studies an SiO_2 fine grained polymorph

(identified as cristobalite) was found to include potassium rich phases. Cristobalite grains were handpicked and analyzed for Rb and Sr. The pyroxene fraction was obtained by magnetic and density separations.

8) Sample 10057,39 is a type A fine grained vesicular crystalline rock, somewhat coarser than rock 17. There was no evidence in the sample of zap craters. A small fragment was analyzed for Rb and Sr.

9) Sample 10069,26 is a fine grained vuggy rock. A fragment was inspected for craters or shocked feldspar crystals. None were found, indicating an interior piece. Rb-Sr analysis was done on part of the fragment.

10) Sample 10071 is a fine grained rock with comparatively few vessicles. It appeared similar to the other fine grained rocks previously analyzed. A fragment was analyzed for Rb and Sr.

4.2.2 Analytical Results

All samples were analyzed for Rb-Sr following the procedure described before. All Sr runs were performed on the Lunatic I and followed the standard procedure established for the basaltic achondrites. Rb runs were performed on a different mass spectrometer. Runs of seawater Sr, Moore County and Angra dos Reis were interspersed between the lunar sample runs. The results for these runs were listed in Table 4.1 and show excellent agreement over the time of these and the previous experiments. A total sample of Olivenza, a chondrite analyzed extensively in this lab (Sanz and Wasserburg 1969), was also analyzed as a standard and the results are listed in Table 2 and agree

very well with the published data of these authors. The Olivenza sample has a very high Rb/Sr ratio compared to the lunar samples.

The analytical results are presented in Table 4.2 . The weight of the samples analyzed is given. Runs yielding Category I and II data were obtained except as discussed below. Sample 84,12 yielded only 40 ratios of Category I. Samples 85,1.11 yielded unstable runs during which Category III data were obtained. Sample 85,1.11 (pyroxene) was comparatively low in Sr and yielded a completely unstable run. Category III data were obtained for sample 17,32 (ilmenite) and for Olivenza. However, these samples are relatively high in $^{87}Rb/^{86}Sr$ and therefore the Rb errors dominate any Sr errors. Excellent runs were obtained for the other samples including all the "total" rock runs.

Figure 5 shows all the data reported here except the highest point for rock 17 (ilmenite) . The basaltic achondrite isochron is shown for comparison. The 85,1.11 "total rock" and "plagioclase" data appear to be higher than the achondrite line suggesting differential Sr evolution. The two fines samples (85,1 and 84,12) lie on the 4.5×10^9 isochron [originating at $(^{87}Sr/^{86}Sr)_{BABI}$] well within experimental error. The glass sample (85,1.28) is anomalous and would give an "age" higher than 5×10^9 years if the $(^{87}Sr/^{86}Sr)_{BABI}$ value was used as initial ratio. This sample has obviously been disturbed. Data for the total rocks 69, 57, and 71 cluster very close to the total rock sample 17. All these points lie distinctly below an isochron of 4.5×10^9 years. The three 17 points shown in Figure 5

define an excellent straight line which has a slope corresponding to an age $3.54 \pm 0.08 \times 10^9$ yr. (best fit three low points only) and an initial ratio $(^{87}Sr/^{86}Sr)_I^{17} = 0.69935 \mp 8$. These values are completely different from the data obtained on the basaltic achondrites or any meteorites (always setting aside the Kodaikanal age of 3.8×10^9 yr.; Burnett and Wasserburg 1967a) . Figure 6 presents only the data on rock 17 including the ilmenite point. It is clear that the data define a linear array and that therefore we may assume that rock 17 has followed the simple Rb-Sr systematics of a closed system with a homogeneous initial Sr composition. A best fit line taking into account errors in both coordinates yields a slope of 0.0512 ± 0.0011 corresponding to an age $\tau = 3.59 \pm 0.08 \times 10^9$ years. The initial Sr composition defined is $(^{87}Sr/^{86}Sr)_I^{17} = 0.69933 \mp 7$. These parameters are in close agreement with the ones presented for only the three lowest points. It is evident that rock 17 was formed at $3.59 \pm 0.08 \times 10^9$ years ago and has not been disturbed since, as far as Rb and Sr are concerned. The data on rock 44 are presented in Figure 7. The points do not define as perfect a linear array as the data for rock 17. A best fit line through these points yields a slope corresponding to an age $\tau = 3.54 \pm 0.38 \times 10^9$ years and an initial ratio $(^{87}Sr/^{86}Sr)_I^{44} = 0.69921 \mp 25$. The cristobalite phase (including the K-rich phases) is only a minor mineral and it is possible that it has been disturbed slightly by an event which did not disturb the major phases. In the case of rock 17 the ilmenite, although a minor phase, does not show any sign of having been

disturbed. It is tempting to consider a line through the 44(total) and 44(pyroxene) data which lie directly on the basaltic achondrite line, thereby obtaining an age of 4.5×10^9 years. Such an age would be incompatible with the cristobalite unless this phase has been disturbed. We shall assume that the latter is not true.

Although the precision for sample 85,1.11 (pyroxene) is bad, a line through the separates corresponds more easily to a 3.5×10^9 yr. isochron than the 4.5×10^9 isochron (Figure 5).

From the data of Olivenza (Table 2) we calculate an age $4.57 \pm 0.10 \times 10^9$ years using the initial ratio $(^{87}Sr/^{86}Sr)_I = 0.6994$ determined by Sanz and Wasserburg (1969). The age these authors obtained was 4.63×10^9 years. Due to the high Rb/Sr in this meteoritic sample any systematic errors in Rb or Sr concentrations measured would have been glaring. Our standard seawater and achondritic runs on the other hand determine our precision in measuring $^{87}Sr/^{86}Sr$.

4.2.3 Discussion

It was noted that all rocks are rather fine grained and similar except rock 44 which is coarse. All fine grained rocks analyzed are very similar in $^{87}Sr/^{86}Sr$ composition and in Rb and Sr concentrations and plot within an extremely small region on a Rb-Sr evolution diagram (Figure 5) . In particular rocks 57 and 71 are overlapping on this graph. The implication is, therefore, that all fine grained rocks are approximately 3.6×10^9 years old and they were formed from a common

reservoir, resulting in rather uniform composition in Rb and Sr. These rocks might actually be fragments of one larger original rock. This tentative conclusion will await further measurements on separated phases of these rocks. The age of rock 17 appears established beyond any doubt.

The age of the moon has been estimated by various circumstantial bits of information. From the data presented here it appears that, if the moon is $\sim 4.5 \times 10^9$ yrs. old, its surface and interior have been affected by rather large scale processes at least until 3.6×10^9 years ago. The nature of these processes cannot be deduced from the data presented here. If we assume that rock 44 is $\sim 3.5 \times 10^9$ years and that 17 and 44 were formed during the same event, this event may have been a meteorite impact which resulted in a melted silicate pool. Rock 44 exhibiting coarser grain structure may have cooled slower, or been deeper than the other rocks. However, at least a second event is needed to bring these rocks on the surface of the moon due to their low radiation ages (PET report). A definition of the initial Sr of rock 44 and of the other rocks may result in a better indication of whether these rocks were created in a single event. Volcanic activity may also result in differences in initial Sr isotopic composition since it does not guarantee isotopic homogeneity. Samples of several terrestrial volcanic rocks obtained from close locations yielded different ($^{87}Sr/^{86}Sr$) ratios indicating that they were not produced from a single homogeneous mantle reservoir (Gast, Tilton and Hedge 1964 ; Lessing and Catanzaro 1964).

By using the $(^{87}Sr/^{86}Sr)_{BABI}$ value and the total rock 17 sample a highest age of 3.8×10^9 years is obtained. Clearly if the parent material of rock 17 is $\sim 4.5 \times 10^9$ years, rock 17 does not represent an unfractionated sample of this parent reservoir. Similarly the glass sample 85,1.28 is a clear case of either Rb loss or Sr acquisition since it gives an apparently high age. The lunar dust (both fine samples) appear to lie on the 4.5×10^9 year isochron originating at $(^{87}Sr/^{86}Sr)_{BABI}$ (this age would be 4% larger, or 4.75×10^9 years if the $(^{87}Sr/^{86}Sr)_{ADOR}$ value were used). This is most probably not an accident. It may mean that the area of the Apollo XI (Mare Tranquillitatis) landing is 4.5×10^9yr with a few extraneous rocks of 3.6×10^9 years but otherwise undisturbed; or this area has been reworked but the lunar dust is a very good average of the original lunar surface, and represents a large enough reservoir so as to have stayed closed to Rb-Sr despite the catastrophic events indicated by the ages of the rocks measured. The relative enrichment of $(^{87}Sr/^{86}Sr)_I^{17} = 0.69933 \pm 7$ with respect to $(^{87}Sr/^{86}Sr)_{BABI}$ is $\epsilon = 5$ (in parts in 10^4). To obtain $\epsilon = 5$ in $\sim 9 \times 10^8$ years (assuming that the moon is 4.5×10^9 years old) we need a parent reservoir of Rb/Sr = 0.01 or $^{87}Rb/^{86}Sr = 0.029$. This is about 40% lower than the values obtained for the fine soil samples. Although the lunar fines may be a good sample of the original reservoir it is not obvious that the measured sample need also be a good representative.

In Figure 8 we show an age-($^{87}Sr/^{86}Sr$) diagram for Sr evolution. This type diagram was discussed in section 3 and also extensively in section 7.4; different cases are shown in Figure 7.3 . In Figure 8 we show the data for lunar rock 17 and 44 and the meteorite Guarena. The extrapolation of Guarena yields almost a vertical line due to the very high Rb/Sr in this body in comparison to the low values obtained for lunar samples. From each of the two lunar rocks we extrapolate by using the average $(Rb/Sr)^f$ in the fines (samples 85,1 and 84,12) and also by using the (Rb/Sr) in each rock. We show the limits $(^{87}Sr/^{86}Sr)_{BABI}$ and $(^{87}Sr/^{86}Sr)_{ADOR}$. We now want to discuss the evolution of terrestrial Rb-Sr in view of the suggestion that the moon may have formed by a fission of the earth at $\sim 3.5 \times 10^9$ years ago (see for example O'Keefe 1969). We will show the data presented is not compatible with this theory. On the earth Rb has been enriched in the crust with respect to the mantle. If we obtain samples from the mantle we may determine the Rb/Sr in this reservoir which is the most probable parent reservoir for forming the moon by fission. We essentially obtain samples of the mantle today when we look at very young oceanic volcanic rocks. In these rocks the $^{87}Sr/^{86}Sr$ measured abundance is as low as 0.702 (Tatsumoto, Hedge and Engel 1965). This is the lowest $^{87}Sr/^{86}Sr$ which may be representative of the earth's upper mantle today. If $^{87}Sr/^{86}Sr$ in the upper mantle is higher the argument which follows is strengthened. If we assume that the earth was formed 4.6×10^9 years ago with an initial composition equal to either $(^{87}Sr/^{86}Sr)_{BABI}$ or $(^{87}Sr/^{86}Sr)_{ADOR}$ and

that the ratio observed in these young rocks is due to the decay of Rb in the mantle we obtain the evolution lines BABI-Earth and ADOR-Earth for the mantle Sr shown in Figure 8. It is clear that the initial Sr composition in rocks 17 and 44 is lower than the mantle isotopic composition at 3.6×10^9 years ago. Therefore we can not form rocks 17 and 44 from the earth 3.6×10^9 years ago as might be thought from the casual coincidence of the age obtained for 17 and 44. If any matter from the earth's crust were to be transferred to the moon during a fission event at 3.6×10^9 years it would make such a process even more unlikely since the crust has a higher Rb/Sr abundance than the mantle.

We now want to find if the lunar rocks and the earth could have formed from a single reservoir before the magic date of 3.6×10^9 years ago. The $(Rb/Sr)^{17}$ line through rock 17 intersects the earth evolution lines above $(^{87}Sr/^{86}Sr)_I^{17}$ so that as explained in section 7.4 there is no $(^{87}Sr/^{86}Sr)$ from which both 17 and the earth could have fractionated. For that matter the $(Rb/Sr)^{17}$ line would not intersect any trajectory, e.g., the Guarena trajectory, at a $^{87}Sr/^{86}Sr$ value close to either $(^{87}Sr/^{86}Sr)_{BABI}$ or $(^{87}Sr/^{86}Sr)_{ADOR}$. This is clear indication that rock 17 has been fractionated at 3.6×10^9 yrs. If we assume that rock 17 was fractionated from the lunar dust (e.g., was formed by melting of the dust) we may follow the evolution of 17 before 3.6×10^9 years along the $(Rb/Sr)^f$ line drawn for the average measured Rb/Sr in the fines. This line intersects $(^{87}Sr/^{86}Sr)_{BABI}$ at 4.06 b.y. and $(^{87}Sr/^{86}Sr)_{ADOR}$ at 4.3 b.y. We may conclude

therefore that either the measured Rb/Sr in the dust is not representative of the average moon soil or that the dust fractionated between 4.1 and 4.3 b.y. Since the dust appears to yield an age of 4.5×10^9 years it is possible that the dust has not fractionated later than 4.5×10^9 years. The value $(^{87}Rb/^{86}Sr)^f = 0.029$ is needed to form rock 17 with only one stage intervening between 4.6 and 3.6 billion years. This may represent the average $^{87}Rb/^{86}Sr$ value for the moon. Since the measured fine soil samples yield 40% higher $^{87}Rb/^{86}Sr$ values this may be an indication that the moon was differentiated and that the lunar "crust" became enriched in Rb in a similar way that the earth's crust is enriched in Rb over the earth's upper mantle. The alternate explanation is that either rock 17 has developed through a multistage process starting in a very low Rb/Sr lunar environment or that the fines samples measured are not a good average for the lunar surficial reservoir from which rock 17 may have formed. It is clear that a multistage evolution is indicated for either the lunar rocks or the lunar dust or the whole moon itself. The nature of the processes involved is not clear at present although it appears that these processes occurred on the moon itself and not for example on the earth prior to a fission event.

From the well defined initial $(^{87}Sr/^{86}Sr)_I^{17} = 0.69933$ we obtained a relative enrichment $\epsilon_{BABI} = 5$ or $\epsilon_{ADOR} = 7$. Some of this enrichment certainly occurred by processes on the moon; if we assume that all this enrichment occurred during a direct assembly of the lunar material from the solar nebula with a lunar Rb/Sr $\simeq 0$ we obtain an interval

$\tau = 15 \times 10^6$ (BABI) or 19×10^6 (ADOR) years for the maximum differential time interval between the formation of the moon and the basaltic achondrites (if the moon separated from this reservoir after the achondrites) .

From Figure 8, the $(Rb/Sr)^f$ lines from rocks 17 and 44 would intersect the Guarena extrapolated line at $(^{87}Sr/^{86}Sr) \approx 0.6985$. This would allow the lunar material to be very primitive and the possibility then exists that the Earth actually formed from this primitive lunar material or from accretion of many such primitive moons.

These data clearly indicate that the moon is $\sim 4.5 \times 10^9$ years old and that differentiation processes either of volcanic or impact origin have occured extensively on the moon at least for 10^9 years after its formation.

4.3 Conclusion

We have shown that precise Sr isotopic measurements yield evidence of differential time evolution of planetary bodies very early in the history of the solar system. We have been able to establish the very short intervals (5×10^6 years) over which direct formation of objects may have occurred. From the results on Guarena and on the lunar rocks it appears that differentiation processes occur for longer periods of time (10^8 - 10^9 years) than were previously considered. This form of detailed history of processes on different objects may result in a better understanding of the formation of the solar system. In view of the similar structure of the lunar and Martian surfaces, and

the observation that the Martian surface appears to have been more active (Leighton et al 1969), Mars most probably has been subjected to reasonably lengthy local differentiation processes, so that only partially fossil-type planets may exist at the present in our solar system. The processes which can be studied on these planets may be simpler than those occuring on the Earth and may clarify early terrestrial evolution (e.g., fractionation of the crust and the mantle) .

References

Aldrich, L.T., Wetherill, G.W., Tilton, G.R. and Davis, G.L. 1956, Phys. Rev., 103, 1045.

Bogard, D.D., Burnett, D.S., Eberhardt, P. and Wasserburg, G.J. 1967, Earth Planet. Sci. Letters, 3, 179.

Burnett, D.S. and Wasserburg, G.J. 1967a, Earth Planet. Sci. Letters, 2, 137.

Burnett, D.S. and Wasserburg, G.J. 1967b, Earth Planet. Sci. Letters, 2, 397.

Duke, M.B. 1963, Thesis, California Institute of Technology

Duke, M.B. and Silver, L.T. 1967, Geochim. Cosmochim Acta, 31, 1637.

Eugster, O., Tera, F. and Wasserburg, G.J. 1969 , J. Geophys. Res. 74 , 3897.

Eugster, O., Tera, F., Burnett, D.S. and Wasserburg, G.J. 1969, submitted to Earth Planet. Sci. Letters.

Flynn, K.F. and Glendenin, L.E. 1959, Phys. Rev., 116, 744.

Ganapathy, R. and Anders, E. 1969, Geochim. Cosmochim. Acta, 33, 775.

Gast, P.W. 1962, Geochim. Cosmochim. Acta, 26, 927.

Gast, P.W., Tilton, G.R. and Hedge C. 1964, Science,145, 1181.

Hohenberg, C.M. 1969a, Geochim. Cosmochim. Acta (in press).

Hohenberg, C.M. and Reynolds, J.H. 1969, submitted to J. Geophys Res.

Lambert, D.L. and Warner 1968, Mon. Not. Roy. Astr. Soc. 140, 197.

Lambert, D.L. and Mallia, E.A. 1968a, ibid, p. 13.

Leighton, R.B., Horowitz, N.H., Murray, B.C., Sharp, R.P., Herriman. A.H., Young, A.T., Smith, B.A., Davies, M.E., Leavy, C.B. 1969 Science 166, 49.

Lessing, P. and Catanzaro, E.P. 1964, J. Geophys. Res. 69, 1599.

Megrue, G.H. 1966, J. Geophys. Res. 71, 4021.

Mueller, H.W. and Zaehringer, J. 1969 in Meteorite Research, p. 845, D. Reidel, Dordrecht.

Nier, A.O. 1950, Phys. Rev. 79, 450.

O'Keefe, J.A. 1969, J. Geophys. Res. 74, 2758.

Podosek, F.A. 1969a, submitted to Geochim. Cosmochim, Acta.

Podosek, F.A. 1969b, submitted to Earth Planet. Sci. Letters.

Preliminary Examination Team Report, 1969, Science 165, 1211.

Reynolds, J.H. 1968, Nature 218, 1024.

Rowe, M.W. and Kuroda, P.K. 1965, J. Geophys. Res. 70, 709.

Sabu, D.D. and Kuroda, P.K. 1967 Nature 216, 442.

Sanz, H.G. and Wasserburg, G.J. 1969, Earth Planet. Sci. Letters 6, 335.

Schnetzler, C.C. and Philpotts, J.A. 1969 in Meteorite Research, Millman Ed., p. 206, D. Reidel Dordrecht.

Schumacher, E. 1956, Z. Naturf. 11a, 206.

Shields, P.M., Pinson, W.H.Jr and Hurley, P.M. 1966, J. Geophys. Res. 71, 2163.

Shields, W.R., Garner, E.L., Hedge, C.E. and Goldich, S.S. 1963, J. Geophys. Res. 68, 2331.

Shima, M. and Honda, M. 1967, Earth Planet. Sci. Letters 2, 337.

Tatsumoto, M. Hedge, C.E. and Engel, A.E.J. 1965 Science 150, 886.

Van Schmus, W.R. and Wood, J.A. 1967, Geochim. Cosmochim. Acta 31, 747.

Wasserburg, G.J., Burnett, D.S. and Frondel, C. 1965, Science 150, 1814.

Wasserburg, G.J., Huneke, J.C. and Burnett, D.S. 1969 Phys. Rev. Letters 22, 1198; J. Geophys. Res. 74, 1969, p. 4221.

Wasserburg, G.J., Schramm, D.N. and Huneke,J.C. 1969, Ap. J. 157, L91.

Wasserburg, G.J.,Steiger, R.H. 1967, in Radioactive Dating and Methods of Low Level Counting, p.331,Int. Atom. Energy Agency, Vienna.

Wasserburg, G. J. 1966, in Advances in Earth Science, P. M. Hurley ed., M.I.T. press, p. 431.

York, D. 1966, Can. J. Phys. 44, 1079.

TABLE 1

Analytical Results of Basaltic Achondrites

Meteorite	Rb 10^{-8} m/g	^{88}Sr 10^{-8} m/g	$^{87}Rb/^{86}Sr$ x 10^{2}	$^{87}Sr/^{86}Sr$ (a)	$(^{87}Sr/^{86}Sr)_I$ (b) (c)
Juvinas	0.199	72.8	0.636	0.69938 ± 4 (d)	0.69897 ± 6
Pasamonte	0.238	73.1	0.760	0.69948 ± 16 (d)	0.69899 ± 18
Sioux County	0.224	68.0	0.767	0.69949 ± 6 (d)	0.69900 ± 8
Nuevo Laredo	0.374	71.7	1.214	0.69984 ± 8 (d)	0.69906 ± 12
Jonzac	0.510	72.0	1.653	0.70006 ± 8 (d)	0.69899 ± 14
Stannern					
1) "total met"	0.813	80.1	2.37	0.70048 ± 6 (d)	0.69895 ± 14
2) plagioclase	3.60	209.6	4.00	0.70144 ± 11	
3) pyroxene	0.081 (e)	9.16	2.1	0.70034 ± 12	
Serra de Mage					
1) "mixture"	0.034 (e)	23.0	0.35	0.69918 ± 6	0.69895 ± 7
2) plagioclase	0.084 (e)	132.3	0.15	0.69912 ± 5	

Table 1 (continued)

Bereba	0.211	69.4	0.701	0.69944 ± 12	0.69899 ± 14
Moore County	0.060	60.7	0.232	0.69914 ± 10 (d)	
				0.69911 ± 4 (f)	0.69896 ± 5
				0.69908 ± 5	
Angra dos Reis 1	0.097	156.8	0.145	0.69890 ± 8	0.69881 ± 9
				0.69895 ± 13	0.69886 ± 14
Angra dos Reis 2	0.044	125.4	0.082	0.69889 ± 4	0.69884 ± 5
				$(^{87}Sr/^{86}Sr)_{BABI}$ = 0.69898 ± 3	
				$(^{87}Sr/^{86}Sr)_{ADOR}$ = 0.69884 ± 4 (g)	
Seawater				0.70912 ± 9 (h)	
				0.70908 ± 8 (d)	
				0.70911 ± 5 (f)	
				0.70910 ± 5 (i)	

(a) Errors correspond to last digits; absolute error from all runs.

(b) Initial $(^{87}Sr/^{86}Sr)$ calculated for $T = 4.5 \times 10^{9}$ yr. and $\lambda = 1.39 \times 10^{-11}$ yr.$^{-1}$.

(c) Error includes contribution from $\delta T = 2.25 \times 10^{8}$ yr. uncertainty.

Table 1 (continued)

(d) From Section 5.

(e) Corrected for 6% blank contribution.

(f) From Section 6.

(g) Calculated from Angra dos Reis only.

(h) From Section 4.

(i) Present work; average of 6 runs for which the total spread of the means of individual runs $\epsilon = \pm 0.00005$

TABLE 2

Analytical Results of Apollo XI Lunar Samples

Sample Number	Text Reference	Weight mg	Rb 10^{-8}m/g (a)	^{88}Sr 10^{-8}m/g (a)	$^{87}Rb/^{86}Sr$ x 10^2	$^{87}Sr/^{86}Sr$ (b)
10085,1	1	8.9	3.47	152.0	5.32	0.70235 ± 7
10084,12	2	74.	3.07	153.4	4.67	0.70206 ±12
10085,1.9	3	2.0	0.803	122.9	1.52	0.70007 ± 9
10085,1.11	4					
i) total		7.6	0.845	254.0	0.776	0.69962 ±13
ii) plagioclase		0.9	1.76	589.4	0.696	0.69954 ±16
iii) pyroxene		2.9	0.51	41.3	2.86	0.70055 ±45
10085,1.28	5	5.0	2.94	146.9	4.67	0.70250 ± 6
10017,32	6					
i) total		7.0	5.89	146.6	9.37	0.70409 ± 8
ii) plagioclase		2.9	1.47	327.5	1.05	0.69991 ± 8
iii) pyroxene		5.1	0.927	79.15	2.73	0.70070 ± 7

TABLE 2 (continued)

iv) ilmenite		12.2	9.13	70.0	30.4	0.71500 ± 17
10044,30.A	7					
i) total		5.9	0.716	170.0	0.982	0.69962 ±12
ii) cristobalite		1.0	5.41	200.9	6.29	0.70236 ± 5
iii) pyroxene		4.7	0.32	29.0	2.59	0.70060 ± 10
10057,39.2	8					
i) total		7.3	7.36	167.4	10.25	0.70469 ± 5
10069,26,G	9					
i)		7.1	6.40	164.8	9.06	0.70404 ± 7
10071	10					
i)		13.1	6.81	155.0	10.24	0.70462 ± 5
Olivenza (c)		12.4	3.04	9.29	76.3	0.74940 ±20

Table 2 (continued)

(a) Rb concentrations are calculated for $^{85}Rb/^{87}Rb = 2.591$; Sr concentrations calculated by assuming normal isotopic abundances $^{86}Sr/^{88}Sr = 0.1194$ and $^{84}Sr/^{88}Sr = 0.006748$.

(b) Errors correspond to the last figures given.

(c) Chondritic meteorite sample; for results of Moore County and Seawater Sr see Table 1 and Figure 2.

Figure 1. Rb-Sr evolution diagram. System S and subsystems A, B, C originate at τ_0 isotopically homogeneous. They evolve undisturbed until τ_1 when they are instantaneously rehomogenized. The new subsystem A', B', C' continue to evolve undisturbed. Total system S remains closed throughout and evolves without discontinuity.

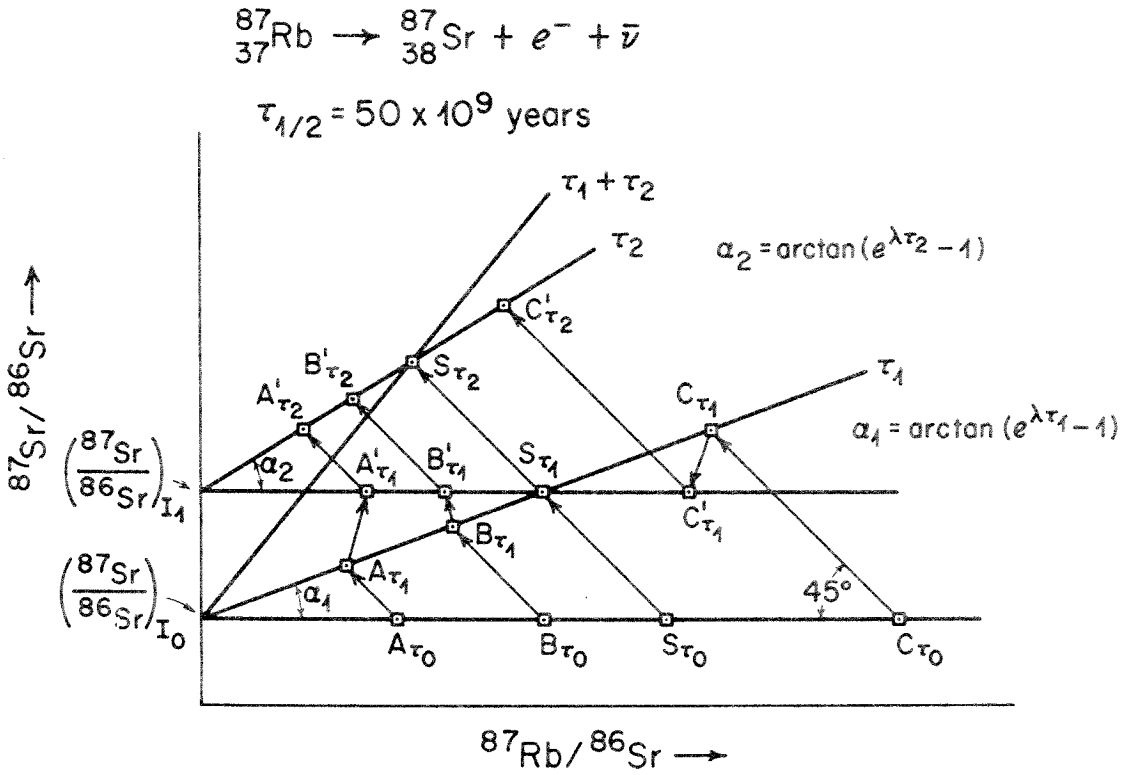
$^{87}_{37}Rb \rightarrow {}^{87}_{38}Sr + e^- + \bar{\nu}$
$\tau_{1/2} = 50 \times 10^9$ years
$\tau_1 + \tau_2$
τ_2
$\alpha_2 = \arctan(e^{\lambda\tau_2} - 1)$
C'_{τ_2}
B'_{τ_2}
S_{τ_2}
A'_{τ_2}
τ_1
C_{τ_1}
$\alpha_1 = \arctan(e^{\lambda\tau_1} - 1)$
$\left(\frac{^{87}Sr}{^{86}Sr}\right)_{I_1}$
α_2
A'_{τ_1}
B'_{τ_1}
S_{τ_1}
C'_{τ_1}
B_{τ_1}
$\left(\frac{^{87}Sr}{^{86}Sr}\right)_{I_0}$
A_{τ_1}
α_1
45°
A_{τ_0}
B_{τ_0}
S_{τ_0}
C_{τ_0}
$^{87}Sr/^{86}Sr \rightarrow$
$^{87}Rb/^{86}Sr \rightarrow$

FIGURE 1

Figure 2. Histogram of seawater strontium runs. Distance corresponding to absolute error of $\pm$ 0.00005 is shown; almost all runs lie within this range and only one run is well outside this range.

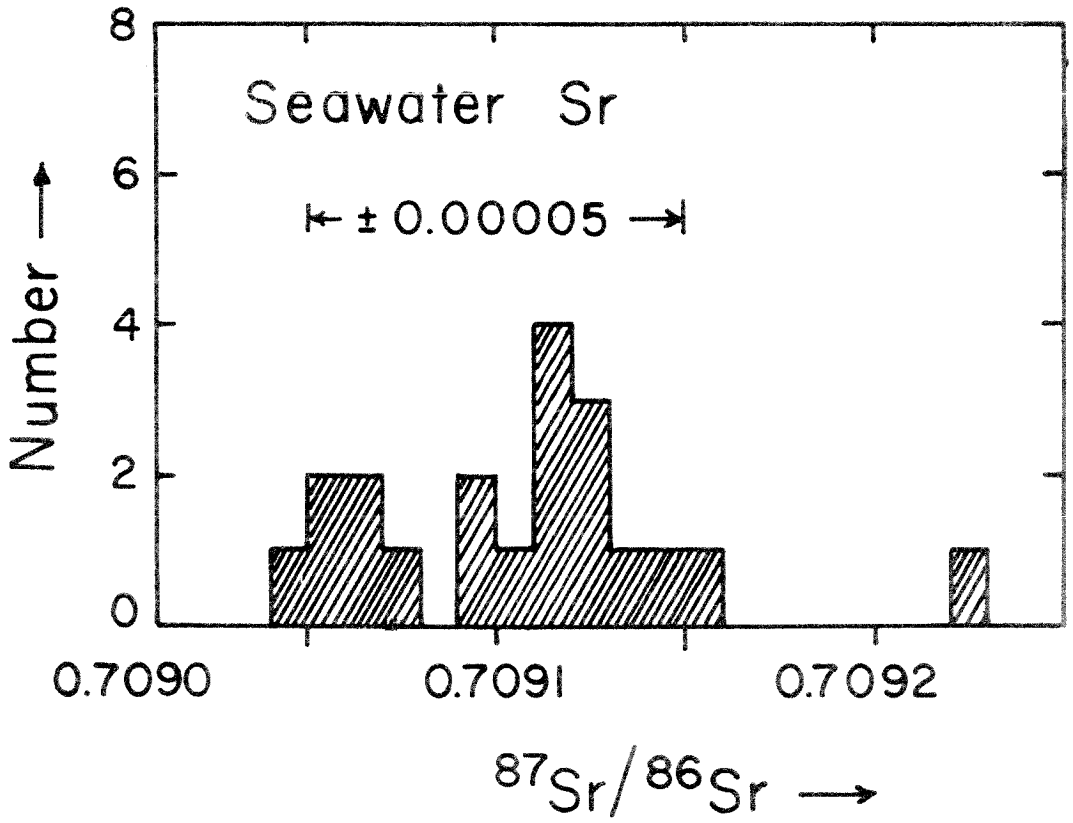
Seawater Sr
← ± 0.00005 →
Number →
8
6
4
2
0
0.7090
0.7091
0.7092
87Sr/86Sr →

FIGURE 2

Figure 3 . Rb - Sr evolution diagram for the basaltic achondrites. Line through data points represents a least squares fit (excluding Angra dos Reis) and determines the age and $(^{87}Sr/^{86}Sr)_{BABI}$. Line segment through Angra dos Reis is parallel to the isochron shown. The enrichment of each meteorite relative to $(^{87}Sr/^{86}Sr)_{BABI}$ is given on the right hand axis. The displacement shown by arrow denotes change in $^{87}Sr/^{86}Sr$ which would be incurred in an environment of chondritic Rb/Sr ($\sim$ 0.25) during 20 m.y.

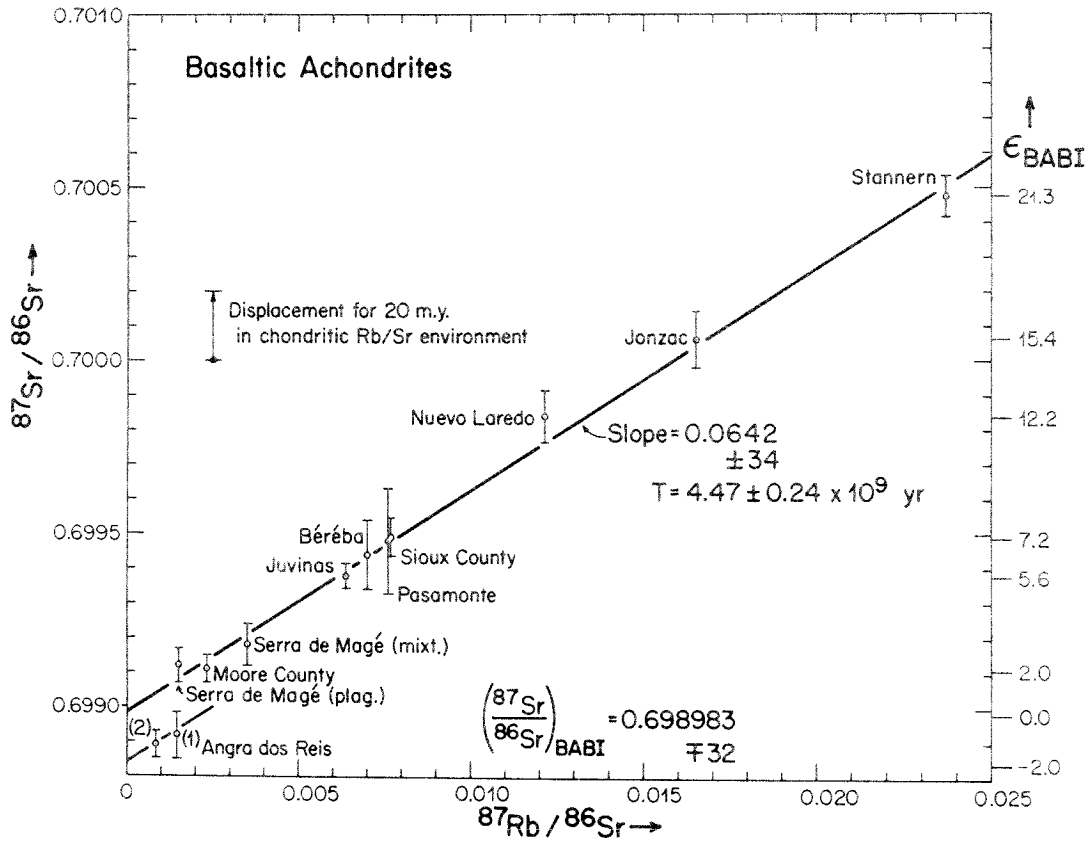
Basaltic Achondrites
0.7010
0.7005
0.7000
0.6995
0.6990
$^{87}Sr / ^{86}Sr \rightarrow$
0
0.005
0.010
0.015
0.020
0.025
$^{87}Rb / ^{86}Sr \rightarrow$
ϵ_{BABI}
21.3
15.4
12.2
7.2
5.6
2.0
0.0
-2.0
Stannern
Jonzac
Nuevo Laredo
Displacement for 20 m.y.
in chondritic Rb/Sr environment
Slope = 0.0642
±34
T = 4.47 ± 0.24 x 10^9 yr
Béréba
Juvinas
Sioux County
Pasamonte
Serra de Magé (mixt.)
Moore County
Serra de Magé (plag.)
(2)
(1)
Angra dos Reis
$\left(\frac{^{87}Sr}{^{86}Sr}\right)_{BABI}$ = 0.698983
∓32

FIGURE 3

Figure 4 . Rb - Sr evolution diagram for Stannern. Relative enrichment of each sample with respect to $(^{87}Sr/^{86}Sr)_{BABI}$ is shown on the right hand axis (parts in 10^4) . Line shown is the basaltic achondrite isochron.

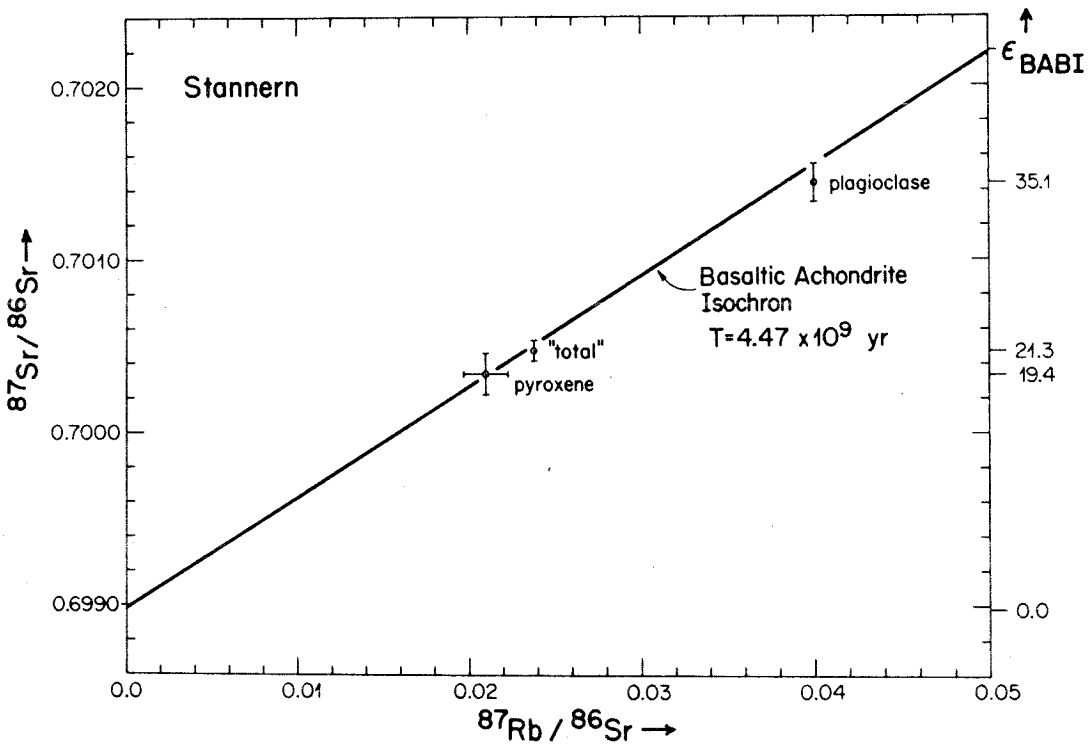
Stannern
0.7020
0.7010
0.7000
0.6990
$^{87}Sr/^{86}Sr$
0.0
0.01
0.02
0.03
0.04
0.05
$^{87}Rb/^{86}Sr$
ϵ_{BABI}
35.1
21.3
19.4
0.0
plagioclase
"total"
pyroxene
Basaltic Achondrite
Isochron
T=4.47 x10^9 yr

FIGURE 4

Figure 5 . Rb - Sr evolution diagram for the lunar samples. Basaltic achondrite isochron is shown for reference only. Isochron $\tau = 3.54 \times 10^9$ years is the best fit line through total rock 17, rock 17 pyroxene (pyx) and rock 17 plagioclase (plag) .

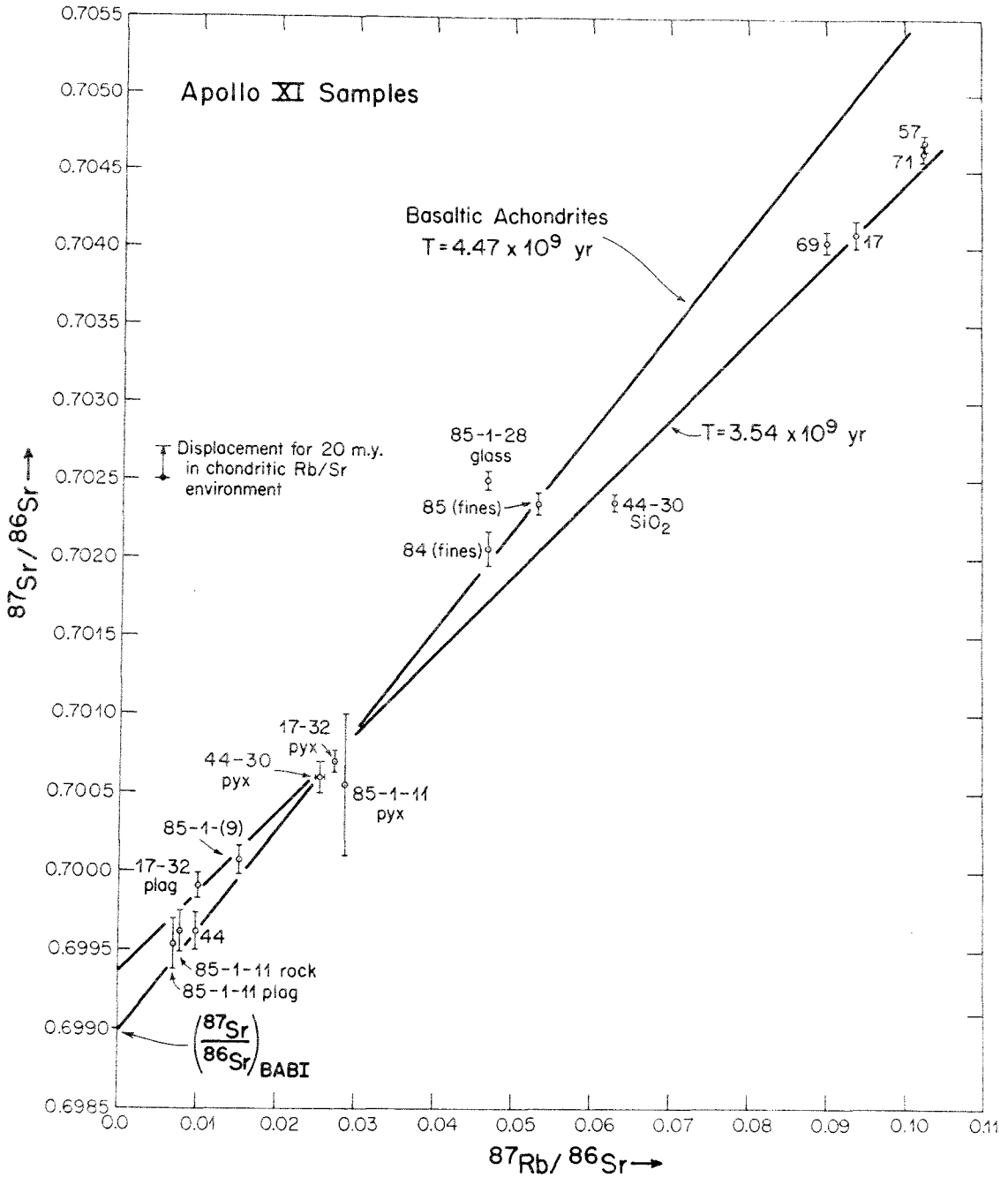
Apollo XI Samples
Basaltic Achondrites
T = 4.47 x 10^9 yr
T = 3.54 x 10^9 yr
Displacement for 20 m.y. in chondritic Rb/Sr environment
85-1-28 glass
85 (fines)
84 (fines)
44-30 SiO2
57
71
69
17
17-32 pyx
44-30 pyx
85-1-11 pyx
85-1-(9)
17-32 plag
44
85-1-11 rock
85-1-11 plag
(87Sr/86Sr)BABI
87Sr/86Sr
87Rb/86Sr
0.7055
0.7050
0.7045
0.7040
0.7035
0.7030
0.7025
0.7020
0.7015
0.7010
0.7005
0.7000
0.6995
0.6990
0.6985
0.0
0.01
0.02
0.03
0.04
0.05
0.06
0.07
0.08
0.09
0.10
0.11

FIGURE 5

Figure 6 . Rb - Sr evolution diagram for rock 17. This diagram includes all four data points for this rock. Best fit line for rock 17 is shown. Basaltic achondrite line is shown for reference.

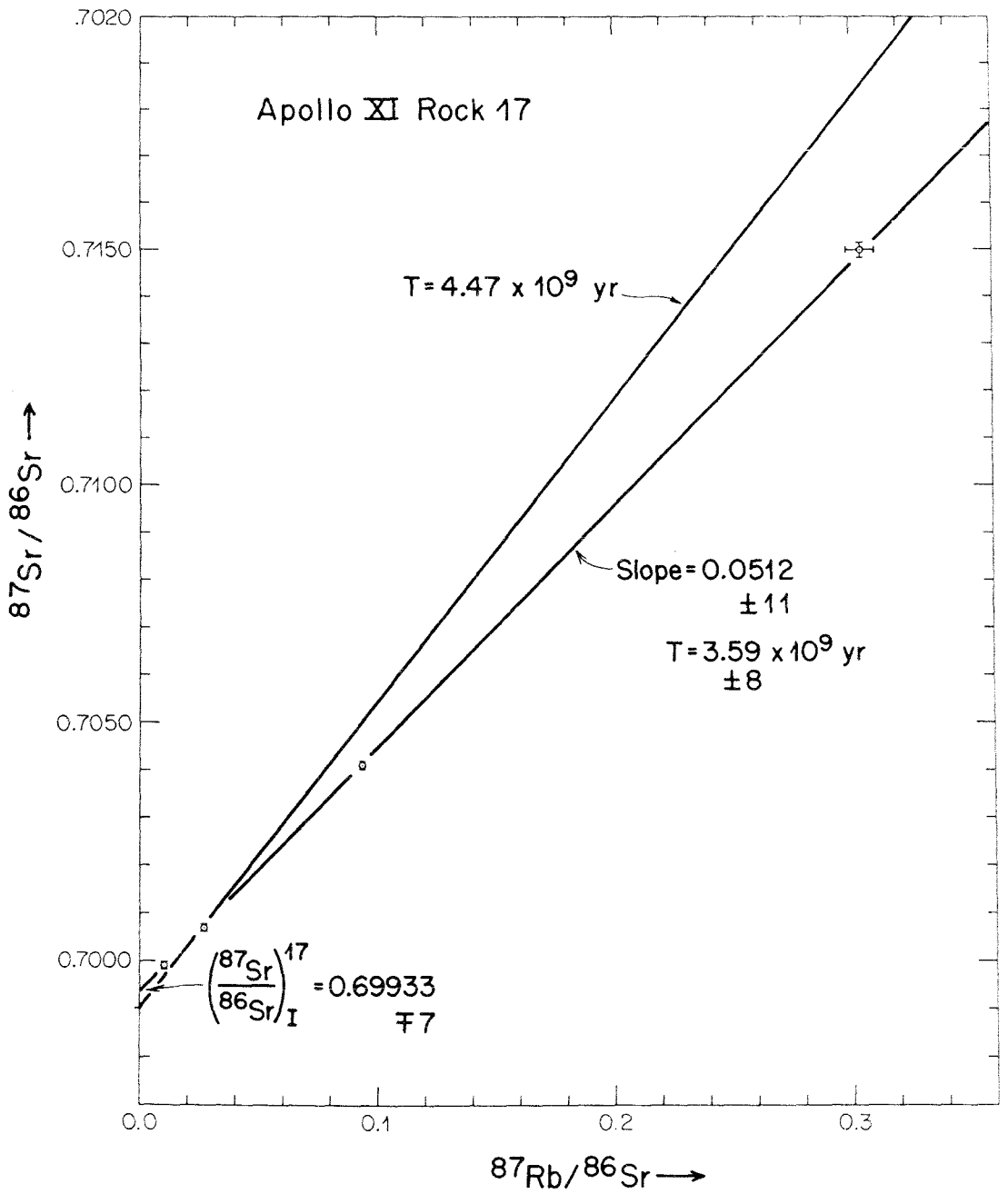
Apollo XI Rock 17
T = 4.47 x 10^9 yr
Slope = 0.0512
±11
T = 3.59 x 10^9 yr
±8
(87Sr/86Sr)I 17 = 0.69933
∓7
87Sr/86Sr
87Rb/86Sr
.7020
0.7150
0.7100
0.7050
0.7000
0.0
0.1
0.2
0.3

FIGURE 6

Figure 7. Rb - Sr evolution for Rock 44. Best fit line is shown through the data points. Basaltic achondrite line is shown for comparison.

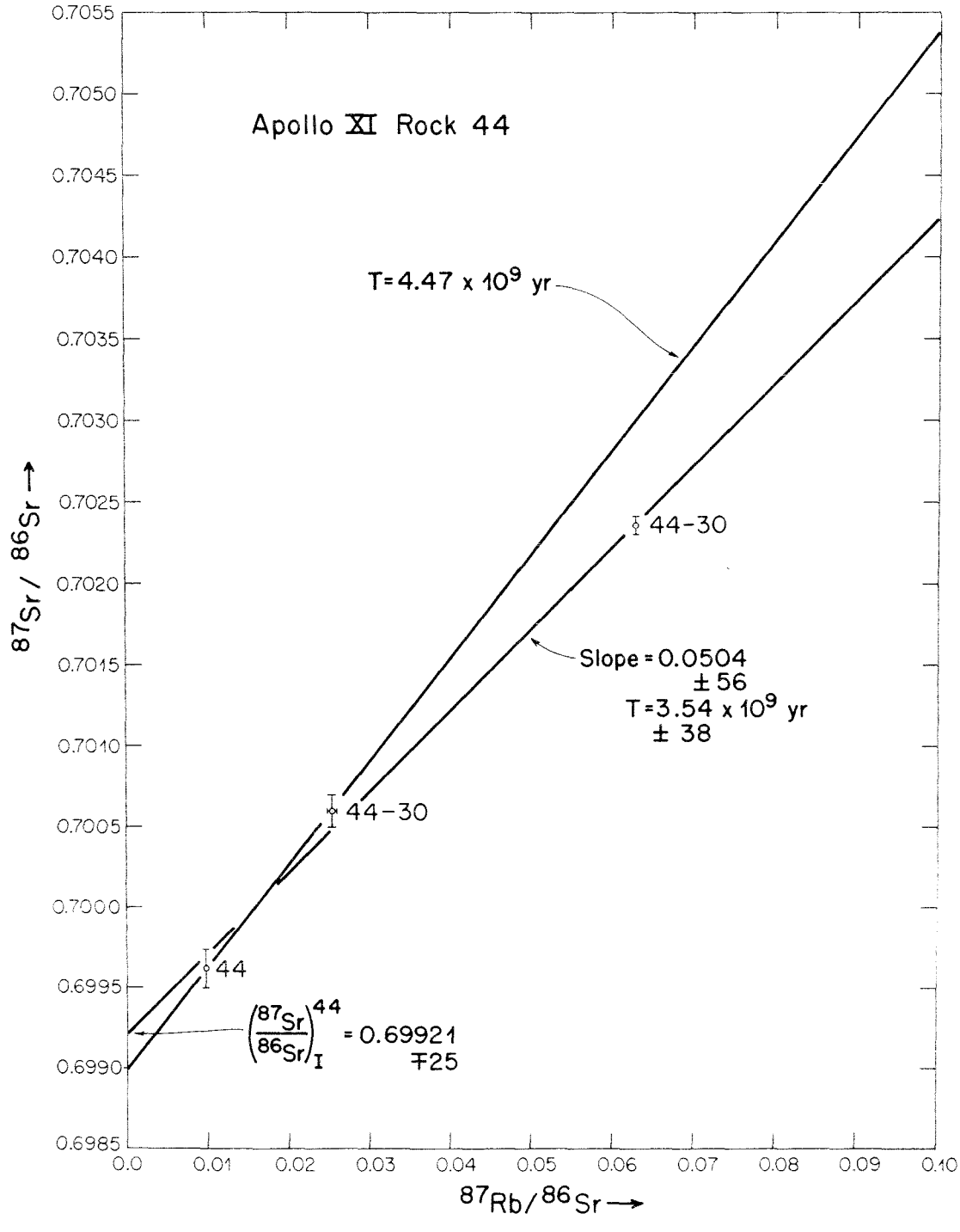
Apollo XI Rock 44
T=4.47 x 10^9 yr
44-30
Slope = 0.0504
± 56
T=3.54 x 10^9 yr
± 38
44-30
44
(87Sr/86Sr)I 44 = 0.69921
∓25
87Sr / 86Sr →
87Rb/86Sr →
0.7055
0.7050
0.7045
0.7040
0.7035
0.7030
0.7025
0.7020
0.7015
0.7010
0.7005
0.7000
0.6995
0.6990
0.6985
0.0
0.01
0.02
0.03
0.04
0.05
0.06
0.07
0.08
0.09
0.10

FIGURE 7

Figure 8. Age-($^{87}Sr/^{86}Sr$) plot for rocks 17 and 44. $(^{87}Sr/^{86}Sr)_{BABI}$ and $(^{87}Sr/^{86}Sr)_{ADOR}$ limiting values are shown. The lines BABI-Earth and ADOR-Earth represent Sr evolution in the earth's mantle during 4.6×10^9 years as deduced from young oceanic basalts. Extrapolation from rocks 17 and 44 is along lines of slope determined by $(Rb/Sr)^f$ in the fines and $(Rb/Sr)^{17 \text{ or } 44}$ as measured for the total rocks. Rock 17 always lies below the earth evolution lines. The meteorite Guarena is shown for comparison.

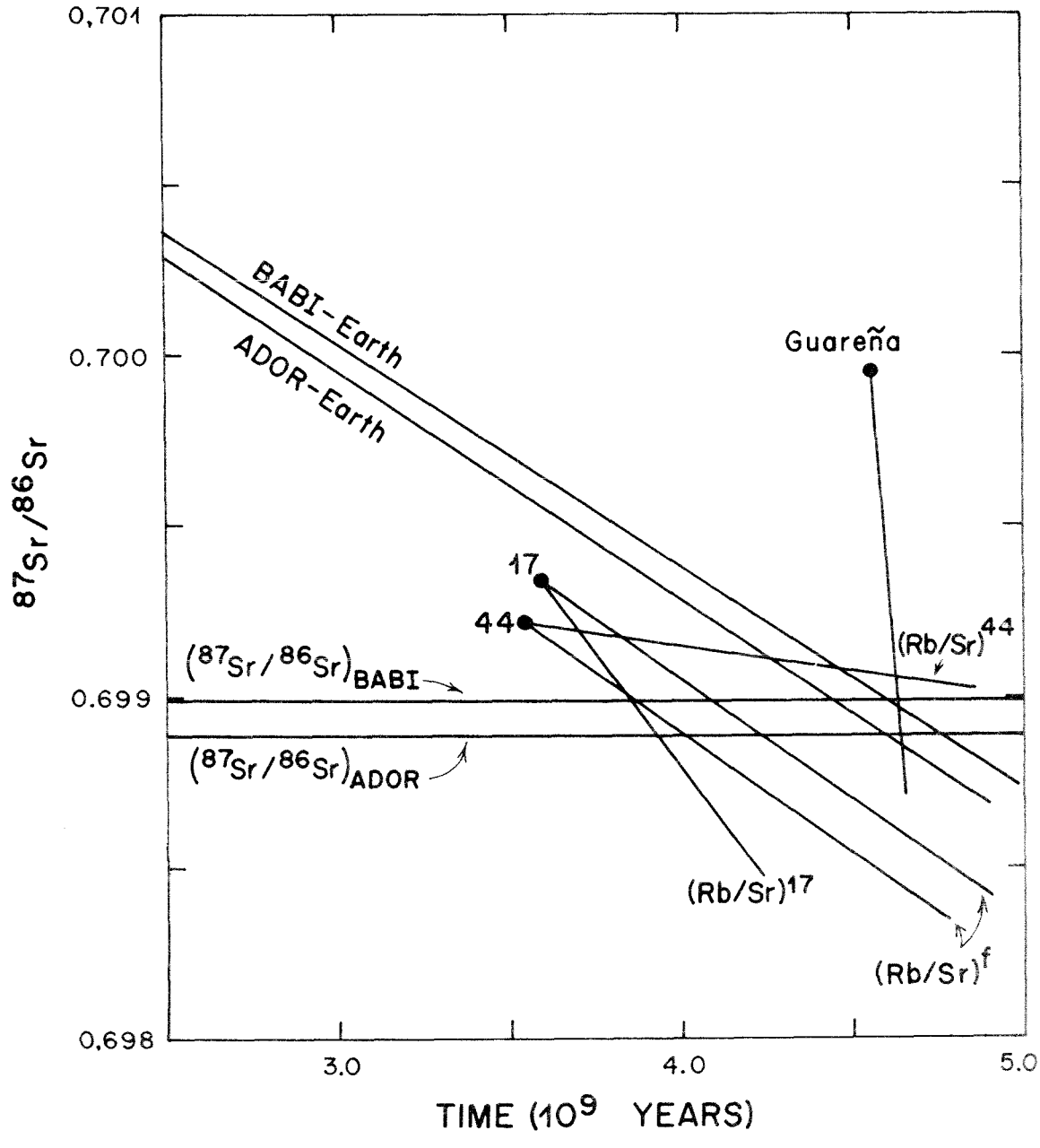
0,701
0.700
0.699
0,698
$^{87}Sr/^{86}Sr$
BABI-Earth
ADOR-Earth
Guareña
17
44
$(Rb/Sr)^{44}$
$(^{87}Sr/^{86}Sr)_{BABI}$
$(^{87}Sr/^{86}Sr)_{ADOR}$
$(Rb/Sr)^{17}$
$(Rb/Sr)^{f}$
3.0
4.0
5.0
TIME (10^9 YEARS)

FIGURE 8

Reprinted from THE REVIEW OF SCIENTIFIC INSTRUMENTS, Vol. 40, No. 2, 288–295, February 1969
Printed in U. S. A.

A Programmable Magnetic Field Mass Spectrometer with On-Line Data Processing*

G. J. WASSERBURG, D. A. PAPANASTASSIOU, E. V. NENOW, AND C. A. BAUMAN
Charles Arms Laboratory of the Geological Sciences, California Institute of Technology, Pasadena, California 91109

(Received 8 July 1968; and in final form, 21 October 1968)

A single focusing, 30.48 cm radius, 60° sector magnet mass spectrometer was constructed with symmetric conjugate foci calculated from fringe field data and corresponding to a beam deflection of 68°. Experimental and calculated optical characteristics agree well. A rotating coil probe and a rate coil are employed as field sensors for a nulling device and for field scanning. The magnetic field can be set to 27 values corresponding to the center of spectral lines and zero lines on both sides of each peak. The automatic scanning consists of: (1) rapid field change between adjacent field values (~500 G/sec); (2) locking in at the preset field values (~0.3 sec); (3) remaining in a channel for a preset time during which the ion beam current is integrated and the data digitized. Repeated arbitrary excursions between channels do not cause effective field variations of more than $|\Delta B/B| = 2\times10^{-6}$. For 0.2 mm source and 0.64 mm collector slit settings, a typical peak at mass 88 is flat for 2.7 G to 0.01% at a 14 kV accelerating potential. Data consist of channel intensity, scale factors, and internally provided clock time; data signals drive a typewriter and tape punch. A cyclic scan of five isotopes including background requires 35 sec. A segment of data (~10 cycles) is processed by the computer and the results returned to the operator.

INTRODUCTION

IN measuring the relative isotopic abundances of elements in small samples with high precision we have been limited by the usual analog techniques of data acquisition (e.g., strip chart recorder, slow field scanning). This limitation has been recognized by Moreland, Stevens, and Walling,[1] who designed systems for digital output with voltage scanning combined with a linear magnetic field sweep. This paper will present a system which eliminates chart reading, operator field scanning, and scale switching. The usual slow field scanning to determine accurately the center and intensity of spectral lines is changed to a step scan mode which permits that a greater percentage of time be spent integrating the ion beam intensity and a reduction of errors due to ion beam instability.

The basic aspects of the system are a programmable magnetic field for mass analysis, a digital voltmeter for ion beam integration, and transmission of the data to an on-line computer. The magnetic field can be set to 27 values corresponding to centers of spectral lines and zeros on either side of the peak. Nine channels are completely independent and carry their own identification. In each of the nine main channels the magnetic field may have values $H_k - H_k'$, H_k, and $H_k + H_k''$; these values are selected in sequence in the automatic scan mode and the ion current in each channel integrated. Any channel may be omitted and the cycle may start at any channel. A schematic mass spectrum showing the field values at which data points are taken and possible scanning sequences are shown in Fig. 1; Table I shows the information obtained in each channel. A schematic of the data processing cycle is shown in Fig. 2. Transmission of data to the computer during automatic scanning proceeds at a rate of up to 15 characters/sec for prolonged periods of time. The signals transmitted are stored in sequence on disk and are accessible to programs stored in the computer. A variety of programs for each element and type of experiment is stored and a particular one may be chosen by typing on the Flexowriter; program parameters may also be transmitted from the Flexowriter and interpreted as such,

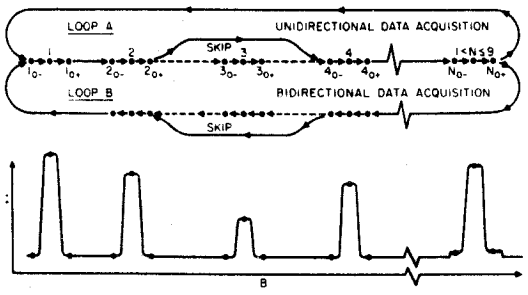

FIG. 1. Magnetic field step scanning. Dots represent field values at which the ion beam is integrated and correspond to points on the mass spectrum shown in the lower diagram. Loops A and B represent unidirectional and bidirectional data acquisition, respectively.

TABLE I. Twenty-seven channel mass analyzer.

a) 9 MAIN CHANNELS. EACH MAIN CHANNEL k IS SET TO 3 FIELD VALUES: $H_k - \Delta H_k'$, H_k, $H_k + \Delta H_k''$, SELECTED IN SEQUENCE IN THE SCAN MODE.

b) DATA OUTPUT AT EACH CHANNEL: ONE 15-CHARACTER WORD

CHARACTER #		INFORMATION
1	(n)	CHANNEL # / MASS IDENTIFICATION
2-7	(n)	INTEGRATED VOLTAGE (VOLT-SECS)
8	(q)	VIBRATING REED, DIGITAL VOLTMETER, SIGNAL POLARITY
9	(n)	TIME INTERVAL FOR INTEGRATION (1,2,4,8 SECS)
10-14	(n)	TIME AT INITIATION OF INTEGRATION
15	(?)	END OF WORD CODE (TAB)

* Contribution No. 1543, Division of the Geological Sciences.

[1] P. E. Moreland, Jr., C. M. Stevens, and D. B. Walling, Rev. Sci. Instrum. 38, 760 (1967).

distinct from the otherwise continuous stream of data. Processing of the data occurs in blocks of variable length ($\sim$several tens of words). The analyzed data are placed in storage at the computer and simultaneously returned to the laboratory on a second typewriter.

DESIGN PARAMETERS

Assuming good ion optical characteristics the critical factors are the ability to center an ion beam in the detector and to change the magnetic field rapidly between programmed field values. For an ion beam width of 0.2 mm and a collector slit of 0.38 mm, the magnetic field stability required is $|\Delta B/B| \leq 5\times10^{-5}$ for a maximum beam translation of 0.025 mm at the detector slit. The corresponding required stability of the accelerating potential is $|\Delta V/V| \leq 1\times10^{-4}$.

The magnetic field scan rate was chosen to provide a short time for field switching with respect to the time needed to obtain ion beam counting statistics of better than 0.1% for a beam of 10^{-12} A ($\sim 6\times10^{6}$ ions/sec).

While it is simple to achieve the field stability required at one point in the magnet gap, it is not evident that a field control which monitors the flux locally is sufficient to regulate the final position of the ion beam. This depends on the total path integral of the magnetic field which may be nonuniform due to hysteresis effects during cycling.

MAGNET CONTROL SYSTEM

Figure 3 is a schematic diagram of the function of the control systems. Each channel has a set of five binary coded switches, which, through relays, select a fraction of the reference voltage from a ratio transformer. A permanent reference magnet rotating at 1800 rpm around a coil provides the primary emf for the ratio transformer. The magnet and coil are placed in a thermostatic oven. A

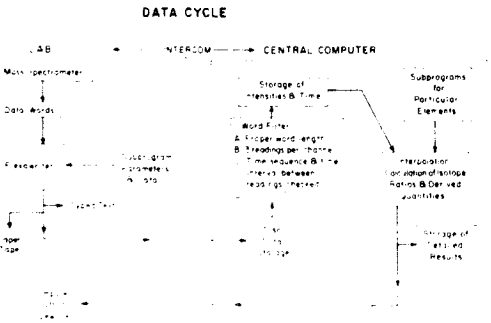

FIG. 2. Block diagram showing data cycle and schematic relationships between spectrometer and on line, time-shared computer (5 min period for set of 10 values of each ratio for five isotopes).

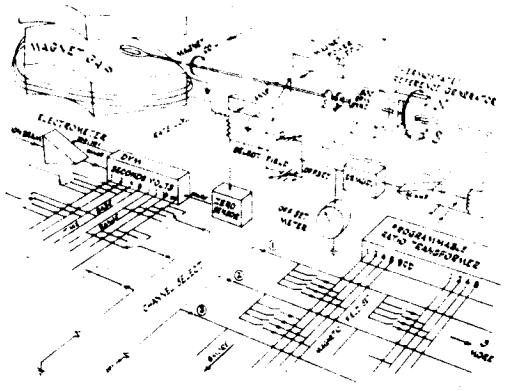

FIG. 3. Schematic of the magnet programming and control system and data acquisition system. A programming panel (not shown) permits (by remote switching) the choice of the numerical values of the magnetic field, time base, DVM, and electrometer ranges for each channel. Upon transfer of data to the memory, the DVM switches channel select (shown as 3) and thus changes the magnetic field set which initiates the slewing mode (see Fig. 4). The zero sensor detects when the new field is achieved and starts the next DVM integration of the ion beam.

second coil extends into the analyzer magnet air gap attached to the end of the same shaft as the rotating permanent magnet. The shaft is placed tangent to the flight tube so that the coil is positioned close to the tube one gap width inside the air gap. The coil is placed along with the shaft and pickup leads in a protective sleeve which has a 6.4 mm diam.

Upon command from the digital voltmeter a new channel is selected which switches in a new fraction of the reference voltage corresponding to a new magnetic field value. This voltage is added to an opposing voltage provided by the rotating coil in the magnet air gap. The resultant emf is amplified and converted to a dc signal by a synchronous rectifier. This signal is applied to an operational amplifier with negative feedback whose output causes the output of the magnet current power supply to change in the signified direction. The current in the magnet changes at a fast rate corresponding to 500 G/sec which we call the slewing mode.

The changing magnetic field creates an emf in the rate coil around the polecap. This voltage is also applied to the operational amplifier and compensates the original signal. At the slewing state the rectifier and amplifier become saturated. Thus the magnetic field overshoots the programmed value and an opposite correction has to be applied by the system, causing some oscillations for a time defined as the "lock in" time (typically $\sim$0.3 sec); thereafter the field remains constant until the next command from the digital voltmeter. The magnetic field as a function of time during automatic step scan is shown schematically on Fig. 4. This system was designed to our

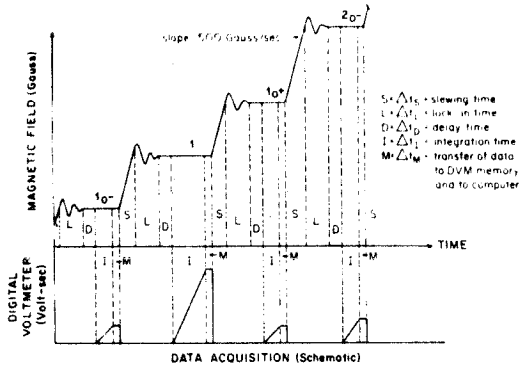

FIG. 4. Magnetic field as a function of time and channel during automatic step scan. The field is switched from channel 1_{0^-} to 1, 1_{0^+}, 2_{0^-}, etc. in the automatic scan mode of Fig. 1. The lower part illustrates the DVM signal. The times involved are as follows (sec): $\Delta t_s \sim 0.04$ for typical jumps in magnetic field; $\Delta t_L \sim 0.3$; $\Delta t_D \sim 1$; $\Delta t_I \sim 1-8$; $\Delta t_M \sim 0.001$. The magnetic field starts to slew automatically when information has been transferred to the DVM one word memory.

specifications by Magnion Inc. using a rotating coil and permanent magnet made by Rawson Inc. An offset voltage supplied by a battery enables us to offset the magnetic field in each channel by up to 10 G on either side of the field setting in the main channel to sample the zeros of each peak. The battery cancels some of the effective rectifier output in such a way that a slightly higher/lower emf from the rotating coil is needed to balance the system. When the step scan is complete, a zero sensor enables the digital voltmeter to start integrating the beam ion intensity for a preset integrating time. At the end of this time interval (Δt_I), the digital voltmeter signals for a change in channel. Scanning is done cyclically and unidirectionally (Fig. 1) to minimize hysteresis effects. By moving the probe in the air gap an optimal position may be found which minimizes hysteresis effects.

DETECTION SYSTEM

The detection system is designed to operate in two distinct modes: (1) pulse counting and (2) analog operation with integration of the ion current using a Faraday cup or an electron multiplier. We will only discuss mode 2. In the analog mode the ion signal is applied to a vibrating reed electrometer (Cary No. 36) with variable feedback resistor (10^{10}, 10^{11}, 10^{12} Ω) with a 0.1 sec time constant for 99% full scale. The output of the electrometer is integrated by a bipolar digital voltmeter for a time interval of 1, 2, 4, or 8 sec. The digital voltmeter (DVM) is equipped with an internal clock with 0.01 sec resolution running continuously from 0 to 1000 sec and recycling. This clock notes and stores the time at the onset of integration. This time is part of the output data and is used for interpolating ion beam intensities. The time intervals of integration, the scale changes on the electrometer (100 V, 10 V), and the DVM range (0.1, 1, 10, 100 V) are provided automatically by a ganged switch which is activated upon entering into a given channel. Each main channel controls its own range and integration interval for maximum sensitivity. In addition, a distinct integration interval may be chosen for the zeros on either side of the peak. In the automatic scan mode a zero sensor initiates the DVM integration after an interval Δt_D from the time the magnetic field is locked in. The interval Δt_D is chosen to avoid any errors due to the time constants for charging up of the system. If the system has an effective time constant τ, the ion beam signal detected will grow exponentially with time from the time the ion beam is switched into the collector. If the signal is integrated for a time Δt_I at a time Δt_D after the beam is in the collector, the resulting measurement will be off the true measurement by a fraction $\epsilon \simeq \tau e^{-\Delta t_D/\tau}/\Delta t_I$. An identical error will be caused by reading the background a time Δt_D after the beam has been switched off the collector; the total error in corrected intensities is thus 2ϵ and depends on how long we wait before integrating the ion signal. To measure this effect we compared the ratios of the ion beam intensities obtained as a function of Δt_D; it was found that $\Delta t_D \simeq 1$ sec reduced any errors to less than 0.01%.

At the end of a DVM reading the output is transferred into the DVM memory and a signal is generated that switches the system to a new channel. While the magnetic field is slewing, the DVM one word memory is typed on the Flexowriter, punched on tape, and the signals transmitted to the computer (Fig. 4). After lock-in at the new channel the zero sensor initiates the DVM integration and the whole process is repeated. The digital voltmeter, the memory unit, and serializer were developed for our re-

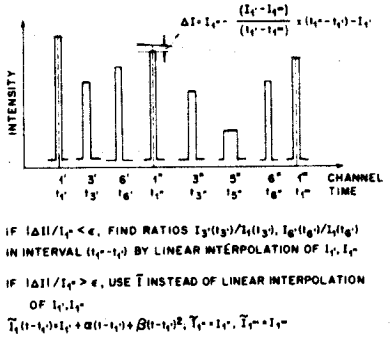

FIG. 5. Interpolation criterion used for calculating isotope ratios. We store in the computer a continuous array of intensities measured, the time of measurement, and the channel identification. Numerals refer to channel numbers and the primes denote successive readings. Channel 1 is here chosen as the index isotope and the criterion is applied to intensities $I_{1'}$, $I_{1''}$, $I_{1'''}$ to calculate ratios in the interval $(t_{1''}-t_{1'})$. For ratios in the interval $(t_{2'''}-t_{1''})$ we use $I_{1''}$, $I_{1'''}$, and $I_{1''''}$ from the continuous array.

quirements by the Non-Linear Systems, Inc. During scanning each channel may correspond simply to one spectral line, or we may assign more than one channel to a spectral line either for achieving better statistics or for a more complicated background monitoring.

COMPUTER PROGRAM

The IBM 1800 computer is used on a time-sharing basis and is capable of performing all the necessary operations for data reduction. The processing of the data consists of two parts: (a) interpretation of the stream of data and reduction to intensities and time at which readings were obtained and (b) calculation by interpolation of isotopic ratios and of any derived quantities of interest.

In dealing with the continuous stream of data it is found to be more efficient that the data stored on disk be analyzed in small blocks. The natural block size corresponds to data transmitted during one complete step scan cycle, e.g., enough data to calculate one ratio for every isotope measured. In this fashion the computer analysis lags at most one step scan cycle behind the actual data obtained.

To avoid possible errors in the incoming data from being interpreted, a word filter was designed which permits only "legal" words to be used by the programs. The filter checks proper word length; verifies that selected characters are as expected (i.e., α-numeric or numeric); and checks that each data word appears in the proper time sequence, and that the zeros for each peak exist and are in proper sequence (i.e., left zero, peak, right zero). Using the legal data words, the spectral line intensities are calculated by subtracting the appropriate zero intensities and correcting for scale factors and integration times (Δt_I). This information along with the time of onset of integration (corrected for Δt_I) is stored in an array. The members of the array are ordered according to channel number and the time of onset of integration. This order corresponds to the normal sequence of scanning (Fig. 1). Channels which have yielded illegal words or have been accidentally or intentionally skipped during a cycle are stored in this array as zeros. The calculation of isotopic ratios is begun upon accumulation of sufficient data. A self-consistent interpolation criterion has been used as indicated in Fig. 5. We choose a high intensity isotope as an index isotope (e.g., No. 1 in Fig. 5) and calculate the ratios of every isotope to this index isotope. This is satisfactory as long as the index isotope has sufficient intensity to yield good statistics. A more sophisticated system is needed if the precision of the index isotope measurement is poor due to statistics, or if the ion beam is highly unstable or granular. Mean ratios, statistical errors, and derived quantities are calculated in sets of ~ 10 ratios for each isotope.

Table II. Beam characteristics.

	(mm)	ΔH equivalent (G)
Potassium ($B = 3500$ G at 14.5 kV)		
Source slit	0.2	...
Collector slit	0.69	4.1
Beamwidth	0.2	1.2
Dispersion (per mass unit)	7.62	45
ΔH_{max} (during repeated cycles)	0.013	0.08
$\frac{\Delta H_{max}}{H} = 2\times10^{-4}$		
Strontium ($B = 5640$ G at 16.0 kV)		
Source slit	0.2	...
Collector slit	0.53	5.0
Beamwidth	0.24	2.3
Dispersion (per mass unit)	3.46	32.3

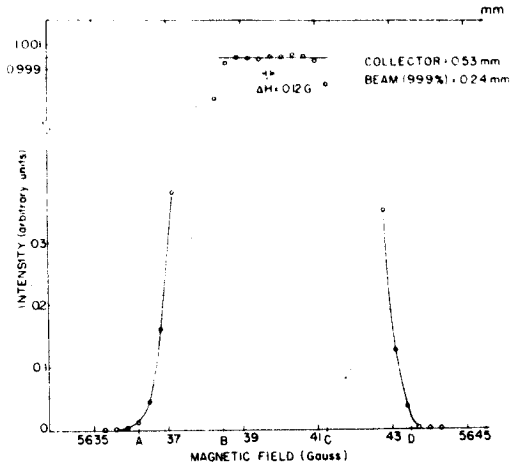

FIG. 6. ^{88}Sr beam profile for collector slit wider than the beamwidth. We obtained intensity readings by changing the magnetic field automatically in small steps, using the mass analyzer. From the distances AB and CD we calculate a beamwidth of 0.24 mm for a 0.2 mm source slit. The gauss equivalent in millimeters is given on the top axis. The signal while the beam is sweeping across the cup is flat to 1×10^{-4} for 2.3 G; beam statistics were a factor of 3 better. The Gauss equivalent scale in millimeters should be multiplied by 2.

Visual beam monitoring is achieved using a recorder (0.2 sec for full scale deflection) in parallel with the digital system with a variable chart speed of 2.54 cm/min to 20.3 cm/sec. The recorder range is controlled by each individual channel being used for optimum sensitivity. To make the visual beam monitoring useful for high precision data, recorder inputs of selected channels are provided with an expanded scale.[2] The magnetic field may also be made to operate in the conventional ramp scan mode in conjunction with analog display on the strip chart recorder.

[2] W. R. Shields, Nat. Bur. Stand. Tech. Note 277 (1966).

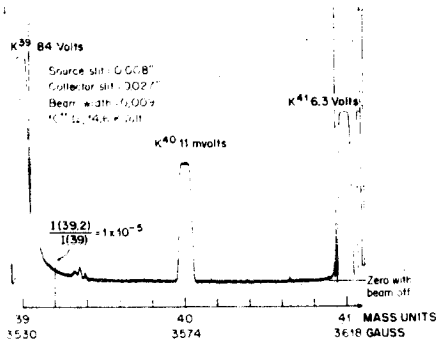

FIG. 7. Potassium spectrum obtained by ramp scanning the magnetic field. Discontinuities in the recorder output correspond to sensitivity changes. The background is very close to the instrument zero shown and remains on the positive side. Small peaks at 39.35 are reflected peaks off a knife-edged baffle.

PERFORMANCE

The operation of the mass spectrometer in the step scan mode depends on our ability to control the magnetic field accurately. In order to determine the reproducibility of the magnetic field settings, we set channels of the magnetic field at the values required to bring a beam halfway in the collector collimating slit. Small instabilities or changes in magnetic field due to repeated cycling thus cause large variations in detected signal intensity.

For this purpose we step scanned cyclically and unidirectionally over the sides and the center of peaks in a potassium spectrum. From the maximum signal intensity changes at the sides of the peaks we find a

$$|\Delta B|_{\max}=0.08\ \text{G}, \quad \text{or} \quad |\Delta B/B| \leqq 2\times 10^{-5},$$

during 9 min for 35 cycles. The equivalent maximum drift in the accelerating voltage is $|\Delta V/V|=4\times 10^{-5}$. This drift is equivalent to a beam translation in the cup of 0.013 mm.

The accelerating voltage is monitored during an experiment using the DVM and is stable to better than 1×10^{-4} over an hour. A 20 MΩ wire wound resistive divider provides the potentials for the focusing plates in the source. The high voltage is provided by a Walden Co. power supply in the range 10-20 kV at 1 mA maximum load. The unit was modified to eliminate warmup drift by keeping the thermostatic reference ovens on continuously. The power supply can conveniently be modified to provide a programmable high voltage.

Table II shows typical sizes of collimating slits and beamwidths obtained for two elements. Wide collector collimating slits are used; however, they can be narrowed down to the limit defined by the effective field drift. For the thermal ionization source for different experiments over periods of months with slightly different loading and focusing conditions in the source, we find an effective magnetic field drift of 0.3 G. It is, therefore, possible at the beginning of an experiment to choose the magnetic field values in the channels to correspond to the masses under investigation. Thus, even very low intensity signals at known masses may be centered in the collector and data acquisition initiated as soon as signals are detected by the DVM. For signals of sufficient intensity, the center of a peak is determined by finding the average of the two field values at which one-half of the beam is in the detector.

Figure 6 shows the top of a typical spectral line obtained by scanning of the B field in small steps and integrating the ion signal with the digital voltmeter. The observed peak top is flat to better than 1×10^{-4} while the beam traverses the collector collimating slit when the electron suppressor is kept at -180 V. The lower part of Fig. 6 shows the initial increase in signal intensity as the ion beam enters the slit; the distance AB corresponds to a beam image at the collector slit of 0.24 mm width and is very close to the size of the source slit used. Uncertainty $\Delta B/B=2\times 10^{-5}$ for locking in at a magnetic field value is shown on the figure and is negligible for beamwidths 0.025 mm narrower than the collector defining slit. The detailed form of beam tails and the possible presence of positive reflected peaks and negative signals due to electrons were investigated by studying the potassium spectrum since $^{39}K/^{40}K=8\times 10^{3}$. A typical spectrum obtained at high beam intensities is shown in Fig. 7. The zero as measured with the beam off is indicated. None of the zero lines and the spectral lines were changed by moving a hand magnet around the tube and in the vicinity of the collector cup and signal lead to the electrometer. The small peaks at mass 39.35 correspond to scattering off a knife-edged baffle placed 3.8 cm in front of the collector slit. At 0.2 m.u. above the center of the mass 39 peak, the intensity has fallen by a factor of 10^5 which corresponds to a tailing of 10^{-5} for peaks separated by 1 m.u. at mass 200. The low mass tail as determined from similar experiments is less than 10% more intense than the high mass tail at symmetric distances from the center of the ^{39}K beam. This condition is obtained using a V-filament (3) and by careful sample loading and focusing in the source.

A study of the characteristics of the mass spectrometer was made by analyzing several samples of strontium extracted from seawater. The sample size ranged from 3×10^{-6} to 5×10^{-9} g of Sr; the latter sample corresponds to 3×10^{-11} g of ^{86}Sr. For each sample load, ratios were obtained as a function of the ion beam intensity in sets of ten during the course of the run. The ratios $^{87}Sr/^{88}Sr$, $^{86}Sr/^{88}Sr$, $^{84}Sr/^{88}Sr$ were measured and the $^{85}Rb/^{88}Sr$ ratio was monitored. To correct for mass discrimination the $^{86}Sr/^{88}Sr$ ratios for each set were used to calculate the discrimination factor by assuming this ratio to be 0.1194; the ratios were then corrected accordingly. Figure 8 shows

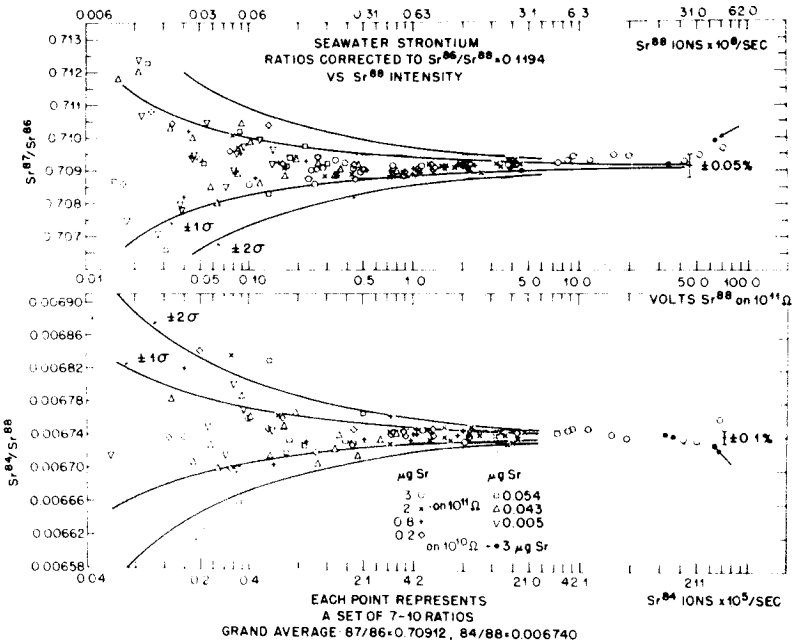

FIG. 8. Isotopic ratios obtained for Sr extracted from seawater as a function of ion beam intensity for samples from 3×10^{-8} to 5×10^{-9} g Sr. Ratios are corrected for mass fractionation. The solid curves represent the expected statistics of the ratios if we assume that statistics are determined by the number of ions. Ratios obtained for ^{88}Sr intensities higher than 10 V on 10^{11} Ω had to be corrected for the voltage coefficient of the resistor which is nonlinear and not well known for high voltages (~50 V). Ratios obtained on the 10^{10} Ω resistor are plotted at the correct ion current but 10× the voltage and did not have to be corrected for voltage coefficient. Two points marked by arrows were obtained during an unstable part of the run while the intensity varied by a factor of 2 (nonmonotonically) in 7 min.

these corrected ratios as a function of beam intensity. It can be seen that for signals ranging from 3×10^{7} to 3×10^{9} ^{88}Sr ions/sec, we obtain ^{87}Sr/^{86}Sr ratios with a total spread less than ±0.05%. From the counting statistics for the number of ^{86}Sr and ^{87}Sr ions collected to form the average of ten ratios, the expected 2σ deviations range from ±0.05% to ±0.005%, correspondingly. At somewhat lower intensities, the data show a wider spread around the average of ^{87}Sr/^{86}Sr=0.70912; this spread is consistent with a $\pm2\sigma$ deviation from counting statistics for the ^{87}Sr and ^{86}Sr. A similar plot for the low abundance isotope ^{84}Sr is shown in the lower part of Fig. 8. In the interval from 6×10^{7} to 3×10^{9} ^{88}Sr ions/sec, the data lie within a ±0.1% band. The counting statistics in this interval determine $\pm2\sigma$ deviations from ±0.1% to ±0.04%. At lower signal intensities the ratios ^{84}Sr/^{88}Sr obtained agree within the $\pm2\sigma$ deviations from counting statistics. At ^{88}Sr intensities lower than 0.05 V, the ^{84}Sr beam was centered in the collec-

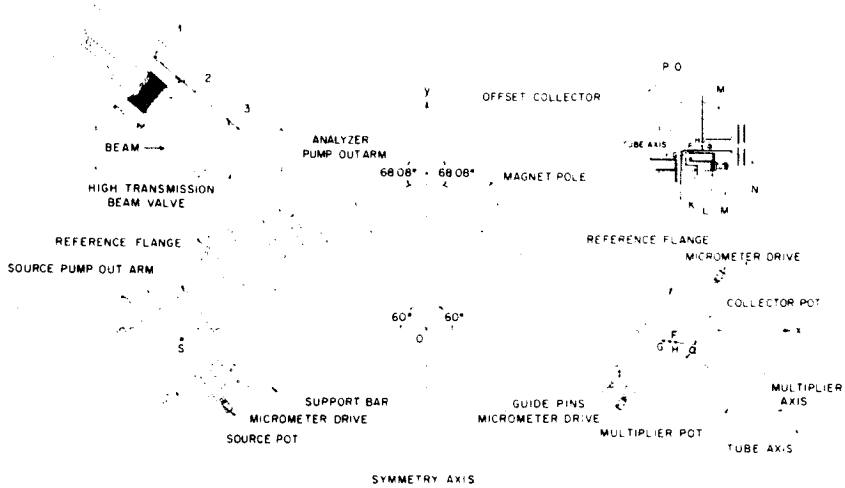

FIG. 9. Schematic drawing of the mass spectrometer. Points S and F are the symmetric foci calculated. The offset collector system is shown in the upper right corner; G and H are the adjustable collimating slits for the simple cup and the multiplier, respectively. K—repeller; L—collector cup; M—shield for simple cup and multiplier; N—multiplier; O—baffle; P—reference flange. Upper left hand shows the beam valve assembly; 1—Viton O rings; 2—valve driver fully retracted; 3—valve seat.

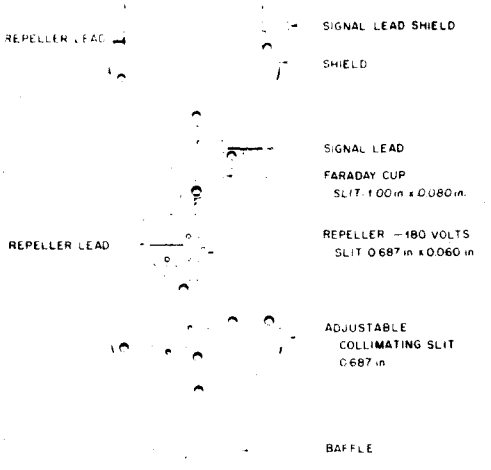

FIG. 10. In-line collector assembly showing complete shield which is placed around the Faraday cup.

tor slit by using the known dispersion of the instrument rather than by watching the analog record. For these Sr experiments we find that the maximum stable beam obtained is proportional to the amount of sample on the filament for this element. For the smallest load of 5×10^{-9} g Sr, we obtained a maximum stable signal of 6×10^{6} ^{88}Sr ions/sec. Measurements were made of isotopic ratios with a beam of 6×10^{3} ions/sec or $\sim10^{-15}$ A for the low abundance isotope. Although this signal is near the noise level of the system, we obtained $\pm10\%$ statistics for the average of 10 ratios by integrating 8 sec at each field value. We conclude that it is possible to obtain $\pm10\%$ statistics with 5×10^{-12} g of a Sr isotope using a Faraday collector.

Very high precision data can be obtained from small samples in short times when we can correct for mass discrimination. When the signal intensity is much greater than the noise level, i.e., for ion currents $\gtrsim7\times10^{-15}$ A, we can obtain results good to within the counting statistics for the number of ions collected by using the digital system and integrating essentially the voltage drop across a resistor. At very high intensities, $\sim10^{-10}$ A, the precision is not improved, even though the counting statistics are better, as we are limited by beam instabilities. For a typical set of 10 ratios we obtain a standard deviation of $\sigma_x\sim0.05\%$. We have observed that if sets of more than 10 ratios are considered, σ_x does not change. Therefore, if the ratios are normally distributed and we obtain approximately 100 ratios (10 sets of 10 ratios) of ^{87}Sr/^{86}Sr, then with $\sigma_x=0.05\%$, the standard deviation of the mean $\sigma_m=0.005\%$ which appears to be the limiting precision of the mean currently available. This is indicated by internal statistics within long runs and by reproducibility of the mean for different runs of the same sample.

DESCRIPTION OF THE INSTRUMENT

A schematic drawing of the mass spectrometer is shown in Fig. 9. The focal points S and F and the beam deflection angle were determined by computer calculations of ion trajectories using the measured magnetic fringe field. A solution was sought with focal points S and F symmetric with respect to the y axis. The coordinates of these focal points are $|x|=58.870$ cm and $y=-2.697$ cm. The beam deflection angle is 68.08° for the 60°, 30.48 cm radius, sector magnetic field used. The line GH is the straight line approximation to the locus of foci and forms an angle $\alpha=26.5°$ with the tube axis. As shown in the upper right hand side of Fig. 9, G is the position of the collimator for the simple Faraday cup and H that for the multiplier.

The construction of the instrument was done with precision of ±0.025 mm over the total length of the instrument for the alignment and positioning of the critical optical elements. The alignment of the tube and reference flanges was done on a boring mill. For this purpose support saddles were placed and screwed into a precision tooling plate on the mill at approximately the proper angles and spacing. These saddles were drilled and bored *in situ* and the tube and beam valve assembly were clamped together; the reference flanges were attached to the tooling plate and locked at the proper relative angles by the 5×5 cm^2 support bar using 12.7 mm guide pins. All welding was performed while the components were clamped. The surface of the reference flanges was finally machined on the boring mill after welding; all distances and angles were measured with reference to the tooling plate and the reference flanges. Alignment holes were bored on the reference flanges on the boring mill and the source and collector assemblies were then mounted using tight guide pins for slit alignment. Stainless steel was used throughout the construction; the tooling plate was made from aluminum and is now used to support the mass spectrometer tube in the horizontal position.

To facilitate magnet alignment the magnet is placed on a cart capable of (a) motion in two orthogonal directions in the horizontal plane and simple rotation in this plane and (b) motion in the vertical direction and tilting off the horizontal plane. The motions in (a) are effected by screw drives, are monitored by indicators, and are easily reproducible to 0.013 mm. The magnet is positioned at its calculated position and the beams obtained are almost theoretical as discussed in the section on performance of the instrument.

The system is differentially pumped by two ion pumps, on either side of the beam valve, which is shown in Fig. 9 in detail; the valve affords full ion beam transmission. Viton O rings are used for gaskets as shown with the O ring

on the driver of the valve out of the ion beam path. Gold and copper gaskets are used for the rest of the machine; a Teflon gasket may be used for the source flange for frequent venting. The analyzer section remains at an equilibrium pressure of 2×10^{-8} Torr as measured at the pump during an experiment; similarly the source section attains a pressure of $\sim5\times10^{-8}$ Torr while running. A Vacsorb pump is used for rough pumping; total pumpdown time is ~15 min for a pressure of 3×10^{-7} Torr after venting the source for sample loading.

A thermal ionization thick lens source with Z-focusing plates is used as designed by Dietz.[3] The final collimating slit is symmetrically adjustable, and the first three plates may be conveniently removed for cleaning after each run.

Two interchangeable collector assemblies have been built for the spectrometer. A schematic plan view of the offset system is shown in Fig. 9. Point G is the collimating slit for the simple cup; this slit is adjustable through a micrometer bellows arrangement. The collector cup is completely enclosed by shield (M) to guard against the electron gas created in the whole region. The signal lead from the cup (not shown here) is also guarded by a cylindrical tube along its path inside the collector pot. The repeller (K) is kept at -180 V and is mounted on a separate insulating stack from the simple cup. The baffle (O) shields the cup from reflected beams and is constructed as a cup to collect most secondaries. The multiplier is also shielded by a can, although complete electron shielding is not as critical.

Figure 10 shows the assembly of a simple in-line cup which may be interchanged with the offset system. In this simpler geometry light tight shielding is easier. Ions and electrons may enter the collector cup only through the collimator slit and the repeller slit which is again kept at -180 V. The beam profiles as discussed before are very good and free of any negative signals or discontinuities in the background resulting from addition of opposite polarity signals.

[3] L. A. Dietz, Rev. Sci. Instrum. **30**, 235 (1959).

ACKNOWLEDGMENTS

The authors wish to thank Pai Young, G. W. Barton, L. A. Dietz, and W. R. Shields for aid and discussion during the design and construction of this instrument. R. E. Haas helped with the computer programming. This research was supported by grants from the National Science Foundation (GP 5391, GP 7976).

EARTH AND PLANETARY SCIENCE LETTERS 5 (1969) 361-376. NORTH-HOLLAND PUBLISHING COMP., AMSTERDAM

INITIAL STRONTIUM ISOTOPIC ABUNDANCES AND THE RESOLUTION OF SMALL TIME DIFFERENCES IN THE FORMATION OF PLANETARY OBJECTS

D.A.PAPANASTASSIOU and G.J.WASSERBURG

The Charles Arms Laboratory of Geological Sciences, California Institute of Technology, Pasadena, California 91109 *

Received 26 February 1969

It is shown that differences in the $^{87}Sr/^{86}Sr$ ratio corresponding to about 10^{-2} % are clearly resolvable using improved instrumental techniques. Several basaltic achondrites having a total spread of 0.2% in $^{87}Sr/^{86}Sr$ were studied and appear to define an identical initial $^{87}Sr/^{86}Sr$ abundance corresponding to 0.698976 ± 0.000055 (maximum uncertainties). These samples are found to lie on a well defined isochron with a slope of 0.0629 ∓ 0.0037 and an age $4.39 \mp 0.26 \times 10^9$ yr, for $\lambda = 1.39 \times 10^{-11}$ yr^{-1}. The maximum deviation of a data point from the best fit line is 6×10^{-3} %. This shows that if the samples were derived from material with chondritic or solar Rb/Sr abundance ratios, they were formed within a time period of 4 m.y. or 1.6 m.y. respectively. The application of such measurements to establish a refined early solar system chronology is discussed.

1. Introduction

The purpose of this investigation is to obtain a precise estimate of the initial strontium isotopic composition at the time of formation of planetary objects in the solar system and to apply high precision measurements to determine the ages of basaltic achondrites. In addition, we will show how small time differences (10^6–10^7 yr) in the time of formation of planetary objects may be resolved.

The $^{87}Sr/^{86}Sr$ ratio in some achondrites was first measured by Schumacher [1], and Herzog and Pinson [2], and later by Webster, Morgan and Smales [3]. These results were of critical importance for determining the age of stony meteorites by assuming that the chondrites evolved from strontium with the initial isotopic composition as found in achondrites. Gast [4] reported several analyses of achondrites which were a substantial improvement over the data of earlier workers. He showed that the initial (I) $(^{87}Sr/^{86}Sr)_I$ was about 0.698 to 0.700 and found no evidence for a value of 0.687 as reported by Schumacher. More recent data of somewhat better precision obtained in this laboratory [5] have confirmed Gast's results. Independent estimates for $(^{87}Sr/^{86}Sr)_I$ values were obtained by Burnett and Wasserburg [6] from two iron meteorites (Toluca and Pine River) which are in agreement with the values from basaltic achondrites.

Determination of an internal isochron [7] for a single meteorite permits an estimate of $(^{87}Sr/^{86}Sr)_I$ in that particular object. The first successful effort in this direction was with the iron meteorite Weekeroo Station [8]. Relatively precise internal isochrons have been obtained for Kodaikanal [9], Norton County [5], and Weekeroo Station [8] which yield ages of 3.81×10^9 yr, 4.70×10^9 yr, 4.37×10^9 yr, and $(^{87}Sr/^{86}Sr)_I$ of 0.713, 0.700 and 0.703, respectively. New results recently presented on Krähenberg by Kempe and Müller [10] and on El Taco by Wasserburg and Burnett [7] give almost identical parameters with those of Norton County. The results

* Contribution no. 1603.

of Shima and Honda [11], obtained by differential dissolution, are subject to large analytical and procedural uncertainties and are therefore not included in this discussion. There is a clear distinction between Kodaikanal and all the other meteorites. Both the age and the initial $(^{87}Sr/^{86}Sr)_I$ are clear indications of a late time of formation. Weekeroo Station appears to be somewhat younger than Norton County in age.

2. Experimental methods

2.1. *Instrumental procedure*

As pointed out previously [5] the initial $(^{87}Sr/^{86}Sr)_I$ ratios are of great significance with regard to resolving small time differences and may permit *qualitative* distinctions in time and Rb-Sr evolution which are not resolvable by the differences in isochron slopes. In order to determine $(^{87}Sr/^{86}Sr)_I$ with some precision it is most reasonable to look at ancient objects such as meteorites or phases in meteorites with low Rb/Sr ratios and small resulting enrichments in $^{87}Sr/^{86}Sr$.

We have utilized measurement techniques with a level of precision about ten times higher than that which was previously obtainable. The isotopic composition of Sr in several basaltic achondrites has been determined using a new programmable magnetic field mass spectrometer with digital output and with on-line data processing [12].

2.2. *Interpolational procedure and statistics*

To reduce errors due to counting statistics we used high beam intensities of $1-8 \times 10^{-11}$ A ^{88}Sr; at currents above 2×10^{-11} A we used a 10^{10} Ω feedback resistor on the vibrating reed electrometer, instead of the 10^{11} Ω resistor used for lower currents, to avoid voltage effects. The filament load was typically 2×10^{-7} g Sr for the achondrite runs.

In all runs, the stability and linearity of the beam is checked by verifying that the middle ^{88}Sr peak of each three sequential ^{88}Sr peaks lies on a line through the two adjacent ^{88}Sr peaks to within better than 0.05%. This time interval corresponds to a time interval at least twice the interpolation time for obtaining ratios $^{86}Sr/^{88}Sr$ and $^{87}Sr/^{88}Sr$. During a run those data which did not satisfy this stability criterion were rejected. When this linearity criterion is satisfied, sets of ratios calculated through a simple linear interpolation and through a quadratic interpolation result in means and standard deviations which agree better than 0.01%.

As a test of the quality of the data obtained for a given experiment, use was made of the ratio of the ^{88}Sr ion beam to itself using the linear interpolation procedure. Consider the set of ^{88}Sr intensities measured at times τ_n throughout an experiment. We form the ratios (for constant $\tau_n - \tau_{n-1}$ intervals for all n)

$$R_n^{88} = \frac{^{88}Sr(\tau_{n-1}) + {}^{88}Sr(\tau_{n+1})}{2\,{}^{88}Sr(\tau_n)}$$

and

$$r_n^{88} = (R_n^{88} - 1) \times 10^4 .$$

A histogram of the values for 169 data points from one run are shown in fig. 1 (top). The distribution r_n^{88} has a mean 0.25, a standard deviation $\sigma(r_n^{88}) = 2.8$, and a standard deviation of the mean $\sigma_M(r_n^{88}) = 0.22$. The variable r_n^{88} appears to be normally distributed and thus the standard deviation of the ^{88}Sr beam itself, $\sigma(^{88}Sr)$, in parts in 10^4, may be computed as $\sigma(^{88}Sr) = \sqrt{\frac{2}{3}}\,\sigma(r_n^{88}) = 2.3$ and can be thought of as a resultant of random variables for counting statistics ($\sigma_C(^{88}Sr)$), beam instability ($\sigma_B(^{88}Sr)$), noise in the vibrating reed ($\sigma_{VR}(^{88}Sr)$) and noise in the digital voltmeter ($\sigma_{DVM}(^{88}Sr)$). These values are given for an average beam intensity of unity. This assumes that the only variation in beam intensity is due to the error variables indicated. We estimate σ_{VR} for 10^{-15} A noise and σ_{DVM} from a 0.01–0.02% instrument reproducibility for different voltage ranges. For an ion beam of 5×10^{-11} A $\sigma_C(^{88}Sr) = 0.5$ and we calculate $\sigma_B = 2.1$.

From the parameters in table 1 we find $\sigma(^{87}Sr) = 4.0$. This yields $\sigma(r_n^{87}) = \sqrt{\frac{2}{3}} \times 4.0 = 4.9$ and is to be compared with the measured value $\sigma(r_n^{87}) = 5.2$ as obtained from the histogram for the internal ratios of ^{87}Sr shown in fig. 1 (middle). A similar comparison for ^{86}Sr (table 1) between $\sigma(r_n^{86})$ calculated and measured shows them to be in essential agreement.

For the $^{87}Sr/^{88}Sr$ ratio there is an additional error due to the correction for discrimination. The correction was made as follows: (a) The discrimination factor was determined for each set of ten ratios of $^{87}Sr/^{88}Sr$ by normalizing the average $(^{86}Sr/^{88}Sr)_m$

INITIAL STRONTIUM ISOTOPIC ABUNDANCES

Table 1
Standard deviations of the random variables for isotopic ratios *

Ratio	σ_C	σ_B	σ_{VR}	σ_{DVM}	$\sigma(r_n)$ calc.	$\sigma(r_n)$ exp.	σ(Sr)	$\sigma(^{87}Sr/^{88}Sr)$ calc.	$\sigma(^{87}Sr/^{88}Sr)$ exp.
r_n^{88}	0.5	2.1**	0.2	1.0		2.8	2.3		
r_n^{87}	1.8	2.1	2.0	2.0	4.9	5.2	4.0		
r_n^{86}	1.4	2.1	2.0	2.0	4.7	5.0	3.8		
$r_n^{87/88}$								4.6	4.3

* For ^{88}Sr ion beam $\sim 5 \times 10^{-11}$ A. All quantities in parts in 10^4 for distributions with means equal to or normalized to unity.
** Calculated from elements in the same row and assumed identical for all other isotopes.

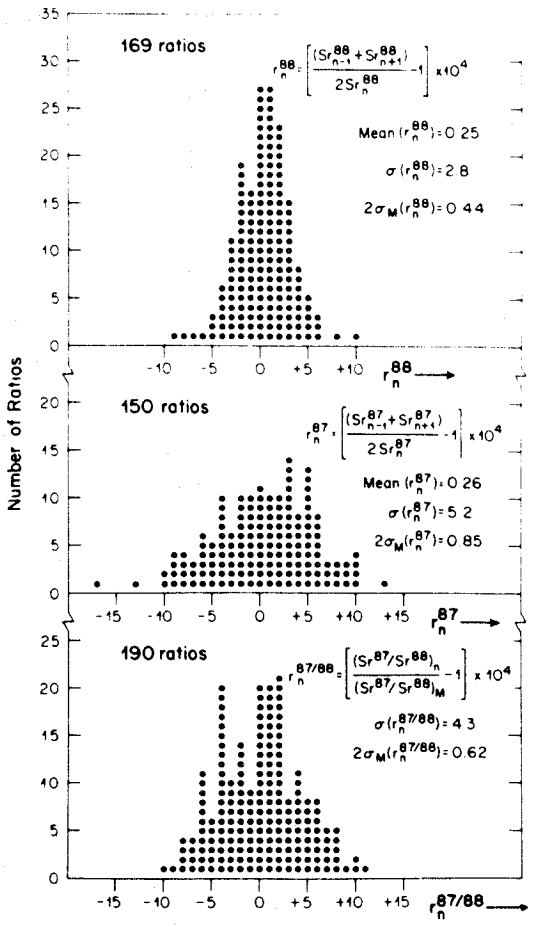

Fig. 1. Frequency distribution of ratios obtained from a single run. Nineteen sets of ten ratios each were obtained for which $\sigma_{10} \leq 0.05\%$ for $^{87}Sr/^{88}Sr$ and ^{88}Sr linearity to 0.05% at $\sim 5 \times 10^{-11}$ A. To obtain statistics of internal beam stability we form the ratios of ^{88}Sr to itself (top) and similarly for ^{87}Sr (middle). Ratios of ^{87}Sr to itself show a higher dispersion due to electronic noise. The means of the r_n^{88} and r_n^{87} distributions differ by less than σ_M from the expected mean of zero. Isotopic ratios $^{87}Sr/^{88}Sr$ corrected for discrimination and normalized to unity (bottom) have a dispersion which agrees with the dispersion calculated from the ^{88}Sr, ^{87}Sr and ^{86}Sr statistics. All deviations and means are given in parts in 10^4.

for each set of ten to 0.1194. Each $^{87}Sr/^{88}Sr$ of the corresponding set was then corrected by the appropriate discrimination factor. These results, normalized appropriately, are shown in fig. 1 (bottom).
(b) The discrimination factor was also determined from each $^{86}Sr/^{88}Sr$ ratio within a set and applied to the corresponding $^{87}Sr/^{88}Sr$ ratio. This point by point correction results in a distribution of $^{87}Sr/^{88}Sr$ ratios which have a mean indistinguishable from the ratio $(^{87}Sr/^{88}Sr)_m$ for a set of ten as calculated by method (a) but with a higher variance. No trend in $(^{87}Sr/^{88}Sr)$ within a set was seen. However, the $(^{86}Sr/^{88}Sr)_m$ for adjacent sets of ten ratios often exhibited monotonic changes of 0.01%. This implies that the changing discrimination within each set of ten ratios introduces an additional spread in the standard deviation of $^{86}Sr/^{88}Sr$.

$$(\sigma_{DISK})^2 = \sum_{n=0}^{\frac{1}{2}N-1} \frac{1}{2}\frac{(2n+1)^2}{(N-1)} q^2\tau^2 ,$$

where q is the rate of change of discrimination (sec^{-1}) and τ is the interval between ^{86}Sr peaks; $\sigma_{DISK} \approx 0.3$

for $N = 10$. Using the values for $\sigma(r_n^{88})$ measured and $\sigma(r_n^{87})$ and $\sigma(r_n^{86})$ calculated, we find, including the discrimination correction according to (a) above, $\sigma(^{87}Sr/^{88}Sr) = 4.6$. The standard deviation for the distribution in fig. 1 (bottom) is $\sigma(r_n^{87/88}) = 4.3$, in good agreement with $\sigma(^{87}Sr/^{88}Sr)$. The comparison of calculated and experimental values is shown in the last two columns of table 1. It is clear that $\sigma(^{87}Sr/^{88}Sr)$ is much larger than the ion counting statistics for these intense beams. As an estimate of the error *of the mean* we chose

$$2\sigma_M(r_n^{87/88}) = \frac{2\sigma(^{87}Sr/^{88}Sr)}{\sqrt{N}} ,$$

where N is the total number of ratios in the run. For the normalized ratios of the experiment shown $2\sigma_M = 0.62$.

For the continuous data acquisition procedure used, corrected ratios were obtained in sets of ten, and the mean $\bar{x}_{10}$ and standard deviation σ_{10} were calculated for each set. At the completion of a run, each set was classified according to three categories: I ($\sigma_{10} \leqslant 0.05\%$), II ($\sigma_{10} \leqslant 0.075\%$) and III ($\sigma_{10} \leqslant 0.15\%$). We rejected any runs in which only category III data were obtained. In order to test the character of the data, the mean $\bar{x}_M$, the standard deviation, and $2\sigma_M$ for all of the data points in each category were calculated for every run. It was found that the means were all equal, independent of the category, to within a factor of 2 better than the $2\sigma_M$ of each category (see table 3). We conclude that the data selection scheme does not introduce any significant bias and that the choice of $2\sigma_M$ for category I and II data is a good estimate of the limits of error.

2.3. *Enriched standards*

A further documentation of the resolution (of 1 part in 10^4) was done by analyses of enriched standards as well as repeat analyses of samples. For this purpose a set of synthetic standards was made up. A solution of Sr extracted from Nuevo Laredo (representing the 0 percent standard) and a solution of Sr extracted from a terrestrial microcline which had a 10% enrichment in $^{87}Sr/^{86}Sr$ relative to Nuevo Laredo, were prepared. Both solutions were passed twice through an ion exchange column to reduce the amount of Rb. Both samples were run twice on the mass spectrometer to determine Sr concentration and $^{87}Sr/^{86}Sr$ immediately before mixing. Mixtures of these two standard solutions were made and run repeatedly on the mass spectrometer. Table 2 shows the data obtained and the calculated enrichments from gravimetry. Fig. 2 shows the average measured values for the standards expressed as an enrichment in parts per ten thousand,

$$\epsilon^{S,G} = \left[\left(\frac{^{87}Sr}{^{86}Sr}\right)^{S,G} - \left(\frac{^{87}Sr}{^{86}Sr}\right)^{S}_{0}\right] \Big/ \left(\frac{^{87}Sr}{^{86}Sr}\right)^{S}_{0} \times 10^4 ,$$

where the superscript may be either G or S. G stands for the expected enrichment from gravimetry, and S for the enrichment measured on the mass spectrometer. In *this* diagram the error bars represent deviations $s = \sqrt{\Sigma(2\sigma_i)^2}\ /n$, where σ_i^2 is the variance of the mean for each of the n runs of a standard. The 45° line is drawn to facilitate the comparison. All means are less than 2×10^{-5} away from the 45° line. Standard IV is not shown but is off the line by 12×10^{-5}. From table 2 it is clear that the data for the 0.3% standard are of poor quality, but, because of the extreme enrichment, no effort was made to obtain refined measurements. From the deviations of the means off the 45° line and the extent of the error bars we conclude that we can resolve 0.01% in $^{87}Sr/^{86}Sr$. The enriched standards were particularly clean, and usually gave runs that were slightly less stable than the achondrite runs.

2.4. *Sr and Rb contamination*

Since we proposed to look at very small enrichments in $^{87}Sr/^{86}Sr$ it was critical to avoid any enrichments due to common Sr contamination or Rb background in the mass spectrometer. Typical Sr blanks obtained were $(0.7 \pm 0.3) \times 10^{-9}$ g Sr with $(^{87}Sr/^{86}Sr)_{blank} \approx 0.710$. For samples near $^{87}Sr/^{86}Sr = 0.700$ the change in $^{87}Sr/^{86}Sr$ due to contamination is 1×10^{-5} for sample sizes of 0.7 μg Sr. We typically used samples of 3 μg Sr for the analyses reported. Samples with much less Sr may present a serious contamination problem. The possible presence of Rb during the Sr mass spectrometric analyses was monitored by measuring mass 85. For composition runs the Rb ratio measured in the beginning of the Sr run of a sample is $^{85}Rb/^{87}Rb = 2.65$. We can clearly detect $^{85}Rb/^{88}Sr = 4 \times 10^{-6}$ corresponding to $^{87}Rb/^{87}Sr = 1.5 \times 10^{-5}$ for nor-

Table 2
Comparison of enriched standards: Gravimetric (G) and Spectrometric (S)

Standard	ϵ^G (a)	$\epsilon^S_{average}$ (a)	$^{87}Sr/^{86}Sr$ (b)	$2\sigma_m \times 10^4$ (b)
0	0.0	0.0	0.699739	0.84
			0.699728	0.58
I	2.69	2.60	0.699919	0.88
			0.699911	0.74
II	4.85	5.04	0.700097	0.83
			0.700074	0.64
III (c)	10.14	9.99	0.700652	0.92
			0.700349	0.99
			0.700457	0.82
			0.700301	0.70
			0.700401	1.05
IV (d)	31.0	29.8	0.701878	1.60
			0.701754	1.15

(a) In units of 10^{-4}, normalized for the 0 standard.
(b) Results of individual runs; all ratios normalized to $^{86}Sr/^{88}Sr = 0.1194$.
(c) Only category II data (~100 ratios per run).
(d) Only category II data (~40 ratios per run).

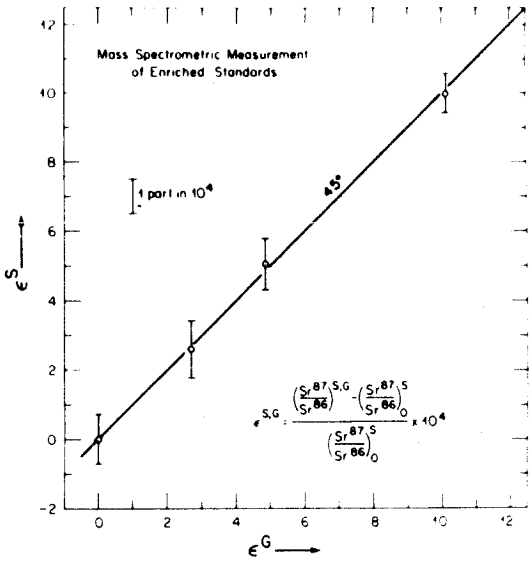

Fig. 2. Correlation of enrichments (ϵ) in $^{87}Sr/^{86}Sr$ (parts in 10^4) for standard solutions calculated from gravimetry (G) and from mass spectrometric measurements (S). Results for four standards are shown; the lowest (zero) standard is used for normalization. Error bars are estimates of error (see text) from the variance of the mean for two to five runs (table 2). Deviation of means from 45° line (3×10^{-5}) confirm a resolution of 1 part in 10^4.

mal Rb. We could always wait long enough during a run so that ^{85}Rb fell below the detectability limit. For samples spiked with both ^{84}Sr and ^{87}Rb tracers the $^{85}Rb/^{87}Rb$ ratio may be lower than that in the sample by a factor of four during Sr analyses. This would correspond to $^{87}Rb/^{87}Sr = 6 \times 10^{-5}$. The mass spectrometer used for Sr analyses has never been used for Rb analyses and no Rb is observed from a blank filament heated for prolonged times at temperatures much higher than required for Sr ionization. We conclude that any Rb present during an analysis must be coming from the sample load on the filament.

When running spiked samples a correction has to be made to obtain $^{87}Sr/^{86}Sr$ in the sample from $^{87}Sr/^{86}Sr$ measured due to ^{87}Sr and ^{86}Sr in the tracer. For $^{88}Sr_{sample}/^{84}Sr_{tracer} \approx 10$ this correction in $^{87}Sr/^{86}Sr$ amounts to two percent. If the composition of the spike is in error due to unknown discrimination by 0.5% per mass unit, the error contributed to $^{87}Sr/^{86}Sr$ is 4.4×10^{-5}. Several samples were spiked so that $^{88}Sr_s/^{84}Sr_t \approx 30$ to 50 reducing the error accordingly. Table 3 shows the ratio $^{88}Sr_s/^{84}Sr_t$ in the measured sample. From the agreement in $^{87}Sr/^{86}Sr$ for composition runs and concentration runs (better than three parts in 10^5) we conclude that this correction does not propagate any significant errors and that the Rb contribution to $^{87}Sr/^{86}Sr$ is negligible.

3. Analytical results

Analyses are presented of six basaltic achondrites. Duke and Silver [13] have presented the most recent survey of the petrology of basaltic achondrites, and give a description of the samples analyzed here. The samples were cleaned on the external surfaces by grinding with a dental burr. The chemical methods used have been described before [9]. Repeated mass spectrometric analyses were made of all samples and the results of the individual runs are shown in table 3. The Sr data are divided into different categories depending on the standard deviation σ_{10} as explained before. In this table, runs 52 and 59 for Juvinas and

Table 3
Basaltic achondrites

Category		I ($\sigma_{10} < 0.05$ %)		II ($\sigma_{10} < 0.075$ %)			III ($\sigma_{10} < 0.15$ %)	
Meteorite	Run	N *	$^{87}Sr/^{86}Sr$	N	$^{87}Sr/^{86}Sr$	N	$^{87}Sr/^{86}Sr$	$^{88}Sr_s/^{84}Sr_t$
Juvinas	52	90	0.699367 ± 57 **	170	0.699374 ± 53	270	0.699369 ± 57	nt ***
	59	170	0.699388 ± 44	220	0.699402 ± 44	290	0.699387 ± 54	12
	74					140	0.699411 ± 110	nt
	75	10	0.699304 ± 158	60	0.699456 ± 84	180	0.699408 ± 88	nt
Pasamonte	72			37	0.699595 ± 151	149	0.699481 ± 155	31
Sioux County	54	60	0.699514 ± 80	170	0.699464 ± 60	290	0.699447 ± 62	nt
	56	70	0.699468 ± 75	176	0.699485 ± 60	186	0.699503 ± 64	11
Nuevo Laredo	66	10	0.699790 ± 109	18	0.699723 ± 144	57	0.699849 ± 157	43
	69			8	0.699582 ± 497	168	0.699830 ± 147	43
Moore County	78					116	0.699100 ± 142	18
	79					119	0.699179 ± 138	18
Jonzac	53	10	0.700415 ± 210	30	0.700088 ± 182	130	0.700088 ± 95	nt
	58	35	0.700199 ± 115	159	0.700058 ± 71	170	0.700050 ± 70	10
	62					109	0.700090 ± 305	nt
	65	8	0.699922 ± 282	36	0.700049 ± 71	142	0.700025 ± 171	nt
	67	44	0.700021 ± 97	109	0.700067 ± 97	216	0.700051 ± 88	nt
Stannern	51	20	0.700470 ± 86	80	0.700454 ± 90	230	0.700436 ± 79	nt
	57	60	0.700496 ± 80	180	0.700477 ± 59	200	0.700475 ± 65	9

*Number of ratios obtained.
**Absolute errors: $\pm 2\sigma_m$.
***No tracer.
All data are normalized to ($^{86}Sr/^{88}Sr$) = 0.1194.

54 and 56 for Sioux County are the best obtained both in terms of dispersion and in terms of total number of ratios (200–300) for $^{87}Sr/^{86}Sr$. The means (I, II, III) for run 52 show a maximum variation of 0.7×10^{-5} and the means for run 59 show a maximum variation of 1.5×10^{-5} for the three different categories of data. The difference between run 52 and run 59 is 2.2×10^{-5}. These variations are well within the error defined by $2\sigma_m \sim 5 \times 10^{-5}$. In addition, runs 74 and 75, during which relatively unstable ion beams were encountered, provide means that are only $\sim 2 \times 10^{-5}$ away from the means of 52 and 59 even though the $2\sigma_m$ for these runs is worse by a factor of two. Run 75 category II is off by $\sim 7 \times 10^{-5}$ for 60 ratios measured; category I for this run contains only 10 ratios which is too small a number for meaningful comparisons even though the means happen to agree well. For the final tabulation only runs 52 and 59 were used.

Runs 54 and 56 offer similar results, with a total spread of 5×10^{-5} for both runs. Runs 51 and 57 for Stannern are at a slightly worse level of precision ($2\sigma_m \sim 8 \times 10^{-5}$) than Sioux County but still offer minimal variations in the means within each run and between the two runs ($\sim 4 \times 10^{-5}$). The Jonzac data which were obtained during less stable runs converge to the mean within a total spread of 7×10^{-5} for the categories II and III. Category I for Jonzac contains few ratios and the results are an indication of the variations expected from only one or two sets of 10 ratios. The average of run 62 has not been used in the final results since $2\sigma_m$ is 3 times larger than for the other analyses; its inclusion would not change any of the results.

Data at the level $2\sigma_m = 1.5 \times 10^{-4}$ were obtained for Pasamonte and Nuevo Laredo (runs 72, 66 and 69) and for Moore County (runs 78, 79). These data will be improved in future measurements. Moore County

Table 4
Analytical results

Meteorite	Rb (10^{-8} m/g)	^{88}Sr (10^{-8} m/g)	$^{87}Rb/^{86}Sr \times 10^2$	$^{87}Sr/^{86}Sr$	$\delta(^{87}Sr/^{86}Sr) \times 10^4$ (a)	$(^{87}Sr/^{86}Sr)_I$ (b)	$\delta(^{87}Sr/^{86}Sr)_I^{total} \times 10^4$ (c)
Juvinas	0.202	73.2	0.644	0.699378	0.36	0.698962	0.57
Pasamonte	0.242	73.5	0.769	0.699481	1.55	0.698985	1.81
Sioux County	0.228	68.4	0.775	0.699491	0.55	0.698990	0.81
Nuevo Laredo	0.380	72.1	1.228	0.699840	0.76	0.699047	1.18
Jonzac	0.519	72.4	1.671	0.700062	0.82	0.698983	1.38
Stannern	0.827	80.5	2.396	0.700475	0.60	0.698928	1.37
Moore County	0.0613	61.0	0.234	0.699140	0.99	0.698989	1.07
				$(^{87}Sr/^{86}Sr)_{BABI} = 0.698990 \pm 47$			
				$(^{87}Sr/^{86}Sr)_{JUSI} = 0.698976 \pm 55$ (d)			
Seawater				0.70912	0.9	(ref. [12])	
				0.70911	0.8	} [this work]	
				0.70905	0.8		

(a) Estimate of absolute error from all runs.
(b) Initial $(^{87}Sr/^{86}Sr)$ calculated for $\tau = 4.5 \times 10^9$ yr and $\lambda = 1.39 \times 10^{-11}$ yr^{-1}.
(c) Error includes contribution from $\delta\tau = 2.25 \times 10^8$ yr uncertainty.
(d) Best value, calculated from Juvinas and Sioux County only; maximum errors given.

is particularly important in defining the initial $(^{87}Sr/^{86}Sr)_I$ ratio. In view of the convergence of the means for similar runs (53 II, 65 III, and from enriched standards' data) we consider these poorer quality data to be reliable.

The final reduced data for the achondrites are given in table 4. Moore County has not been used in determining the isochron or in any of the arguments presented due to its poor precision with respect to Juvinas and Sioux County. However, Moore County is consistent with the data presented. Table 4 also includes our value for seawater Sr from ref. [12] and the value from some additional measurements. The results for the achondrites are plotted on an Sr evolution diagram in fig. 3. The total range in $^{87}Sr/^{86}Sr$ is 0.2%. The errors plotted are estimates (similar to s for the enriched standards) based on the best runs for each sample. The achondrite data represented in this figure appear to follow the systematics of a set of closed Rb-Sr systems of the same age and the same initial strontium isotopic composition. The line shown was calculated from a least squares fit with a weighting function according to the errors of each data point. The line has a slope of 0.0629 ∓ 0.0037 corresponding to an age of $4.39 \mp 0.26 \times 10^9$ yr, for $\lambda = 1.39 \times 10^{-11}$ yr^{-1}. The initial ratio from the best fit line for these basaltic achondrites is $(^{87}Sr/^{86}Sr)_{BABI} = 0.698990 \pm 0.000047$ (basaltic achondrite best initial $\equiv$ BABI). It is evident that the basaltic achondrites yield a well defined isochron. The deviations from the best fit line for each individual run are plotted in parts in 10^4 in fig. 4. The isochron determined is in agreement within experimental errors with that found for chondrites (see for example the recent work of Gopalan and Wetherill [14]), and is independent justification for assuming that the chondrites and achondrites may be considered to lie *approximately* on the same isochron. This isochron is not of the high precision as that obtained for Norton County and Krähenberg but is in reasonably good agreement with them. The $(^{87}Sr/^{86}Sr)_I$ for those meteorites appears to be slightly above that reported here and may represent a real difference in age or Rb-Sr evolution, although the precision of the previously published values is not sufficient to demonstrate this.

Potassium-argon ages have been measured for the achondrites reported here. The ages range from

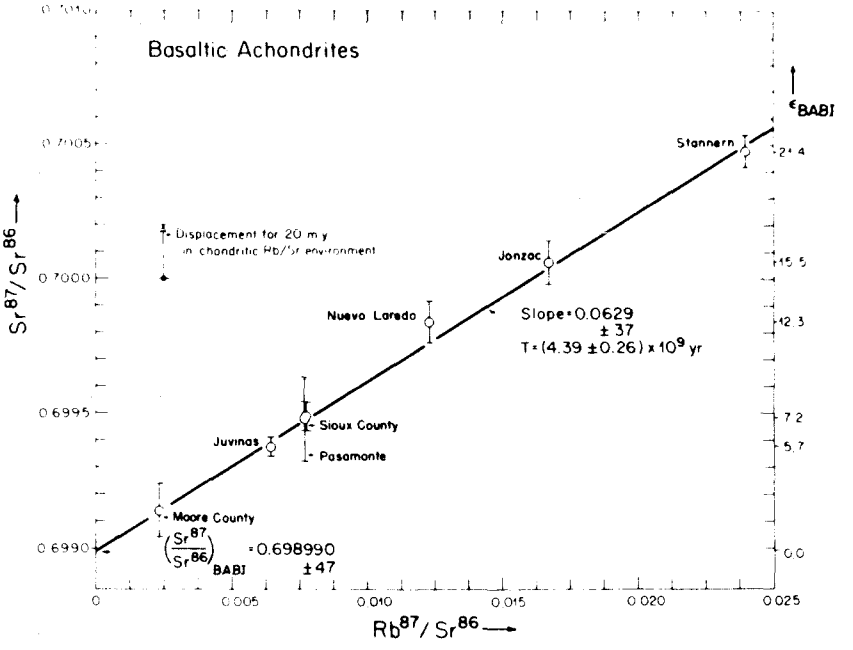

Fig. 3. Strontium evolution diagram for basaltic achondrites. Line through data points was obtained by usual least squares fit and determines age and $(^{87}Sr/^{86}Sr)_{BABI}$. See text for the determination of the initial $(^{87}Sr/^{86}Sr)$ ratio in a different way. The enrichment of each meteorite relative to $(^{87}Sr/^{86}Sr)_{BABI}$ is given on the right hand axis. The displacement shown by arrow denotes change in $(^{87}Sr/^{86}Sr)$ which would be incurred in an environment of chondritic Rb/Sr (~ 0.25) during 20 m.y. For the deviation of the data points from the best fit line see also fig. 4 ($\lambda = 1.39 \times 10^{-11}$ yr^{-1}).

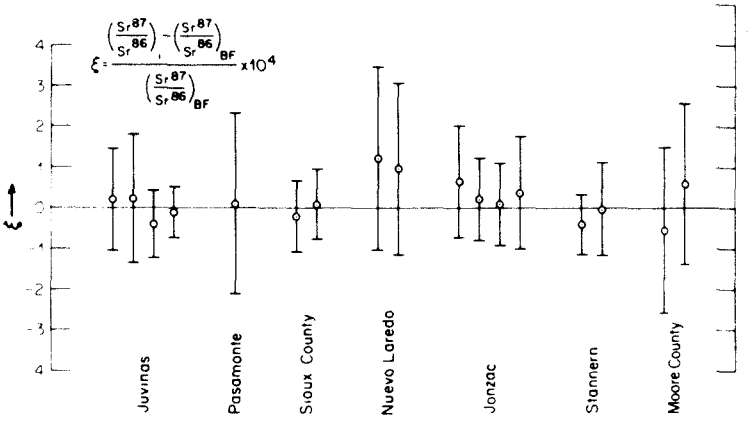

Fig. 4. Relative displacement (ξ) in parts in 10^4 of means of individual runs for basaltic achondrites from the best fit line (BF) of fig. 3. Error bars shown are $\pm 2\sigma_m$ for each run. Agreement of means for repeat runs of each meteorite are better than σ_m.

3.2×10^9 yr for Sioux County [15] to an estimated value of 4.4×10^9 yr for Jonzac [17]. Megrue [16] has reported on K-Ar correlation from different phases of Stannern and Juvinas ($\sim 4.0 \times 10^9$ yr). These argon ages indicate these meteorites to be ancient objects. Any precise interpretation of the K-Ar ages would appear to be very uncertain (see recent discussion and compilation by Heymann, Mazor and Anders [17]). The validity of Megrue's interpretation of the K-Ar ages as representing a physically meaningful event is subject to question [9].

Since the basaltic achondrites may not have co-existed with an Rb-rich reservoir for more than a few million years, younger K-Ar ages must reflect only minor thermal metamorphism which in addition did not obliterate the ^{244}Pu produced fission Xe observed in the Ca-rich achondrites [18]. From our Sr data we can place lower limits for the age of particular basaltic achondrites if we assume that they evolved from the *maximum* (errors included) initial ratio $(^{87}Sr/^{86}Sr)_{JUSI} = 0.699031$ which is determined from Juvinas and Sioux County independently from the best fit isochron (see section 4). For Stannern we obtain a minimum age $\tau = 4.2 \times 10^9$ yr. This value is slightly higher than the K-Ar age of 3.98×10^9 yr given by Megrue [16].

4. Initial $^{87}Sr/^{86}Sr$

Insofar as we may independently estimate the age (i.e., possibly ^{40}K–^{40}Ar, or ^{207}Pb–^{206}Pb as in the case of Nuevo Laredo [19]), it is evident that the initial $^{87}Sr/^{86}Sr$ is much more precisely determined than the age since the fractional change

$$\frac{d \ln (^{87}Sr/^{86}Sr)}{d (\ln \tau)} \ll 1$$

because of the low Rb/Sr ratio ($\sim \frac{1}{3}$) for most meteoritic materials. Let us consider the uncertainty in the initial (I) $(^{87}Sr/^{86}Sr)_I$ ratio resulting from both the uncertainty $\delta\tau$ in the age and the uncertainty $\delta(^{87}Sr/^{86}Sr)_m$ in the measured (m) $(^{87}Sr/^{86}Sr)_m$ ratio. We assume that the objects under investigation are closed Rb-Sr systems. Fig. 5 is a schematic diagram showing the initial ratio $(^{87}Sr/^{86}Sr)_I$ as calculated from a data point of age τ. The error in

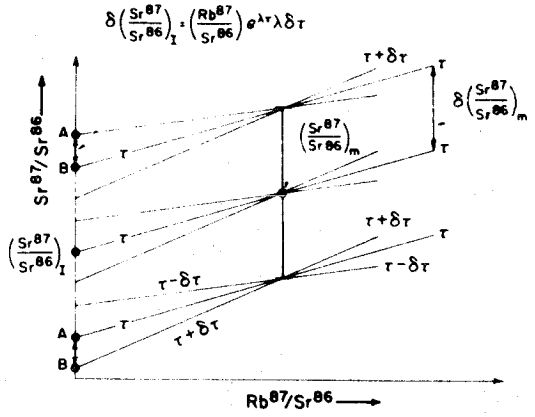

Fig. 5. Schematic illustration of the determination of initial $(^{87}Sr/^{86}Sr)_I$ from a given measured $(^{87}Sr/^{86}Sr)_m$. Uncertainty $\pm\delta\tau$ in the slope for age τ results in additional error AB to the error of the measured ratio, $\delta(^{87}Sr/^{86}Sr)_m$. AB depends on $\delta\tau$ and on the extrapolation distance and is the dominant error for high $^{87}Rb/^{86}Sr$.

$(^{87}Sr/^{86}Sr)_I$ contributed by $\delta\tau$ is $\delta(^{87}Sr/^{86}Sr)_I = (^{87}Rb/^{86}Sr)_m \exp(\lambda\tau)\, \lambda\delta\tau$ and is represented by the segment AB. In order to optimize the usefulness of the present results it is desirable to have the uncertainty $\delta(^{87}Sr/^{86}Sr)_I \ll \delta(^{87}Sr/^{86}Sr)_m$. We have typically obtained a precision for the basaltic achondrites of $\delta(^{87}Sr/^{86}Sr)_m \sim 7 \times 10^{-5}$. If we consider an uncertainty in τ of $\delta\tau = 225 \times 10^6$ yr, corresponding to a 5% uncertainty in the age, we obtain $(^{87}Rb/^{86}Sr)_m = 0.021$ when the two errors are equal. The samples Juvinas, Pasamonte and Sioux Co. have $(^{87}Rb/^{86}Sr)_m$ ratios about a factor of four less than this. It follows that the error in $(^{87}Sr/^{86}Sr)_I$ for these samples is to this order, independent of the error in τ.

The error $\delta(^{87}Sr/^{86}Sr)_I$ is given in fig. 6 as a function of the Rb/Sr ratio and the $(^{87}Sr/^{86}Sr)_m$ ratio for closed systems of age 4.5×10^9 yr and $\delta\tau = 225 \times 10^6$ yr. For $(^{87}Sr/^{86}Sr)_m = 0.702$ we obtain $\delta(^{87}Sr/^{86}Sr)_I = 1.6 \times 10^{-4}$ and for $(^{87}Sr/^{86}Sr)_m = 0.706$ we obtain $\delta(^{87}Sr/^{86}Sr)_I = 3.6 \times 10^{-4}$. These errors are all much larger than the precision of the measurements. In comparison, if $\delta\tau = 100$ m.y. (e.g. for Norton County) samples of phases with $(^{87}Sr/^{86}Sr)_m = 0.702$ or 0.706 will yield $\delta(^{87}Sr/^{86}Sr)_I = 7 \times 10^{-5}$ and 1.6×10^{-4} respectively. It follows that for $(^{87}Sr/^{86}Sr)_m = 0.702$ and only a two percent uncertainty in the age, the error

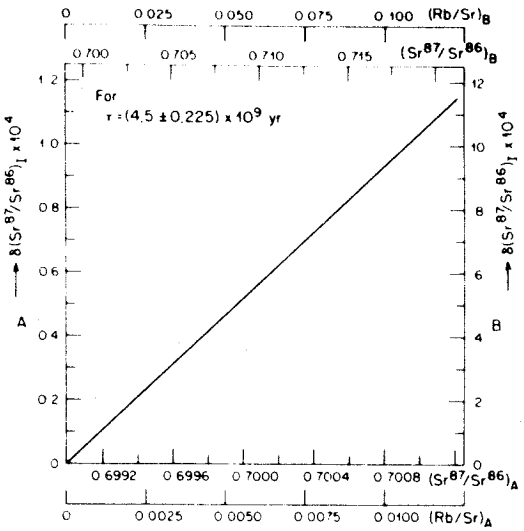

Fig. 6. Determination of the absolute error $\delta(^{87}Sr/^{86}Sr)_I$ in parts in 10^4 resulting from an extrapolation from a point of measured (Rb/Sr) to Rb/Sr = 0 for an assumed age 4.5 b.y. and a 5% uncertainty in the age. Left vertical axis (A) corresponds to lower horizontal axis, $(Rb/Sr)_A$, and right axis (B) to upper axis. On a separate scale we give the present (i.e., measured) $^{87}Sr/^{86}Sr$ of a particular closed system of the same age which evolved from $(^{87}Sr/^{86}Sr)_I = 0.699$. Only the $(^{87}Sr/^{86}Sr)_A$ and $(^{87}Sr/^{86}Sr)_B$ scales are not commensurate.

$\delta(^{87}Sr/^{86}Sr)_I$ is equal to the precision in $(^{87}Sr/^{86}Sr)_m$.

Column seven of table 4 gives the best estimate of $(^{87}Sr/^{86}Sr)_I$ for each of the samples measured assuming an age of 4.5×10^9 yr; column eight shows the maximum error $\delta(^{87}Sr/^{86}Sr)_I^{total}$ which includes $\delta(^{87}Sr/^{86}Sr)_m$ and the error $\delta(^{87}Sr/^{86}Sr)_I$ contributed by an uncertainty $\delta\tau = 2.25 \times 10^8$ yr. This range in age includes all of the Rb-Sr and ^{207}Pb-^{206}Pb values reported in the literature with the exclusion of Kodaikanal. These values are independent of any assumed relationship between the samples. The most precise values for the initial strontium are obtained from Juvinas and Sioux County (JUSI) and yield $(^{87}Sr/^{86}Sr)_{JUSI} = 0.698976 \pm 0.000055$. The errors given here are extreme limits. The value obtained is virtually identical with that obtained from the best fit line, $(^{87}Sr/^{86}Sr)_{BABI} = 0.698990 \pm 0.000047$.

5. Time resolution of a two-stage model

The relative initial $(^{87}Sr/^{86}Sr)_I$ ratios are a sensitive indicator of the differential history of various bodies. Let us assume the existence of a well mixed universal reservoir (r) with a defined $(^{87}Sr/^{86}Sr)_I^r$ and a given Rb/Sr abundance at time $\tau = 0$. In this system, for short times ($\lambda\Delta\tau \ll 1$) the $^{87}Sr/^{86}Sr$ will increase according to

$$(^{87}Sr/^{86}Sr)^r_{\Delta\tau} = (^{87}Sr/^{86}Sr)^r_I + \lambda\Delta\tau(^{87}Rb/^{86}Sr)^r_{\Delta\tau}. \quad (1)$$

Using the symbol ϵ for enrichment in parts in 10^4 relative to the value in the reservoir at $\tau = 0$,

$$\epsilon \equiv \frac{(^{87}Sr/^{86}Sr)^r_{\Delta\tau} - (^{87}Sr/^{86}Sr)^r_I}{(^{87}Sr/^{86}Sr)^r_I} \times 10^4 ,$$

we obtain

$$\Delta\tau = 1.74 \frac{\epsilon}{Rb/Sr} , \quad (2)$$

for $\lambda = 1.39 \times 10^{-11}$ yr^{-1}, and for $\Delta\tau$ in million years [(Rb/Sr) = 0.346 × ($^{87}Rb/^{86}Sr$)]. The smallest experimentally measured value of ϵ for such samples corresponds to a resolution in time interval $\Delta\tau$ which depends on the Rb and Sr elemental abundances in the reservoir. In fig. 7, we plot the relation (2) for different values of ϵ. For a typical chondrite, $^{87}Sr/^{86}Sr$ has changed from 0.699 to 0.745 in 4.6×10^9 yr, or 0.01/b.y.; to obtain an enrichment $\epsilon = 1$ in a chondritic reservoir requires a time interval $\Delta\tau = 7$ m.y. For the abundances observed in the solar photosphere, Rb/Sr = 0.65, we obtain time intervals as shown on the right strip of fig. 7, and in particular for $\epsilon = 1$, $\Delta\tau = 2.7$ m.y. Even for enrichments as large as $\epsilon = 10$ the time interval is small, only 27 m.y. In contrast, for a Rb/Sr = 0.003, which is typical of basaltic achondrites, we obtain $\Delta\tau = 640$ m.y. for $\epsilon = 1$ reflecting the rising lack of resolution in $\Delta\tau$ for systems with a very low radioactive parent-daughter ratio.

We may now consider the relation among systems (i) that become chemically fractionated and physically separated from the reservoir at different times $\Delta\tau_i$ with ratios of $(^{87}Rb/^{86}Sr)^i_{\Delta\tau_i^+}$ at $\Delta\tau_i^+$ of

$$\left(\frac{^{87}Rb}{^{86}Sr}\right)^i_{\Delta\tau_i^+} = \left(\frac{^{87}Rb}{^{86}Sr}\right)^i_{\tau} \exp[\lambda(\tau - \Delta\tau_i)] ,$$

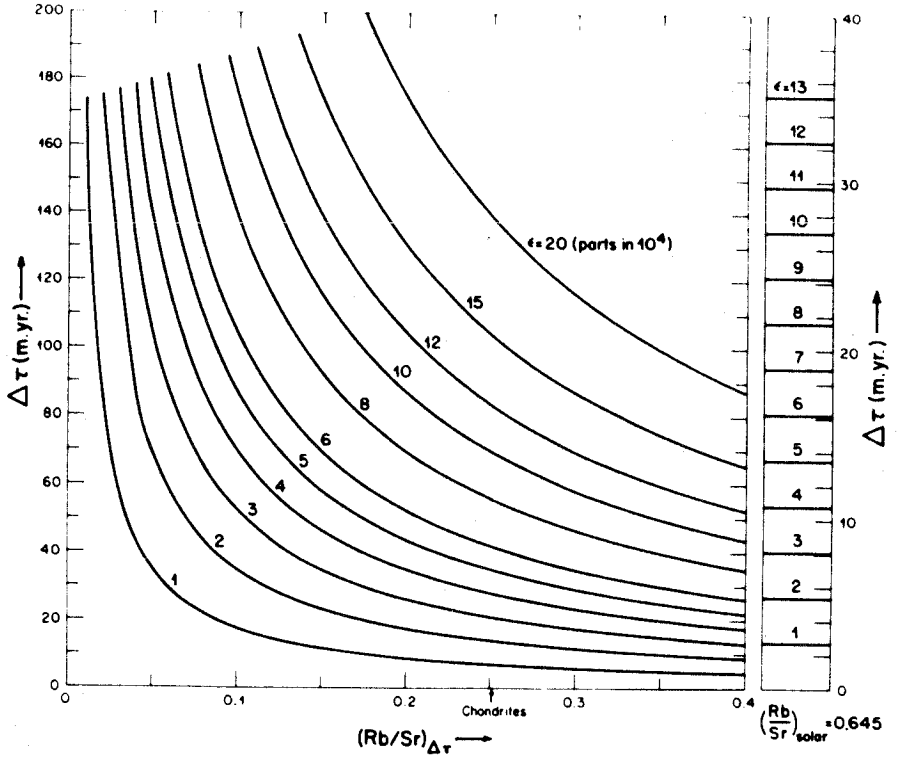

Fig. 7. Time interval in millions of years required to obtain different relative enrichments of $^{87}Sr/^{86}Sr$ (ϵ, parts in 10^4) from res dence in an environment of given $(Rb/Sr)_{\Delta\tau}$ abundance at the end of the interval $\Delta\tau$. The interval $\Delta\tau$ becomes shorter for given ϵ for higher Rb/Sr. The finer $\Delta\tau$ intervals obtained for Rb/Sr as measured in the solar photosphere are shown on the right hand strip.

where τ stands for the present. Subsequently to the fractionation and separation from the universal reservoir the systems i evolve according to

$$\left(\frac{^{87}Sr}{^{86}Sr}\right)^i_\tau = \left(\frac{^{87}Sr}{^{86}Sr}\right)^r_I + \left(\frac{^{87}Rb}{^{86}Sr}\right)^r_{\Delta\tau_i} \lambda\Delta\tau_i + \left(\frac{^{87}Rb}{^{86}Sr}\right)^i_\tau [\exp(\lambda(\tau-\Delta\tau_i))-1]. \quad (3)$$

Fig. 8 shows three such systems as they appear today on an Rb-Sr evolution diagram. The time sequence of separation is $\Delta\tau_1 < \Delta\tau_2 < \Delta\tau_3$ corresponding to

$$\left(\frac{^{87}Sr}{^{86}Sr}\right)_{\Delta\tau 1} < \left(\frac{^{87}Sr}{^{86}Sr}\right)_{\Delta\tau 2} < \left(\frac{^{87}Sr}{^{86}Sr}\right)_{\Delta\tau 3}.$$

As is clear from the diagram there is no *a priori* relationship among the points representing the systems P1, P2, P3, except that the slopes of the line segments drawn reflect the ages of the systems. By rearranging eq. (3) and taking $\lambda\Delta\tau_i \ll 1$, we obtain

$$\left(\frac{^{87}Sr}{^{86}Sr}\right)^i_\tau = \left\{\left(\frac{^{87}Sr}{^{86}Sr}\right)^r_I + \left(\frac{^{87}Rb}{^{86}Sr}\right)^i_\tau [\exp(\lambda\tau)]\right\} + \left(\frac{^{87}Rb}{^{86}Sr}\right)^r_{\Delta\tau_i} \lambda\Delta\tau_i - \left(\frac{^{87}Rb}{^{86}Sr}\right)^i_\tau \lambda\Delta\tau_i \exp(\lambda\tau). \quad (4)$$

The term in brackets on the right hand side of eq. (4) represents the $(^{87}Sr/^{86}Sr)_\tau$ of a system which was fractionated from the reservoir at time $\tau = 0$ with $(^{87}Sr/^{86}Sr)^r_I$ but with $^{87}Rb/^{86}Sr$ such that at time τ it is the same as that of system i. Fig. 9 (top) shows

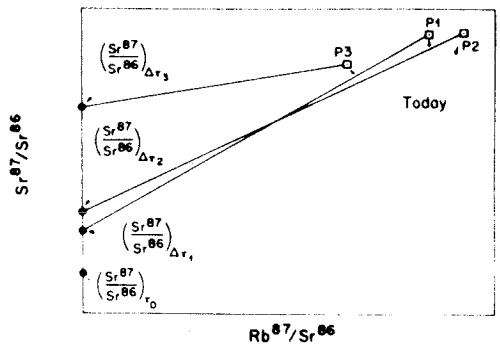

Fig. 8. Points P1, P2 and P3 represent present ratios of Rb-Sr systems experimentally measurable and are in general uncorrelated. The differential evolution of the systems is manifested by the departure of the measured points from regularity. From the points (today) we must conclude, if the systems remained closed, that either $\tau_3 > \tau_1 > \tau_2$ or that they originated from reservoirs with different initial ratios. In particular if they originated from the same reservoir at successive times $\Delta\tau_3 > \Delta\tau_2 > \Delta\tau_1$ from τ_0 they would have evolved from initial ratios $(^{87}Sr/^{86}Sr)_{\Delta\tau_1}$ as shown.

the trajectories of two such systems on an Rb-Sr evolution diagram. The two-stage system, TS, starts at $(^{87}Sr/^{86}Sr)_I^r$ and $(^{87}Rb/^{86}Sr)_0^r$, point A. The $^{87}Sr/^{86}Sr$ grows in for a time $\Delta\tau$ and the $^{87}Rb/^{86}Sr$ decays to $(^{87}Rb/^{86}Sr)_{\Delta\tau}^r$ - as indicated by the single arrow, point B. At this time the system is separated from its Rb-rich reservoir and the $^{87}Rb/^{86}Sr$ ratio decreased to $(^{87}Rb/^{86}Sr)_{\Delta\tau+}^{TS}$, as indicated by the horizontal dashed arrow, point C. The system then evolved along the double arrow to the point TS. System U starts at D and follows the trajectory of an undisturbed (U) system of age τ, initial $(^{87}Sr/^{86}Sr)_I^r$, and present $(^{87}Rb/^{86}Sr)_\tau^U$ values. The reservoir has developed to R during this time. The distance between the $(^{87}Sr/^{86}Sr)_\tau$ of TS and U is

$$\Delta\left(\frac{^{87}Sr}{^{86}Sr}\right) = \left\{\left(\frac{^{87}Rb}{^{86}Sr}\right)_{\Delta\tau}^r - \left(\frac{^{87}Rb}{^{86}Sr}\right)_0^U\right\} \lambda\Delta\tau \,.$$

If

$$\frac{(^{87}Rb/^{86}Sr)_0^U}{(^{87}Rb/^{86}Sr)_{\Delta\tau}^r} \ll 1 \,,$$

the system may be reduced to the impulsive case

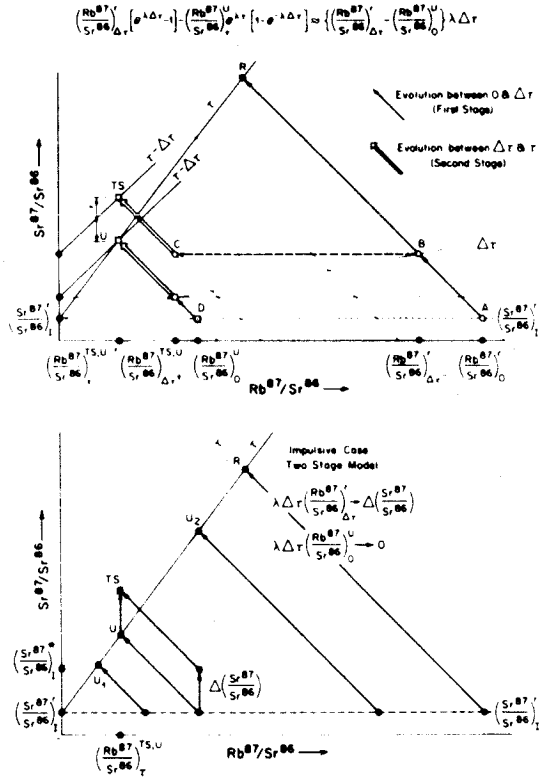

Fig. 9. (top) Strontium evolution diagram. The two-stage system (TS) originates in reservoir r at point A. The reservoir evolves to B during an interval $\Delta\tau$ at which time TS is chemically fractionated and separated from the reservoir (trajectory BC) with a ratio $(^{87}Rb/^{86}Sr)_{\Delta\tau+}^{TS}$ at C. The system evolves thereafter from C to TS (double arrow) during a time $(\tau - \Delta\tau)$. For comparison, system U has the same present $(^{87}Rb/^{86}Sr)_\tau^U$ that TS has and evolved as a closed system during a time τ from the $(^{87}Sr/^{86}Sr)_I^r$ ratio at D. The expression for the displacement TSU is given. The reservoir has evolved to R at the present. The limiting case (injection of ^{87}Sr) is shown in the lower diagram. System TS lies on an isochron of identical age as system U, but which originates at $(^{87}Sr/^{86}Sr)_I^* \equiv (^{87}Sr/^{86}Sr)_I^r + \Delta(^{87}Sr/^{86}Sr)$.

shown in fig. 9 (bottom). In the bottom diagram, systems U, U_1, U_2, and R developed undisturbed. System TS was disturbed at time zero by the addition of pure ^{87}Sr. This instantaneous change $\Delta(^{87}Sr/^{86}Sr)$ would occur if system TS coexisted for an infinitesimal time interval in a system of infinitely large $^{87}Rb/^{86}Sr$ at

any time τ. Again, U is the comparison system which has the same $(^{87}Rb/^{86}Sr)^{U}_{\tau}$ ratio as TS. Both U and TS lie on different isochrons of the same age.

For the more general case of two systems i and j chemically fractionated and separated from the reservoir r at times $\Delta\tau_i$ and $\Delta\tau_j$ with different $(^{87}Rb/^{86}Sr)^{k}_{\Delta\tau}$, k = i or j, we define the difference D:

$$D\left(\frac{^{87}Sr}{^{86}Sr}\right)^{ij} \equiv \left(\frac{^{87}Sr}{^{86}Sr}\right)^{i}_{\tau} - \left(\frac{^{87}Sr}{^{86}Sr}\right)^{j}_{\tau}$$

$$- \left[\left(\frac{^{87}Rb}{^{86}Sr}\right)^{i}_{\tau} - \left(\frac{^{87}Rb}{^{86}Sr}\right)^{j}_{\tau}\right](e^{\lambda\tau} - 1)$$

$$= \lambda\Delta\tau_{ij}\left(\frac{^{87}Rb}{^{86}Sr}\right)^{r}_{\Delta\tau_j} \qquad (5)$$

$$+ e^{\lambda\tau}\left[-\lambda\Delta\tau_i\left(\frac{^{87}Rb}{^{86}Sr}\right)^{i}_{\tau} + \lambda\Delta\tau_j\left(\frac{^{87}Rb}{^{86}Sr}\right)^{j}_{\tau}\right],$$

where $\Delta\tau_{ij} \equiv \Delta\tau_i - \Delta\tau_j$, and where we used $(^{87}Rb/^{86}Sr)^{r}_{\Delta\tau_j} \approx (^{87}Rb/^{86}Sr)^{r}_{\Delta\tau_i}$. The term $\Delta\tau_{ij}$ is the difference in the times at which the systems (i and j) were removed from the reservoir (r). For a reference age τ, the difference $D(^{87}Sr/^{86}Sr)^{ij}$, which is expressed in terms of experimentally measurable quantities, will depend on $(^{87}Rb/^{86}Sr)^{r}_{\Delta\tau_k}$, the difference in age $\Delta\tau_{ij}$ and the products $(^{87}Rb/^{86}Sr)^{k}_{\tau}\lambda\Delta\tau_k$. For determining $\Delta\tau_{ij}$ we require that

$$\left[\left(\frac{^{87}Rb}{^{86}Sr}\right)^{k}_{\tau}\Delta\tau_k \Big/ \left(\frac{^{87}Rb}{^{86}Sr}\right)^{r}_{\Delta\tau}\Delta\tau_{ij}\right] \ll 1, \qquad (6)$$

which is achieved for low $(^{87}Rb/^{86}Sr)^{k}_{\tau}$. We pick τ such that $\Delta\tau_k \ll \tau$. For the basaltic achondrites $(^{87}Rb/^{86}Sr)^{k} \cong 0.006$; for $\Delta\tau_i \approx 100$ m.y. and $(^{87}Rb/^{86}Sr)^{r}_{\Delta\tau} \approx 0.7$, for a chondritic reservoir, this condition is well satisfied for $\Delta\tau_{ij} \approx 7$ m.y. It should be noted that, for small time differences of separation, $\Delta\tau_{ij} \sim 10^6$ yr, it is necessary to choose τ with correspondingly greater accuracy in order to determine $\Delta\tau_{ij}$. However, we may choose a given system j = 0 as a reference system for which $\Delta\tau_0 = 0$. This avoids the necessity of using approximation (6), and we may then construct a sequential time classification for different samples using the values of $\Delta\tau_{i0}$ determined from D^{i0} (with due consideration of the error in τ).

The maximum difference which can be formed for all of the data points is $D(^{87}Sr/^{86}Sr)^{ij}_{max} = 9 \times 10^{-5}$ which yields $(\Delta\tau_{ij})_{max} = 9 \times 10^6$ yr for an Rb/Sr ratio of 0.25. If we exclude Nuevo Laredo, $D(^{87}Sr/^{86}Sr)^{ij}_{max} = 4 \times 10^{-5}$ and $(\Delta\tau_{ij})_{max} = 4 \times 10^6$ yr, indicating that all these samples were formed within this extremely narrow time band, and that Nuevo Laredo is $\sim 7 \times 10^6$ yr younger than the other meteorites. The Rb/Sr ratio in the photosphere as reported in detail by Lambert [20] is 0.65 ± 0.33. The uncertainties cited here are considered by Lambert (personal communication) to represent the *limits* of error. There is thus no indication of an Rb/Sr ratio significantly lower than ~0.25 for the solar system abundances from considerations of Lambert's observations or the average results on chondrites. If this high ratio (Rb/Sr = 0.65) is representative of the solar abundance then, for $D(^{87}Sr/^{86}Sr)^{ij}_{max} = 4 \times 10^{-5}$, the maximum time difference between the separation of the basaltic achondrites from the solar nebulae is $(\Delta\tau_{ij})_{max} = 1.6 \times 10^6$ yr.

The time resolution represented by these considerations is far smaller than the classical Kelvin-Helmholtz contraction time ($\sim 3 \times 10^7$ yr) or any of the more detailed time scales leading up to hydrogen burning for the sun (for example, see ref. [21], table 3). If the planets condensed over the whole time period during which the proto-sun was transferring angular momentum, it follows that a time of $\sim 10^6$ yr should be considered in calculations of this process [22]. The relationship of the solar evolution time scales and the times required to form planetary objects is not at present understood. Our results mean that if the planetary objects investigated were condensed out of the solar or planetary nebulae at different times $\sim 2 \times 10^6$ yr we would observe effects. Since our data indicate no differential effects we conclude that the times of condensation were less than this, assuming that the samples studied are representative of several planetary bodies.

In the preceding discussion we considered possible parent systems with Rb/Sr ratios much larger than those in basaltic achondrites. As pointed out by Gast [26] the terrestrial Rb/Sr ratio is low as compared with the chondritic ratio. If the basaltic achondrites are derived from planets with a low Rb/Sr parent material, such as the earth, our resolution of time is proportionately poorer. For example for Rb/Sr = 0.02, $(\Delta\tau_{ij})_{max} = 50$ m.y. for $D(^{87}Sr/^{86}Sr)^{ij}_{max} = 4 \times 10^{-5}$.

An alternative to the preceding broad generalizations is to assume that the samples analyzed represent the debris of one body which formed and differentiated rapidly or was initially well mixed and had a low Rb/Sr ratio.

No gross differences ($\epsilon \sim 20$) appear from considering the less precise data on initial $^{87}Sr/^{86}Sr$ in a variety of other types of meteorites (chondrites, enstatite achondrites, and iron meteorites) of quite different cosmic ray exposure ages. The only clear exceptions are Kodaikanal and Weekeroo Station.

Estimates of these differential times $\Delta\tau_{ij}$ can be made for the earth as compared with the basaltic achondrites. Measurements of terrestrial $(^{87}Sr/^{86}Sr)$ for many recent basaltic rocks [23] and other rocks [24] give values from 0.7025 to as low as 0.7011. This value is clearly an upper limit to the initial $^{87}Sr/^{86}Sr$ for the earth. The near equality of $^{87}Sr/^{86}Sr$ in some terrestrial samples with the value found in basaltic achondrites was first recognized by Gast [26] to have time-genetic implications. If the earth is *younger* than the basaltic achondrites and if it formed from a reservoir characterized by $(^{87}Sr/^{86}Sr)_{BABI}$ and with chondritic Rb/Sr abundance ratios, or solar photosphere Rb/Sr abundance ratios the maximum age difference is $\Delta\tau = 210$ m.y. or $\Delta\tau = 80$ m.y. respectively. This is a strict upper limit since a substantial part of this enrichment is due to Rb decay subsequent to the formation of the earth. An extensive search for old terrestrial samples containing more primitive Sr will be carried out in order to establish stricter limits.

Considering the nature of lunar surface material both with respect to its chemical composition [25] and probable great age it should prove possible to place much stricter limits on the differential formation time for the moon and the achondrites when materials are returned from the forthcoming Apollo mission.

We now examine the extension of these arguments to a three-stage model. A system i starts evolving at $\tau = 0$ in a reservoir A for an interval $\Delta\tau_i^A$ and continues to evolve for a subsequent interval $\Delta\tau_i^B$ in a second reservoir B until its final chemical fractionation and separation from reservoir B. We may form the difference $D(^{87}Sr/^{86}Sr)_\tau^{ij}$ for two such systems i and j, and neglecting terms of order $\lambda\Delta\tau_k(^{87}Rb/^{86}Sr)^k$,

$$D\left(\frac{^{87}Sr}{^{86}Sr}\right)_\tau^{ij} = \left(\frac{^{87}Rb}{^{86}Sr}\right)_{\Delta\tau}^{A} \lambda(\Delta\tau_i^A - \Delta\tau_j^A) + \left(\frac{^{87}Rb}{^{86}Sr}\right)_{\Delta\tau}^{B} \lambda(\Delta\tau_i^B - \Delta\tau_j^B) . \quad (7)$$

For this model, the vanishing of D does not necessarily imply simultaneity. To obtain some limits on the total time difference $\Delta\tau_{ij}$ between systems i and j $[\Delta\tau_{ij} = (\Delta\tau_i^A + \Delta\tau_i^B) - (\Delta\tau_j^A + \Delta\tau_j^B)]$ we can consider the case where A is an environment of solar Rb/Sr abundance and B an environment of chondritic Rb/Sr abundance. The minimum and maximum values of $\Delta\tau_{ij}$ *for a given value of* D are obtained for residence only in A or B respectively. These limits (1.6 and 4 m.y. respectively) are the same as those discussed earlier. The two systems i and j, however, may be subjected to compensating enrichments in the two successive reservoirs which would tend to increase $\Delta\tau_{ij}$ for a given value of D. Such compensating enrichments for many different bodies are not very probable.

By the same argument if different basaltic achondrites were formed according to this particular three-stage model from different chondrites, strict limits (~ 2 m.y.) can be placed on the time interval between the formation of these chondrites from the solar nebula.

The basaltic achondrites are certainly not primary bodies which condensed directly from the solar or planetary nebula. They are most probably the result of magmatic differentiation from some more primitive material as manifested by their textures and chemical composition.

A variety of arguments have been presented against the basaltic achondrites being derived from chondritic material [13, 26]. These arguments are based on differences in isotopic [27] as well as chemical abundances. The chemical and physical evolution of meteorites is at best only poorly understood and any inferred genetic relationships remain obscure.

In our discussion of the Rb-Sr evolution of various objects, we refer to chondritic Rb/Sr abundance ratios of ≈ 0.25. This value is typical of both the very abundant normal chondrites and the rare carbonaceous chondrites. Models in which the chondritic *ratio* is assumed do not necessarily imply that the material itself is of total chondritic composition.

The same arguments applied to the formation of basaltic achondrites from the planetary nebulae or the chondrites can be applied to the problem of the metamorphism of the chondrites. Such metamorphism with concommitant redistribution of elements (Fe, Mg, Rb? Sr?) would result in higher apparent "initial" ($^{87}Sr/^{86}Sr$). In the case of metamorphism the problem of defining the Rb/Sr in the "universal" reservoir is eliminated since we may measure the Rb/Sr in the total meteorite and $(^{87}Sr/^{86}Sr)_{BABI}$ may be used as the reference value. A time interval $\Delta\tau_{BACH}$ is thus defined depending on the enrichment of the meteoritic $(^{87}Sr/^{86}Sr)_I$ over $(^{87}Sr/^{86}Sr)_{BABI}$ due to the Rb decay in the meteorite before the metamorphism,

$$\Delta\tau_{BACH} \equiv [(^{87}Sr/^{86}Sr)_I^{met} - (^{87}Sr/^{86}Sr)_{BABI}] \times [\lambda(^{87}Rb/^{86}Sr)^{met}]^{-1}$$

In particular, if we can separate Ca-rich, Rb-poor phases from chondrites with low enough $^{87}Rb/^{86}Sr$, we can detect differences in $(^{87}Sr/^{86}Sr)_I$ due to metamorphism. During preliminary investigations we have separated 10^{-3} g of whitlockite, 99% pure, from the St.Séverin amphoterite. From a run of comparatively poor quality we obtain $(^{87}Sr/^{86}Sr)_m$ = 0.70357 ± 0.0002 and $(^{87}Rb/^{86}Sr)_m$ = 0.058, Rb = 0.61 ppm, Sr = 30 ppm. For this Rb/Sr ratio we obtain $\delta(^{87}Sr/^{86}Sr)_I = 0.0002$ for $\delta\tau = 2.25 \times 10^8$ yr. By correcting for Rb decay over 4.5×10^9 yr we obtain $(^{87}Sr/^{86}Sr)_I^{met} = 0.6998 \pm 0.0004$. For $(^{87}Rb/^{86}Sr)_m = 0.175$ measured for a "total" sample of this meteorite we obtain $\Delta\tau_{BACH}$ = 320 ± 160 m.y. for the time of metamorphism in St. Séverin. An attempt is under way to improve the precision of this result. If instead of metamorphism, the $(^{87}Sr/^{86}Sr)_I^{met}$ for St. Séverin is higher than $(^{87}Sr/^{86}Sr)_{BABI}$ due to enrichment in the solar reservoir we obtain for the differential formation of St. Séverin and the basaltic achondrites $\Delta\tau$ = 31 ± 15 m.y.

6. Conclusions

The time resolution for the models proposed is comparable to the "sharp isochronism" reported by Hohenberg, Podosek and Reynolds [28] using the ^{129}I - ^{129}Xe decay scheme. The intervals measured by these two methods are not in principle the same. The ^{129}I - ^{129}Xe method determines cooling time differences among objects with respect to gas retention. The Rb-Sr method determines differences in time of formation of objects which are not necessarily cold. Hohenberg et al. determined that 10 chondrites cooled to a temperature at which ^{129}Xe (produced by ^{129}I decay) is retained to within 2.5 m.y. of each other. Unfortunately there is no overlap between our samples and theirs. While the basaltic achondrites appear to represent a very narrow time window and the chondrites studied by Hohenberg et al. also represent a narrow time window it is evident that these are fundamentally different times since the chondrites show marked excess of ^{129}Xe while the achondrites show (in one case) a marked fission excess in the heavy xenon isotopes but no detectable ^{129}Xe excess. This is presumably due to the longer half life of ^{244}Pu and would imply that the achondrites are "younger" than the chondrites with regard to heating. It remains to be demonstrated that this is actually compatible with the $(^{87}Sr/^{86}Sr)_I$ values in chondrites.

The precision in measuring $(^{87}Sr/^{86}Sr)$ obtained opens up a new dimension in applications. We may now be able to determine internal isochrons for the basaltic achondrites (e.g., Stannern). Furthermore, precise isochrons can be obtained for samples even when the variation in Rb/Sr is very small resulting in only a small difference in $^{87}Sr/^{86}Sr$. For geologic problems our resolution in $^{87}Sr/^{86}Sr$ can result in the age determination of samples as young as 5×10^4 yr for Rb/Sr = 300. This Rb/Sr ratio is typically found in a large number of biotites. This will furnish a link to the ^{14}C dating method and a check of K-Ar dating for young rocks. The only obvious difficulty is the problem of defining an initial strontium in a given rock sample. However, the Rb-Sr systematics displayed by different mineral phases and total rock samples should make any natural contamination problems manifest.

Acknowledgement

The samples studied were obtained through the generous cooperation of several institutions: G.Kurat, Naturhistorisches Museum, Vienna (Jonzac, Stannern);

C.B.Moore, Ninninger Collection, Arizona State University (Juvinas, Moore County, Pasamonte, Sioux County); L.T.Silver, California Institute of Technology (Nuevo Laredo); and P.Pellas and F.Kraut, Musé National d'Histoire Naturelle, Paris (St. Séverin). This work was supported by grants from the National Science Foundation (GP-7976, GP-9114), and in part by a contract from the National Aeronautics and Space Administration (NRG-05-002-044). We were privileged to have the benefit of frequent discussions with D.S.Burnett, and constructive criticisms from W.A.Fowler, P.Gast and G.Wetherill. We would like to thank Pai Young and Uwe Derksen for their efforts in maintaining the Lunatic I spectrometer in the operating condition necessary for this work. Both of us would like to thank Professor T.Lauritsen for having directed one of us (D.A.P.) into this field.

References

[1] E.Schumacher, Alterbestimmung von Steinmeteoriten mit der Rubidium-Strontium-Methode, Z.Naturforsch. 11a (1956) 209.
[2] L.F.Herzog and W.H.Pinson, Rb/Sr age, elemental and isotopic abundance studies of stony meteorites, Am. J. Sci. 254 (1956) 555.
[3] R.K.Webster, J.W.Morgan and A.A.Smales, Some recent Harwell analytical work on geochronology, Trans. Am. Geophys. Union 38 (1957) 543.
[4] P.W.Gast, The isotopic composition of strontium and the age of stone meteorites – I, Geochim. Cosmochim. Acta 26 (1962) 927.
[5] D.D.Bogard, D.S.Burnett, P.Eberhardt and G.J.Wasserburg, Rb^{87}-Sr^{87} isochron and K^{40}-Ar^{40} ages of the Norton County Achondrite, Earth Planet Sci. Letters 3 (1967) 179.
[6] D.S.Burnett and G.J.Wasserburg, Rb^{87}-Sr^{87} ages of silicate inclusions in iron meteorites, Earth Planet. Sci. Letters 2 (1967) 397.
[7] G.J.Wasserburg and D.S.Burnett, The status of isotopic age determinations on iron and stone meteorites, Intern. Symposium on Meteorite Research, Vienna (1968), in: Meteorite Research, ed. Millman (D.Reidel Publ. Co.) to be published.
[8] G.J.Wasserburg, D.S.Burnett and C.Frondel, Strontium-rubidium age of an iron meteorite, Science 150 (1965) 1814.
[9] D.S.Burnett and G.J.Wasserburg, Evidence for the formation of an iron meteorite at 3.8×10^9 yr, Earth Planet. Sci. Letters 2 (1967) 137.
[10] W.Kempe and O.Muller, The stony meteorite Krahenberg: Its chemical composition and the Rb-Sr age of the light and dark portions, Meteorite Research, ed. Millman, to be published.
[11] M.Shima and M.Honda, Determination of rubidium-strontium age of chondrites using their separated components, Earth Planet. Sci. Letters 2 (1967) 337.
[12] G.J.Wasserburg, D.A.Papanastassiou, E.V.Nenow and C.A.Bauman, A programmable magnetic field mass spectrometer with on line data processing, Rev. Sci. Instr. (February, 1969).
[13] M.B.Duke and L.T.Silver, Petrology of eucrites, howardites and mesosiderites, Geochim. Cosmochim. Acta 31 (1967) 1637.
[14] K.Gopalan and G.W.Wetherill, Rubidium-strontium age of hypersthene (L) chondrites, J. Geophys. Res. 73 (1968) 7133.
[15] T.Kirsten, D.Krankowsky and J.Zähringer, Edelgas- und Kalium-Bestimmungen an einer grösseren Zahl von Steinmeteoriten, Geochim. Cosmochim. Acta 27 (1963) 13.
[16] G.H.Megrue, Rare-gas chronology of calcium-rich achondrites, J. Geophys. Res.71 (1966) 4021.
[17] D.Heymann, E.Mazor and E.Anders, Ages of calcium-rich achondrites, I. Eucrites, Geochim. Cosmochim. Acta 1968 (preprint).
[18] M.W.Rowe and P.K.Kuroda, Fissiogenic xenon from the Pasamonte meteorite, J. Geophys. Res. 70 (1965) 709.
[19] C.C.Patterson, Age of meteorites and the earth, Geochim. Cosmochim. Acta 10 (1956) 230.
[20] D.L.Lambert and B.Warner, The abundances of the elements in the solar photosphere – V, The Alkaline Earths, Mg, Ca, Sr, Ba, Mon. Not. Roy. Astr. Soc. 140 (1968) 197. D.L.Lambert and E.A.Mallia, The abundances of the elements in the solar photosphere VI, Rubidium, Mon. Not. Roy. Astr. Soc. 140 (1968) 13.
[21] I.Iben Jr., Stellar evolution, I. The approach to the main sequence, Appl. J. 141 (1965) 993.
[22] F.Hoyle, On the origin of the solar nebula, Royal Ast. Soc. Quart. J. 1 (1960) 28.
[23] M.Tatsumoto, C.E.Hedge and A.E.Engel, Potassium, Rubidium, Strontium, Thorium, Uranium and the ratio Sr^{87}/Sr^{86} in Oceanic Tholeiitic Basalt, Science 150 (1965) 886.
[24] C.E.Hedge and F.G.Walthall, Radiogenic Strongtium-87 as an index of geologic processes, Science 140 (1963) 1214.
[25] A.L.Turkevich, E.J.Franzgrote and J.H.Patterson, Science 158 (1967) 635; Science 160 (1968) 1108; Science 162 (1968) 117.
[26] P.W.Gast, Limitations on the composition of the upper mantle, J. Geophys. Res. 65 (1960) 1287.
[27] H.P.Taylor, Jr., M.B.Duke, L.T.Silver and S.Epstein, Oxygen isotope studies of minerals in stony meteorites, Geochim. Cosmochim. Acta 29 (1965) 489.
[28] C.M.Hohenberg, F.A.Podosek and J.H.Reynolds, Xenon-Iodine dating: Sharp isochronism in chondrites, Science 156 (1967) 233.

EARTH AND PLANETARY SCIENCE LETTERS 7 (1969) 33–43. NORTH-HOLLAND PUBLISHING COMP., AMSTERDAM

INITIAL STRONTIUM FOR A CHONDRITE AND THE DETERMINATION OF A METAMORPHISM OR FORMATION INTERVAL

G.J.WASSERBURG, D.A.PAPANASTASSIOU and H.G.SANZ *
*Charles Arms Laboratory of Geological Sciences **, California Institute of Technology, USA*

Received 5 August 1969

A precise Rb-Sr internal isochron was determined for Guareña, an H6 chondrite, yielding an age of $4.56 \pm 0.08 \times 10^9$ years. Rb-poor, Sr-rich phosphate phases (whitlockite and apatite) were obtained resulting in a precise measurement of the initial Sr isotopic composition $(^{87}Sr/^{86}Sr)_I = 0.69995 \mp 0.00015$. It is shown that from precise age and initial $(^{87}Sr/^{86}Sr)_I$ measurements we can obtain information on the differential evolution of Rb-Sr systems involving either simple metamorphism of closed systems or multi-stage processes. The high initial ratio obtained for Guareña with respect to the value for the basaltic achondrites is the first clear demonstration of differential Sr evolution of a chondrite and affords the simple explanation of Guareña having been metamorphosed 74 million years after its formation. This approach may yield a "time" evolution index for the classification of meteorites.

1. Introduction

This paper demonstrates the feasibility of obtaining a precise initial (indicated by the subscript I) $(^{87}Sr/^{86}Sr)_I$ for a chondrite by measuring phases with very low Rb/Sr in the meteorite. This approach has been shown to have the potential of yielding much more refined genetic information than can be obtained by doing the conventional "total rock" analyses on meteorites. Papanastassiou and Wasserburg [1] *** reported on preliminary results obtained for the St. Severin amphoterite. From the enrichment of the measured $(^{87}Sr/^{86}Sr)_I$ in St. Severin over the precise initial ratio obtained for the basaltic achondrites $[(^{87}Sr/^{86}Sr)_{BABI}]$ they calculated a time interval for metamorphism of this meteorite assuming the enrichment was due to the decay of ^{87}Rb in this object. This interval,

$$\Delta\tau_{BACH} \equiv [(^{87}Sr/^{86}Sr)_I - (^{87}Sr/^{86}Sr)_{BABI}] \times [\lambda(^{87}Rb/^{86}Sr)_I]^{-1},$$

is equal to 320 ± 160 m.y. for St. Severin. However, St. Severin is not an optimal case for such a calculation because the Rb/Sr in the total meteorite is less by a factor of four than in typical chondrites, resulting in a diminished time resolution.

Sanz and Wasserburg [2] have recently demonstrated the feasibility of obtaining a relatively precise ^{87}Rb–^{87}Sr internal isochron for the Olivenza (LL5) chondrite by analyzing individual chondrules and different density fractions. These authors have reviewed the previous attempts at obtaining internal isochrons for chondrites.

The emphasis in the present investigation is placed on $(^{87}Sr/^{86}Sr)_I$, which is of great significance in resolving qualitative, small time differences not resolvable by the differences in isochron slopes. To determine this initial ratio, Ca-rich phases exhibiting very low enrichments of $^{87}Sr/^{86}Sr$ were separated from the meteorite Guareña which fell in Guareña, Badajoz (Spain) on July 20, 1892. S.Calderon and F. Quiroga [3] described the fall and reported on the petrology. By courtesy of the Museo Nacional de Ciencias Naturales de Madrid, a mass of Guareña was shipped to this laboratory for investigation.

* On leave from the Junta de Energia Nuclear, Direccion de Quimica e Isotopos, Madrid, Spain.
** Contribution Number 1655.
*** Hereafter referred to as Paper I.

2. Experimental methods

2.1. *Sampling*

Three different types of samples were prepared:

A) a powdered total meteorite sample from which only the metallic phase was removed;

B) a non-magnetic mineral separate obtained by repeated passing of a sieved sample through a Frantz magnetic separator; and

C) density fractions from sieved samples.

The letters (A, B and C) correspond to the entries in table 1. The sample fractions obtained are described below:

A) *Whole Meteorite.* Two parallel cuts were made on the main mass using a diamond blade and no lubricant. A sample fragment (17 g) was ground, and the metallic phase was removed by a covered hand magnet. The remaining sample (12.5 g) was split into several whole meteorite fractions.

B) *Frantz Separate.* A sieved sample of 100 g (60–150μ) was used for magnetic separations *only*. Repeated passes were made through the Frantz by gradually increasing the magnetic field and by decreasing the tilt of the trough to 1.5° at a constant 15° inclination. A new trough was machined for this instrument from Al and was modified by covering it completely with a thin Al plate so as to eliminate cross contamination from previous samples passed through the Frantz. After each pass, the magnetic and nonmagnetic fractions were monitored for enrichments in phosphate minerals. Manipulations were performed by placing a sample on a stainless steel microscope slide locked on an *x-y* micrometer stage (see fig. 1). A Singer micromanipulator (Mark I) with a fine-tipped tungsten needle wetted with an appropriate agent was used for picking up individual grains and transferring them to a separate slide. For the purpose of counting phosphate grains, the sample was placed on one slide and a drop of HCl placed on the second slide. The stage was translated until the HCl drop was below the needle and a grain was lowered into it. Phosphate grains became cloudy and covered with bubbles upon contact with the acid and dissolved readily. Usually, 100–200 grains were picked for counting. For the purpose of picking grains for chemical analysis, a clean stainless steel slide with a trough filled with a heptadecane-hexadecane mixture (2:1) was used. This setup is shown in fig. 1a. The needle of the micromanipulator was dipped in the trough and then raised. The stage was moved until the desired grain appeared in the field of view. It was then touched with the needle to which it adhered by surface tension. The stage again was moved so that the trough was in the field of view and the needle with the attached grain was lowered into the trough. This breaks the surface tension and releases the grain immediately. An adjustable stop (S in fig. 1a) was used to stop the Y motion of the stage when the trough was in the center of the field of view. This operation could be carried out with high speed and with positive action without removing the operator's eyes from the ocular. The grains in the trough could be quantitatively transferred by rinsing them out with acetone.

The final separates were checked for purity using an electron microprobe. Grain mounts were set up as shown in fig. 1b. Pieces of double-stick scotch tape were placed on a stainless steel microscope slide with engraved circular marks. Using the micro-manipulator, grains were ordered in parallel rows in each circle. A brass disc with appropriately located circular openings was lowered on the slide and the openings carefully filled from the side with epoxy resin from an eye dropper to minimize the formation of air bubbles. A thin glass slide was used for firm backing. After the epoxy had set, the scotch tape was removed and the grain mount polished. Almost every grain mounted was exposed upon polishing. Grain counts were then obtained by electron beam scanning. The phosphate counts were in agreement with the acid dissolution results. The microprobe analysis showed that two-thirds of the phosphates were whitlockite and one-third chlorapatite (5% Cl, 0.5% F). An analysis of the olivine gave $Fo_{82}Fa_{18}$ and an analysis of the feldspar gave $Ab_{76}Or_4An_{20}$. The purest phosphate fraction obtained by using *only* the Frantz (sample B in table 1) gave a microprobe grain count of 12% feldspar and 88% phosphate.

C) *Density fractions.* A sieved sample of 193 g (60–105μ) was obtained for mineral separations using methylene iodide-acetone mixtures. Both components of the mixtures had been filtered before using and were stored in plastic bottles. All laboratory ware was teflon or polyethylene. No centrifuging was necessary to obtain good separa-

Table 1
Analytical results.

Sample	Weight dissolved mg	Rb 10^{-8} mol/g	^{88}Sr 10^{-8} mol/g	$^{87}Sr/^{86}Sr$	$^{87}Rb/^{86}Sr$
GUAREÑA		(a)	(a)	(a) (b)	(b)
A) Whole meteorite					
1) EZ-a	43.3	3.78	10.08	0.75665 ± 8	0.873 ± 17
2) E-α	97.8	4.11	11.00	0.75710 ± 50	0.869 ± 12
3) E-x	35.0	4.21	11.30	0.75680 ± 110	0.864 ± 11
B) "Phosphate" (Frantz only)	6.0	9.77	68.16	0.72155 ± 12	0.334 ± 7
C) Density fractions					
I. CH_2I_2–CH_3COCH_3					
1) $\rho > 3.3$	264.0	1.64	4.348	0.75827 ± 7	0.875 ± 18
2) $\rho < 2.7$ (feldspar)	59.4	28.4	78.19	0.75435 ± 11	0.845 ± 17
3) $3.09 < \rho < 3.20$ (phosphate)	5.9	1.10	60.24	0.70283 ± 7	0.0427 ± 9
II. CH_2I_2–CH_3COCH_3 Phosphate & Frantz					
1) No treatment	4.1	0.95	64.24	0.70225 ± 12	0.0345 ± 7
2) CH_2I_2 (24 h)	3.2	0.90	61.23	0.70234 ± 13	0.0344 ± 7
3) Supernatant (0.5N HCl)	1.8	0.88	67.57	0.70189 ± 9	0.0304 ± 6
III. $C_2H_2I_2$–CH_3COCH_3 (15 min) phosphate	3.8	1.20	43.15	0.70416 ± 12	0.0647 ± 13
IV. $C_2H_2Br_4$–CCl_4					
1) $\rho < 2.9$ (feldspar)	3.4	33.8	97.29	0.75240 ± 8	0.808 ± 16
2) $\rho > 2.9$ (phosphate)	3.4	1.17	63.82	0.70261 ± 8	0.0425 ± 8
MOORE COUNTY	–	0.060	61.0	0.69914 ± 10 (c)	0.00230 ± 5
				0.69912 ± 5 (d)	
				0.69910 ± 6 (d)	
SEAWATER				0.70912 ± 9 (f)	
				0.70908 ± 8 (c)	
				0.70911 ± 5 (d,e)	

(a) Rb concentrations calculated using $^{85}Rb/^{87}Rb = 2.591$. Sr results have been normalized to $^{86}Sr/^{88}Sr = 0.1194$ and calculated using $^{84}Sr/^{88}Sr = 0.00675$ in natural strontium.
(b) Errors correspond to the last significant figures.
(c) From reference [1]; (d) present work; (e) average of 9 runs for which the total spread of the means of individual runs $\epsilon = \pm 0.00005$; (f) from reference [4].

tions. Fractions $\rho > 3.3$, $\rho \approx 3.14$ (phosphate), and $\rho < 2.7$ (feldspar) were obtained. We obtained 40 mg phosphate 90% pure, and passed it through the Frantz several times to obtain 99% pure phosphate (Sample C.I.3). A part of this sample was further separated on the Frantz, and aliquots were taken for the leaching experiments described later. The lower purity fractions obtained as a by-product of the Frantz processing which yielded sample B were subjected to a density separation using methylene iodide and acetone. The total exposure time of this sample (C.III) to the heavy liquids was ~ 15 min, and the sample contained about 7% impurities (approximately equal amounts of feldspar and of olivine and pyroxene).

A different separation was performed by using only $C_2H_2Br_4$ ($\rho = 2.96$) and CCl_4 on a sample which

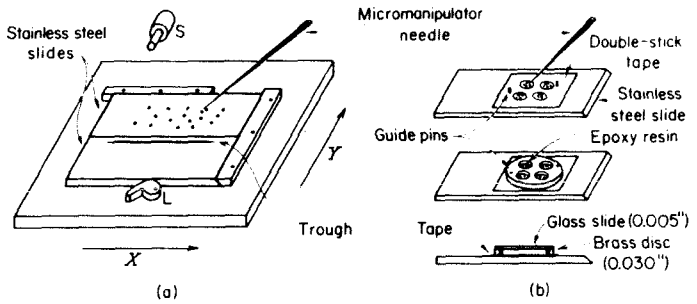

Fig. 1. Grain handling. X-Y stage with two stainless steel slides locked in position by L for picking grains from one slide, using the micromanipulator, and releasing them in the trough which is filled with a viscous liquid. Stop S is used to center the trough in the field of vision without removing eyes from the ocular (not shown). (b) Grains are ordered on double-stick tape inside of engraved circles (top); a brass disc is positioned using guide pins and the holes are filled with epoxy resin (middle); further backing is provided by a glass slide (bottom). All grain manipulations are performed under a microscope using a manipulator. Handing of individual grains down to a couple of microns is simple.

was originally enriched by using only the Frantz.

2.2. *Analytical procedure*

The chemical procedure and all laboratory ware used are the same as that described by Sanz and Wasserburg [2]. The average blank estimate (ABE) is 0.5 ng Sr and 0.04 ng Rb. The small phosphate samples required less handling and are subject to slightly less contamination than the ABE. ^{87}Rb and ^{84}Sr tracers were added to all samples before digestion. Strontium analyses were carried out on the Lunatic I, a digital, on-line mass spectrometer [1,4]. Two Sr analyses on whole meteorite samples of Guareña were reported previously [2] and are included here in table 1. These analyses were carried out on a conventional mass spectrometer and exhibit larger errors but are in good agreement with the Lunatic I data. All Sr analyses were made using a Faraday cup collector. At ion currents less than 2×10^{-11} A, we used a $10^{11}\ \Omega$ vibrating reed electrometer feedback resistor; at higher currents a $10^{10}\ \Omega$ resistor was used. All runs reached at least 2×10^{-11} A beam intensity. All Rb analyses were performed on a third conventional mass spectrometer equipped with an electron multiplier. Maximum errors of 2% are assigned to the $^{87}Rb/^{86}Sr$ ratio arising mostly from the unknown mass discrimination for Rb. Errors are assigned to the $^{87}Sr/^{86}Sr$ in the case of Lunatic I runs according to the scheme of Paper I. Only Category I and Category II data are used in table 1. Careful assignment of errors to $^{87}Sr/^{86}Sr$ is important when the contribution of the $^{87}Rb/^{86}Sr$ error to the calculation of $(^{87}Sr/^{86}Sr)_I$ is small. This contribution is attenuated by the factor $(e^{\lambda\tau} - 1) \approx 0.06$ for $\tau = 4.6$ b.y., so that a 2% error in $^{87}Rb/^{86}Sr$ results in 0.01% error in $(^{87}Sr/^{86}Sr)_I$ when $^{87}Rb/^{86}Sr = 0.05$. Most of our phosphate separates are below this value of $^{87}Rb/^{86}Sr$. Contribution of ^{87}Rb to the ^{87}Sr peak during a mass spectrometer run was monitored by scanning the mass 85 region. This contribution is negligible for all samples except C.II.2. The change in $^{87}Sr/^{86}Sr$ due to contamination from our average blank level of 5×10^{-10} g Sr is 3×10^{-5} for the smallest phosphate sample (acid leach). No corrections for blanks were made for either Sr or Rb since the correction uncertainty is the same as the correction itself.

3. Analytical results

The analytical data are shown in table 1 and are plotted in fig. 2. The points define a linear array, and we may therefore assume that Guareña follows the simple Rb-Sr systematics of a closed system. The insert in fig. 2 (lower right) shows the data for the

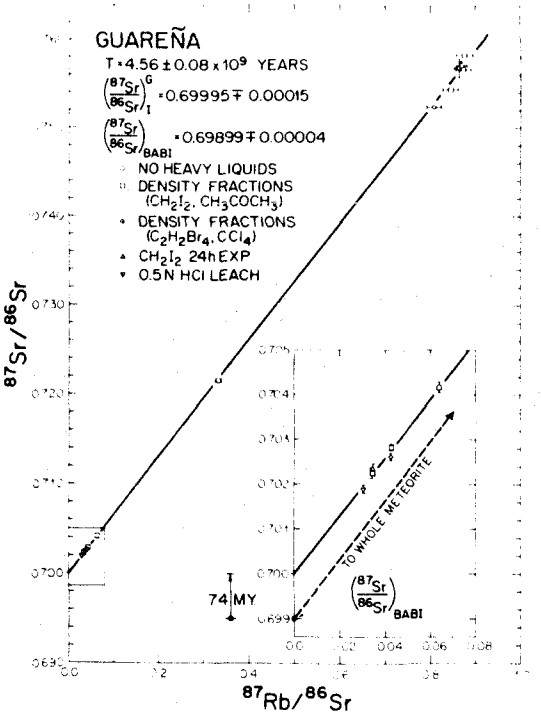

Fig. 2. Rb-Sr evolution diagram for Guareña (H6 chondrite). Least squares best fit isochron is shown in the main diagram and in the lower right insert. The initial ratio obtained is higher and different from $(^{87}Sr/^{86}Sr)_{BABI}$ and offers the first clear indication of differential Sr evolution of a stone meteorite. Dashed arrow is drawn through $(^{87}Sr/^{86}Sr)_{BABI}$ and the whole meteorite analyses, and is distinct from the isochron through the data points.

various phosphate samples. Table 1 also includes some repeat measurements on Moore County which were obtained immediately before or after phosphate runs. Due to its extremely small enrichment, Moore County approximately defines $(^{87}Sr/^{86}Sr)_{BABI}$. We also show our previous and our most recent measurements of Sr extracted from seawater.

From the microprobe grain counts of the phosphate separates, it is clear that the main Sr impurity consists of feldspar grains. Thus, all the "phosphate" points are mixtures of phosphate and feldspar and accordingly fall on a mixing line for the two components. However, the whole meteorite points and the $\rho > 3.3$ fraction cannot be just a mixture of only the trace phosphate and feldspar minerals. Some important Sr-containing fraction which is not identified must be present since the feldspar and whitlockite cannot account for all the strontium in the whole meteorite. Thus, we are not simply observing a mixing line [5].

It has been shown [6] that the trace apatite minerals may pick up radiogenic ^{87}Sr from the more abundant surrounding minerals which show much higher enrichments in $^{87}Sr/^{86}Sr$ (e.g., the feldspar). The dispersion of our data *excluding* the phosphate fractions is not enough to determine a precise age or an initial $^{87}Sr/^{86}Sr$ for this meteorite. However, for the purposes of this paper, we shall assume that the phosphate phase has not been disturbed or contaminated and that the data yield a meaningful age and $(^{87}Sr/^{86}Sr)_I$ for Guareña.

A best fit line through the data following the treatment of York [7] yields an age $\tau = 4.56 \pm 0.08 \times 10^9$ yr (3σ errors) for $\lambda_{^{87}Rb} = 1.39 \times 10^{-11}$ yr^{-1}. The initial ratio for Guareña $(^{87}Sr/^{86}Sr)_I^G = 0.69995 \mp 0.00015$. Half of this error in initial Sr is attributable to measurement errors and half is due to the extrapolation to $^{87}Rb/^{86}Sr = 0$. $(^{87}Sr/^{86}Sr)_I$ for Guareña is very precisely defined and is distinctly different from $(^{87}Sr/^{86}Sr)_{BABI} = 0.69899 \pm 0.00004$ [1]. Except for the special case of Kodaikanal [8] and the slightly uncertain case of Weekeroo Station [9], this is the only clear-cut difference in $(^{87}Sr/^{86}Sr)_I$ found for meteorites. Previous work has always been consistent with $(^{87}Sr/^{86}Sr)_I = 0.699$ within the rather large experimental errors.

Since this clearly measurable difference between $(^{87}Sr/^{86}Sr)_{BABI}$ and the Guareña $(^{87}Sr/^{86}Sr)_I^G$ has rather important implications and depends critically on the phosphate fractions, we tried several leaching experiments to determine if the heavy liquid separations disturbed the samples. Sample C.II was obtained from C.I.3 by several passes through the Frantz. C.II was split into three aliquots. Aliquot C.II.1 received no further treatment; C.II.2 was placed in methylene iodide for 24 hr and then rinsed with acetone; C.II.3 was leached with 0.5 N HCl for five min during which all the phosphate was dissolved while most of the impurities were not. The supernatant solution (HCl soluble) from this leaching procedure was analyzed for Sr and Rb. In addition, sample C.III was obtained by methylene iodide-acetone separation for

only 15 min, instead of the several hours used for sample C.I.3. For comparison with the methylene iodide separates, samples C.IV were obtained by using filtered tetrabromoethane and carbon tetrachloride on a sample which had not been exposed to any heavy liquids. From the insert in fig. 2, it is clear that the samples exposed to methylene iodide-acetone for different times show no effects of differential exposure to these reagents. Sample C.II.2 was corrected conservatively for a slight ^{87}Rb contribution to ^{87}Sr during the mass spectrometer run (0.01%). No difference is apparent between using CH_2I_2 and CH_3COCH_3 or $C_2H_2Br_4$ and CCl_4. Such a difference could be caused by leaching due to differences in the polar nature of the solutions or by different contamination levels. The acid leached sample (C.II.3) does not show preferential leaching of Rb or Sr; however, this is due most probably to the very low percentage of insoluble impurities in the original sample. During the heavy liquid separation of sample C.IV weighing 13 mg (50% phosphate), we obtained samples C.IV.1 and C.IV.2, each weighing 3.4 mg only, for a total recovery from heavy liquids of 52%. A similar absolute amount of sample lost during heavy liquid mineral separations was reported by Sanz and Wasserburg [2]. In agreement with these authors, we find no differential effect from the use of heavy liquids, but caution is still advisable since a large fraction of the sample is often not recovered. Our results for the acid leach do not appear in any way to be out of line, although such a procedure has been shown to be unreliable [2] in other cases where the mineral separates were not of high purity.

In an effort to even further establish that there were no anomalous effects due to the use of the heavy liquid separations, sample B was obtained by using *only* magnetic separations without any contact with the heavy liquids. In addition, the whole meteorite samples were also totally dissolved and did not come into contact with the heavy liquids. A line drawn through sample B and the Lunatic I total meteorite point yields an age 4.53×10^9 yr and an intercept $(^{87}Sr/^{86}Sr)_I^G = 0.69982$ and is the same to within experimental and interpolational error as $(^{87}Sr/^{86}Sr)_I^G$. We conclude that the difference between $(^{87}Sr/^{86}Sr)_I^G$ and $(^{87}Sr/^{86}Sr)_{BABI}$ is real and clearly measurable.

4. Discussion

The determination of an internal isochron for a Rb-Sr system yields the age τ_I since the last Sr isotope homogenization and the Sr isotopic abundance $(^{87}Sr/^{86}Sr)_I$ at the time of this homogenization. If we can also measure the present value $(^{87}Rb/^{86}Sr)_P$ in the total system, we can calculate $(^{87}Rb/^{86}Sr)_I$. The significant question is how the system arrived, τ_I years ago, at the state described by $(^{87}Rb/^{86}Sr)_I$ and a homogeneous $(^{87}Sr/^{86}Sr)_I$. If the total system remained closed at times $\tau \geqslant \tau_I$, we can determine the average $(^{87}Sr/^{86}Sr)_\tau$ for short intervals $\Delta\tau = \tau - \tau_I$ ($\lambda\Delta\tau \ll 1$). We obtain $(^{87}Sr/^{86}Sr)_\tau = (^{87}Sr/^{86}Sr)_I - \lambda(\tau - \tau_I)(^{87}Rb/^{86}Sr)_I$. On a $[\tau, (^{87}Sr/^{86}Sr)_\tau]$ diagram this is the equation of a straight line originating at τ_I and $(^{87}Sr/^{86}Sr)_I$ and with the negative slope $-\lambda(^{87}Rb/^{86}Sr)_I$. This construction is shown in fig. 3a for a system A. Riley and Compston [10] have previously discussed similar constructions with a slight change in variables for the purpose of obtaining the age and initial Sr isotopic composition of a system. The purpose of our construction is to determine the qualitative evolution of a system prior to the time of its last Sr homogenization.

In Paper I we obtained $(^{87}Sr/^{86}Sr)_{BABI}$ as the initial isotopic abundance for the basaltic achondrites. This is the lowest Sr isotopic abundance obtained with high precision. Slightly lower initial Sr isotopic abundances have been reported but with a precision at least a factor of ten worse than $(^{87}Sr/^{86}Sr)_{BABI}$. The average solar system Sr isotopic abundance must have crossed $(^{87}Sr/^{86}Sr)_{BABI}$ at some early unknown time τ_{BABI}. Irrespective of τ_{BABI} we can examine the evolution of any system since the solar system had the composition $(^{87}Sr/^{86}Sr)_{BABI}$. In particular, for a system A with age τ_I^A, if $(^{87}Sr/^{86}Sr)_I^A > (^{87}Sr/^{86}Sr)_{BABI}$, this clearly indicates the system A was formed or disturbed after the solar system had evolved past $(^{87}Sr/^{86}Sr)_{BABI}$. In fig. 3a we obtain the intersection A′ of the constant $y = (^{87}Sr/^{86}Sr)_{BABI}$ line and the line extrapolated from A with slope $-\lambda(^{87}Rb/^{86}Sr)_I^A$, and we define a unique time interval $\Delta\tau_{BACH}^A = \tau_{BABI}^A - \tau_I^A$, following the notation of Paper I. This interval represents the time required for system A to evolve

from $(^{87}Sr/^{86}Sr)_{BABI}$ to $(^{87}Sr/^{86}Sr)_I^A$ as a closed system. At τ_I^A system A is isotopically homogenized, the phases become closed to Rb and Sr and thereafter evolve undisturbed.

If τ_F is the time at which two systems, A and B, are fractionated and separated simultaneously from a single reservoir of a uniform $(^{87}Sr/^{86}Sr)_{BABI}$ composition, they will evolve along different straight lines originating from the point $[\tau_F, (^{87}Sr/^{86}Sr)_{BABI}]$ as shown in fig. 3b. The two systems are homogenized at intervals $\Delta\tau^A_{BACH}$ and $\Delta\tau^B_{BACH}$ after τ_F and thereafter evolve undisturbed as closed systems. The simultaneity of formation of A and B (that is, the coincident solution τ_F) gives credence to the intervals $\Delta\tau_{BACH}$, which can always be constructed, and also fixes $\tau_{BABI} = \tau_F$. If we obtain systems which extrapolate back to a single point, we can form a definite time sequence for these systems according to their relative $\Delta\tau_{BACH}$ values. Such a sequence would also be associated with a major event of fractionation and formation of planetary objects at a determinable time τ_F.

Any system may undergo a more complicated evolution, including Rb-Sr fractionation before τ_I, than the simple single-stage evolution described above. Fig. 3 c shows a possible two-stage trajectory A_2A_1A for system A. Stage AA_1 has a slope determined by $(^{87}Rb/^{86}Sr)_I^A$. Stage A_2A_1 has an undetermined

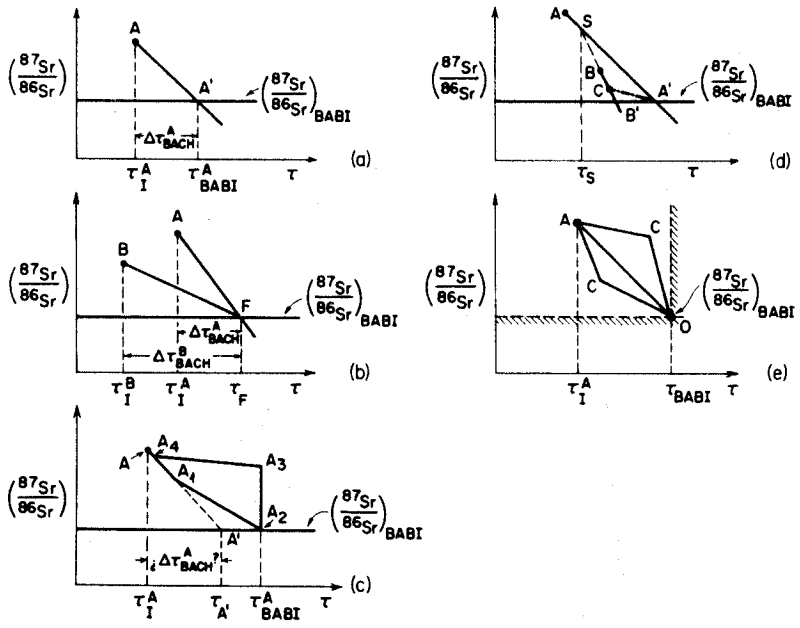

Fig. 3. Age – $^{87}Sr/^{86}Sr$ diagrams for the evolution of systems prior to their final Sr isotopic homogenization. Slope of lines drawn reflects $^{87}Rb/^{86}Sr$ in the total systems. (a) Definition of $\Delta\tau$BACH. (b) Coincidence of origin of two $\Delta\tau$BACH intervals unequivocally fixes both intervals and also τ_F as a time of formation of planetary objects. (c) Possible evolution of a system: each straight line defines a stage of closed system evolution; each intersection of two lines of different slope (proportional to $^{87}Rb/^{86}Sr$) defines an event of Rb-Sr fractionation after Sr re-equilibration. Trajectories A'A, A_2A_1A and $A_2A_3A_4A$ are all compatible with the observable quantities at A; (d) For the two systems as shown the position of the intersection S of AA' and BB' requires a differential evolution stage A'C independently of the $(^{87}Sr/^{86}Sr)_{BABI}$ value; (e) Knowledge of both τ_{BABI} and $(^{87}Sr/^{86}Sr)_{BABI}$. System A had at least a two-stage evolution (OCA) unless it had the right Rb/Sr to evolve from $(^{87}Sr/^{86}Sr)_{BABI}$ to $(^{87}Sr/^{86}Sr)_I^A$ in time $\tau_{BABI} - \tau_I^A$ (that is, along OA with slope equal to $-\lambda\xi$).

slope; however, for a two-stage evolution, if system A had the composition $(^{87}Sr/^{86}Sr)_{BABI}$ at times greater than (or smaller than) $\tau_{A'}$, slope A_2A_1 must be smaller than (or greater than) slope AA_2. For example, a system with trajectory A_2A_3 originating at A_2 with infinite Rb/Sr requires an extra stage A_3A_4 if we want to evolve to A with the experimentally determined slope equal to AA', assuming that system A remained closed at τ_I^A.

We would like to discuss the general case of two systems, A and B, and to show that it is possible to determine when at least a two-stage evolution is required for one of the two systems. We can use $(^{87}Sr/^{86}Sr)_{BABI}$ as the basis for the comparison, even though objects could have formed before or after the time at which at the solar system crossed this ratio. In fig. 3d we show the two systems, A and B, the extrapolated lines AA' and BB' with slopes $-\lambda(^{87}Rb/^{86}Sr)_I^A$ and $-\lambda(^{87}Rb/^{86}Sr)_I^B$ respectively, and the intersection S of lines AA' and BB' at τ_S and $(^{87}Sr/^{86}Sr)_S$. Several cases are possible depending on the location of S with respect to systems A and B. If $(^{87}Sr/^{86}Sr)_S$ is greater than either $(^{87}Sr/^{86}Sr)_I^A$ or $(^{87}Sr/^{86}Sr)_I^B$, there exists no Sr isotopic composition of a reservoir from which both systems, A and B, could have fractionated and evolved to τ_I^A and τ_I^B in a single stage with no intermediate Rb-Sr fractionation. For the particular case shown in fig. 3d, system B must have evolved at least in an intermediate stage A'C. This conclusion is true even if we did not know the value of $(^{87}Sr/^{86}Sr)_{BABI}$. The two-stage evolution for either system B or system A is the simplest trajectory required; a more complicated history is, of course, allowed.

If the intersection S occurs in the region

$$\min[(^{87}Sr/^{86}Sr)_I^A\ ,\ (^{87}Sr/^{86}Sr)_I^B] > (^{87}Sr/^{86}Sr)_S > (^{87}Sr/^{86}Sr)_{BABI}\ ,$$

there exists a value $(^{87}Sr/^{86}Sr)_S$ for a reservoir from which A and B could have fractionated and formed in a single process. The time of this event is also determined. If the Rb/Sr in the solar reservoir were known, the time required for evolution in this reservoir from $(^{87}Sr/^{86}Sr)_{BABI}$ to $(^{87}Sr/^{86}Sr)_S$ can be determined and possibly establish an interval for the direct formation of objects from the solar reservoir. If $(^{87}Sr/^{86}Sr)_S < (^{87}Sr/^{86}Sr)_{BABI}$, the intersection S may be actually meaningful in as much as fractionation and separation of objects can occur before the solar system crossed $(^{87}Sr/^{86}Sr)_{BABI}$. In this case τ_S may be considerably larger than both τ_I^A and τ_I^B and therefore objects A and B would be prime candidates for a search for effects resulting from short-lived radioactivities or primary irradiation, if these effects were not obliterated by the metamorphic events at τ_I^A and τ_I^B. If such effects are not found, or if τ_S is unreasonably high, we could conclude that S is not meaningful and that therefore in the simplest case either A or B underwent a two-stage evolution. If $(^{87}Sr/^{86}Sr)_S < 0$ such a two-stage evolution would be absolutely required. Therefore, we can, in principle, almost by inspection of the trajectories of two systems, A and B, on a $[\tau,(^{87}Sr/^{86}Sr)_\tau]$ diagram determine whether we can order the systems according to their $\Delta\tau_{BACH}$ or what the minimum number of required evolution stages is and the relative type of Rb-Sr fractionation which is necessary for consistency of the refined Rb-Sr data. Measurements of effects of other elements will impose further restrictions on the systems studied.

For this discussion, we did not make any assumptions about the time τ_{BABI} at which the solar system crossed $(^{87}Sr/^{86}Sr)_{BABI}$. However, limits can be placed on τ_{BABI} from the ages of meteorites measured by internal isochrons and the approximately equal ages obtained for groups of meteorites. If we fix τ_{BABI}, we obtain fig. 3e for any system A. There exists a value $\zeta = (^{87}Rb/^{86}Sr)$ for which A can evolve directly from $(^{87}Sr/^{86}Sr)_{BABI}$ to $(^{87}Sr/^{86}Sr)_I^A$ in the fixed interval $(\tau_{BABI} - \tau_I^A)$. If $(^{87}Sr/^{86}Sr)_{BABI}$ is the lowest $(^{87}Sr/^{86}Sr)_I$ for a homogenized reservoir from which systems developed, the regions in fig. 3e $(^{87}Sr/^{86}Sr) < (^{87}Sr/^{86}Sr)_{BABI}$ and $\tau > \tau_{BABI}$ are forbidden for individual systems.

If system A has $(^{87}Rb/^{86}Sr)_I^A \neq \zeta$ (corresponding to segment AO) we require at least a two-stage evolution after $(^{87}Sr/^{86}Sr)_{BABI}$ with an intermediate stage OC of appropriately lower or higher $(^{87}Rb/^{86}Sr)$ than ζ if $(^{87}Rb/^{86}Sr)_I^A$ is higher or lower than ζ, respectively. We obtain for the trajectories in fig. 3e,

$$(^{87}Sr/^{86}Sr)_I^A - (^{87}Sr/^{86}Sr)_{BABI} = \lambda\zeta(\tau_{BABI} - \tau_I^A),$$

or

$$(^{87}Sr/^{86}Sr)_I^A - (^{87}Sr/^{86}Sr)_{BABI} = \lambda(^{87}Rb/^{86}Sr)_C(\tau_{BABI} - \tau_C) + \lambda(^{87}Rb/^{86}Sr)_I^A(\tau_C - \tau_I^A)$$

where all time differences are positive. The total time difference $(\tau_{BABI} - \tau_I^A)$ can be arbitrarily partitioned between the intermediate stage OC and stage CA. Any independently determined event in the history of system A in the interval $\tau_{BABI} - \tau_I^A$ may be used to partition this interval and to determine $(^{87}Rb/^{86}Sr)$ in the intermediate stage OC.

The preceding general discussion can be applied to Guareña which is the first system for which an age τ_I and a very precise $(^{87}Sr/^{86}Sr)_I$ were determined. We calculate $\Delta\tau_{BACH} = 74 \pm 12 \times 10^6$ yr for either slow cooling or a metamorphic event resulting in complete Sr isotopic homogenization. Even though we can define a precise time $\Delta\tau_{BACH}$ of metamorphism for Guareña, it is not clear what temperature and pressure are involved in a meteoritic environment in the apparent absence of water. The existence of a metamorphism interval is consistent with the classification of Guareña as an H6 recrystallized chondrite by Van Schmus and Wood [11]. If we now fix $\tau_{BABI} = 4.7 \times 10^9$ yr, we require an intermediate stage of evolution. However, the error in the age of Guareña and the possible range of τ_{BABI} allow a single-stage evolution from $(^{87}Sr/^{86}Sr)_{BABI}$ to $(^{87}Sr/^{86}Sr)_I^{Guareña}$.

While Guareña is the first meteorite for which precise data exist, we may, for the purpose of discussing the case of two systems, consider also the iron meteorite Weekeroo Station. Burnett and Wasserburg [9] have determined an age $\tau_I^W = 4.37 \times 10^9$ yr and $(^{87}Sr/^{86}Sr)_I^W = 0.703 \mp 0.001$ by analyzing silicate inclusions of this meteorite. Rb/Sr in the "whole" meteorite is not meaningful in the usual sense, however, we can take an average present $(^{87}Rb/^{86}Sr)_p \approx 0.70$ from the data presented. The results are plotted in fig. 4. The intersection of the extrapolated lines for Guareña and Weekeroo Station falls above $(^{87}Sr/^{86}Sr)_I^{Guareña}$, and thus we formally require that Guareña or Weekeroo Station evolve through some intermediate stage. We show, in particular, an intermediate stage G'W'' for the Weekeroo Station silicate inclusions. The errors for Weekeroo Station are large and, therefore, in fact, we cannot *require* a differential multistage evolutionary history for these meteorites even though a differential history is clearly indicated by the difference in their initial Sr isotopic composition. The error envelopes for Weekeroo Station and Guareña would overlap at $\tau = 4.7$ b.y. and the simplest possible explanation is that both Guareña and the silicate inclusions formed at $\tau_{BABI} \approx 4.7$ b.y. and underwent different cooling or metamorphic histories. Since the Rb/Sr in both meteorites is approximately the same and also similar to a typical "chondritic" Rb/Sr reservoir as discussed in Paper I, the ages of Guareña and Weekeroo Station might actually represent different times of separation of these bodies from such a reservoir followed by fast cooling. This model would also circumvent the problem of isotopically equilibrating physically separated silicate inclusions in Weekeroo

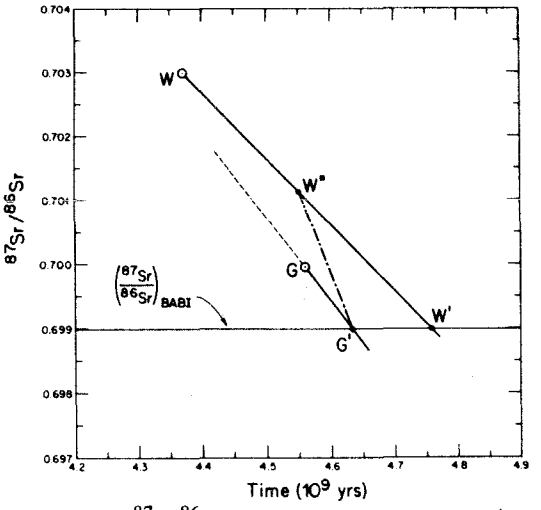

Fig. 4. Age – $(^{87}Sr/^{86}Sr)$ plot for Weekeroo Station (WW') and Guareña (GG'). Stage G'W'' is indicated as a possible two-stage model. A multi-stage model is required since the intersection of WW' and GG' falls above Guarena. Errors of the Weekeroo Station data (not shown) do not allow a firm conclusion.

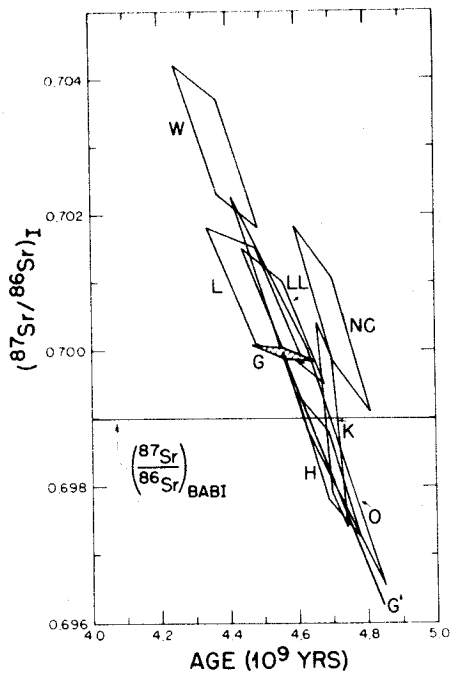

Fig. 5. Age – $(^{87}Sr/^{86}Sr)_I$ anticorrelation plot. We show error envelopes for internal isochrons of Weekeroo Station (W, [9]); Norton County (NC, [15]); Krähenberg (K, [16]); Olivenza (O, [2]); and Guarena (G-hatched polygon). We also show error envelopes for isochrons for the L, LL and H chondrite groups [12–14]. Error envelopes correspond to least squares errors as stated by each author. Guareña is not compatible with the H-group data. However, an extrapolation along line GG′ drawn from the center of envelope G and with slope proportional to Rb/Sr in the whole Guareña meteorite yields an intersection with the H-group data in the interval 4.60–4.78 b.y., so that Guareña could have formed in this interval and been metamorphosed at 4.56 b.y. No attempt at normalizing isotopic data between different workers has been made.

Station at 4.37 b.y. if it formed at ~ 4.7 b.y.

Kaushal and Wetherill [12] recently obtained an isochron for the H-group chondrites. Our *whole* meteorite data agrees well with the isochron presented. However, a more meaningful comparison involves an age – $(^{87}Sr/^{86}Sr)_I$ anticorrelation plot [2]. We have shown in fig. 5 error envelopes for individual meteorites and groups of meteorites. The envelopes correspond to ± 3σ errors for a least squares fit according to a York-type program [7] used by each author. We have drawn simple polygonal envelopes. A formal study of the detailed shape of such envelopes and of the statistical significance of their intersections will be undertaken. We have shown the data for the H, L, LL group chondrites [12–14] and the internal isochron data for Weekeroo Station [9], Norton County [15], Kraehenberg [16] and Olivenza [2]. The ± 3σ data for Guareña yield τ_I = $4.56 \pm 0.08 \times 10^9$ yr and $(^{87}Sr/^{86}Sr)_I$ = 0.69995 ∓ 0.00012 and result in a very small error envelope which does not intersect the H-group chondrites. However, if we extrapolate back in time using Rb/Sr of Guareña, we find an intersection at 4.70 b.y. A consistent explanation would be that Guareña as a total meteorite was formed along with the H-group chondrites but was subjected to metamorphism 4.56 b.y. ago. This is analogous to geological studies were "total rock" points yield higher ages than separated minerals from each rock [17] if the total rocks remained closed. The Guareña data intersect the L and LL-group chondrites and Olivenza. It appears that such intersections are more a sign of large, analytical errors from less precise work than an indication of a genetic relationship. In particular, from the disagreement of Guareña and the H-group chondrites it follows that different meteorites may only approximately be considered as originating with the same $(^{87}Sr/^{86}Sr)_I$ and that certainly evidence of events on a fine time scale is lost by whole meteorite studies. It should be noted that the comparison of data from different laboratories is made difficult both by the lack of high quality comparisons of adequate standards and the considerable difference in the quality of the data reported by different workers.

Acknowledgements

We thank Mr. J.Brown for his competent and meticulous work in obtaining the phosphate separates. This research was principally supported by grants from the National Science Foundation (GP-9433 and GP-9114).

References

[1] D.A.Papanastassiou and G.J.Wasserburg, Initial strontium isotopic abundances and the resolution of small time differences in the formation of planetary objects, Earth Planet. Sci. Letters 5 (1969) 361.

[2] H.G.Sanz and G.J.Wasserburg, Determination of an internal $^{87}Rb-^{87}Sr$ isochron for the Olivenza chondrite, Earth Planet. Sci. Letters 5 (1969).

[3] S.Calderon and F.Quiroga, Estudio petrografico del meteorito de Guareña, Badajoz, Anal. Soc. Espaň. Hist. Nat. Madrid 22 (1893) 127.

[4] G.J.Wasserburg, D.A.Papanastassiou, E.V.Nenow and C.A.Bauman, A programmable magnetic field mass spectrometer with on-line data processing, Rev. Sci. Instrum. 40 (1969) 288.

[5] G.J.Wasserburg and D.S.Burnett, The status of isotopic age determinations on iron and stone meteorites, in: Meteorite Research, Millman, ed. (D.Reidel Publ. Co., Dordrecht, Holland, 1969) p. 467.

[6] R.H.Steiger and G.J.Wasserburg, Comparative U-Th-Pb systematics in 2.7×10^9 yr plutons of different geologic histories, Geochim. Cosmochim. Acta, November 1969 (in press).

[7] D.York, Least squares fitting of a straight line, Can. J. Phys. 44 (1966) 1079.

[8] D.S.Burnett and G.J.Wasserburg, Evidence for the formation of an iron meteorite at 3.8×10^9 yr, Earth Planet. Sci. Letters 2 (1967) 137.

[9] D.S.Burnett and G.J.Wasserburg, $^{87}Rb-^{87}Sr$ ages of silicate inclusions of iron meteorites, Earth Planet. Sci. Letters 2 (1967) 397.

[10] G.H.Riley and W.Compston, Theoretical and technical aspects of Rb-Sr geochronology, Geochim. Cosmochim. Acta 26 (1962) 1255.

[11] W.R.Van Schmus and J.A.Wood, A chemical-petrologic classification for the chondrite meteorites, Geochim. Cosmochim. Acta 31 (1967) 747.

[12] S.K.Kaushal and G.W.Wetherill, $^{87}Rb-^{87}Sr$ age of bronzite (H group) chondrites, J. Geophys. Res. 74 (1969) 2717.

[13] K.Gopalan and G.W.Wetherill, Rubidium-strontium age of hypersthene (L) chondrites, J. Geophys. Res. 73 (1968) 7133.

[14] K.Gopalan and G.W.Wetherill, Rubidium-strontium age of amphoterite (LL) chondrites, J. Geophys. Res. (1969) in press.

[15] D.D.Bogard, D.S.Burnett, P.Eberhardt and G.J.Wasserburg, $^{87}Rb-^{87}Sr$ isochron and $^{40}K-^{40}Ar$ ages of the Norton County achondrite, Earth Planet. Sci. Letters 3 (1967) 179.

[16] W.Kempe and O.Mueller, The stony meteorite Kraehenberg: its chemical composition and the Rb-Sr age of the light and dark positions, in: Meteorite Research, Millman, ed. (D.Reidel Publ. Co., Dordrecht, Holland, 1969) p. 418.

[17] M.A.Lanphere, G.J.Wasserburg, A.L.Albee and G.R. Tilton, Redistribution of strontium and rubidium isotopes during metamorphism, World-Beater complex, Panamint Range, California, in: Isotopic and Cosmic Chemistry, Craig, Miller and Wasserburg, eds. (North-Holland Publ. Co., 1964).